UNIVERSITÀ DEGLI STUDI
DI GENOVA

OSPEDALE POLICLINICO SAN MARTINO
Sistema Sanitario Regione Liguria
Largo Rosanna Benzi, 10 - 16132 GENOVA

Corso di Dottorato in Biotecnologie in Medicina Traslazionale

Curriculum Di Biotecnologie Cellulari E Molecolari

XXX ciclo

TARGETING HIGH GRADE GLIOMAS IN MURINE PRECLINICAL MODELS

Author: Francesco Alessandrini

Supervisor: Prof. Paolo Malatesta

Contents

Introduction

Gliomas

Gliomas constitute a heterogeneous group of tumor originating in the brain. Gliomas represent almost 80% of the primary cerebral tumors and are composed by cells similar to glial cells. The heterogeneity of the different phenotypes of glial cells are reflected on that of gliomas, including tumors composed from astrocytes, oligodendrocytes, choroid plexus cells or radial glia cells [1]. The incidence of gliomas is 6 cases per 100'000 people every year, higher in male than in female (7.14/100'000 and 5.06/100'000 respectively, [2]).

Historically, gliomas have been diagnosed and classified based on histopathology, although over time the information regarding the molecular nature of the tumor lesions has been added to the classic grading for a better classification. In the updated central nervous system (CNS) tumor classification, published in 2016 by the World Health Organization (WHO), some tumors are defined by a combination of microscopic morphologic and molecular and genetic factors, whereas others continue to be defined by morphology alone (Figure 1).

The main classification recommended by WHO is based on the resemblance of cellular component of gliomas to normal isotypes (astrocytomas, oligodendrogliomas and mixed oligoastrocytomas) and their grade of malignancy, from I to IV, that depends by tumor aggressiveness and the histopathological features of tumor tissue, such as cellularity, cytonuclear atypia, mitotic activity, microvascular proliferation and necrosis [3].

Grade I is applied to lesions with low proliferative potential and the possibility to cure following surgical resection alone. Grade II is referred to generally infiltrative tumors that, despite low -

level proliferative activity, often recur. Some type II tumors tend to progress to higher grades of malignancy, for example, low-grade diffuse astrocytomas that transform to anaplastic astrocytoma and glioblastoma. Similar transformation occurs in oligodendroglioma and oligoastrocytomas. Patients with grade II gliomas typically survive more than 5 years. Neoplasms designated grade III are lesions with histological evidence of malignancy, including nuclear atypia and brisk mitotic activity, and are most often lethal for patients within 3 years. Grade IV is assigned to cytologically malignant, mitotically active, necrosis-prone neoplasms typically associated with rapid pre- and postoperative disease evolution and a fatal outcome. Widespread infiltration of surrounding tissue and a propensity for craniospinal dissemination characterize some grade IV neoplasms. Not more than 30% of patients with grade IV gliomas survive more than two years.

Recent molecular advances revealed that canonic histologically defined categories of gliomas correlate well with relatively few recurrent molecular features [5, 6]. Thus, these alterations have become entity-defining features, overcoming the more conventional histologic assessment. Gliomas of all histologic grades can be subdivided broadly into 3 groups dependent on only 2 parameters: the deletion of both the short arm of chromosome 1 (1p) and the long arm of chromosome 19 (19q, 1p/19q co-deletion), and the mutational status of isocitrate dehydrogenase 1 (IDH1), or its mitochondrial cousin, isocitrate dehydrogenase 2 (IDH2).

We can define three main groups of gliomas: i) astrocytoma, IDH-mutant; ii) astrocytoma, IDH–wild type; and iii) oligodendroglioma, IDH-mutant and 1p/19q-codeleted (Figure 2). The fourth possible category, that of 1p/19q-codeleted tumors lacking *IDH* mutation, represents an exceedingly rare entity.

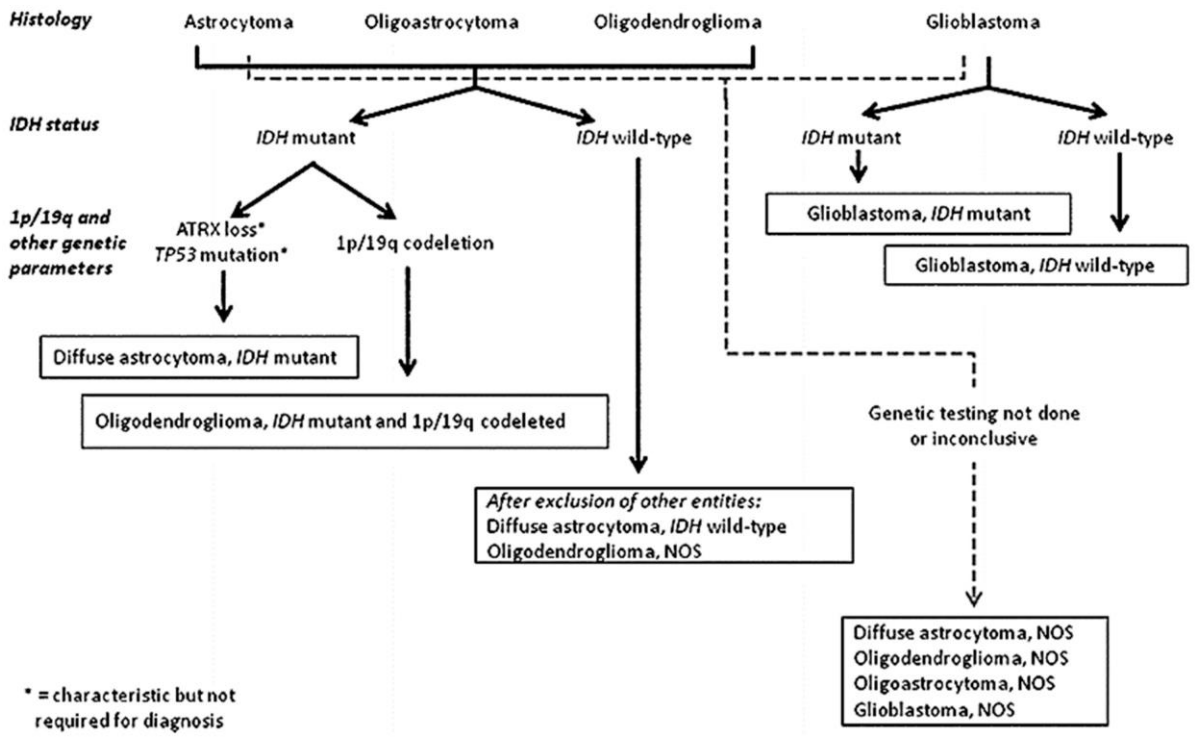

Figure 1

A simplified algorithm for classification of the diffuse gliomas based on histological and genetic features from 2016 CNS WHO project. A caveat to this diagram is that the diagnostic "flow" does not necessarily always proceed from histology first to molecular genetic features next, since molecular signatures can sometimes outweigh histological characteristics in achieving an "integrated" diagnosis [4].

Glioblastomas

Glioblastoma multiforme (GBM) is the most common primary malignant brain tumor, accounting for approximately 60%–70% of gliomas [7] and about 210,000 new cases are diagnosed each year worldwide [2], usually occurring after the age of 40 years and with a peak of incidence between 50 and 70 years of age. Many genetic and environmental factors have been studied in GBM but no risk factor that accounts for a large proportion of GBM has been identified and like many cancers are sporadic [8].

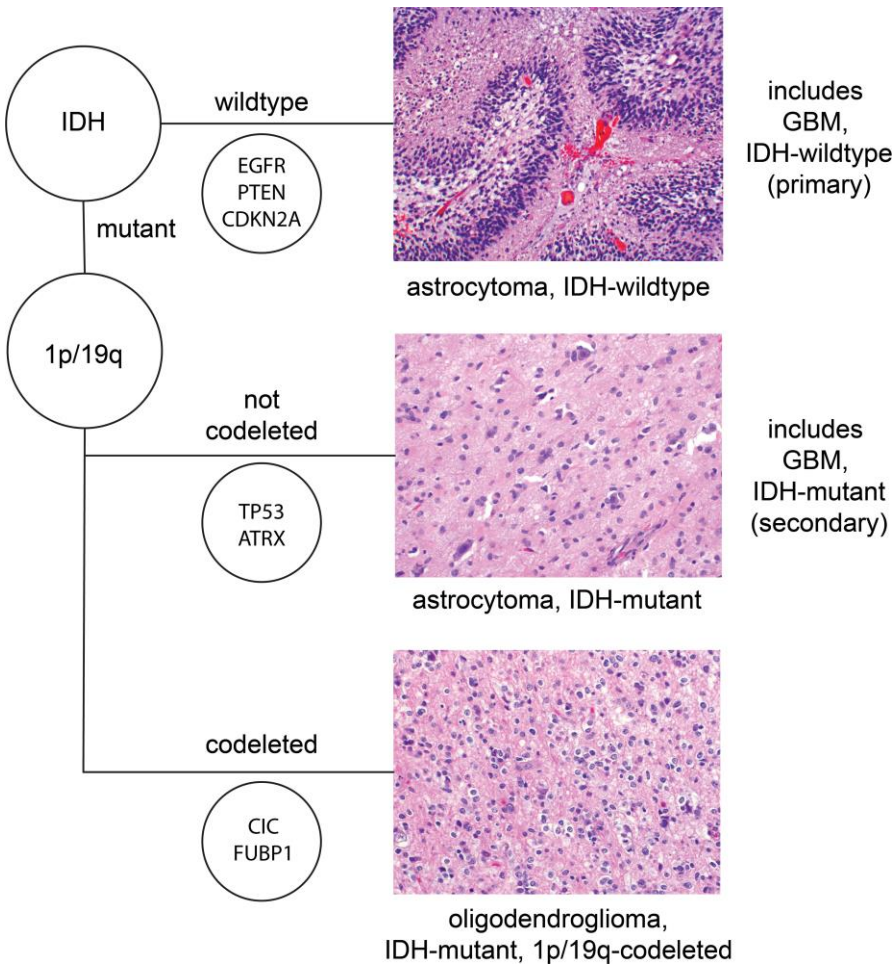

Figure 2

World Health Organization classification of infiltrating gliomas. The diagram represents the 3 major categories of adult diffusely infiltrating gliomas based on IDH1/2 mutational status and 1p/19q codeletional status, along with representative additional recurrent somatically altered genes for each group, and histologic images stained with hematoxylin-eosin [9].

GBMs are typically poorly-marginated, diffusely infiltrating necrotic masses localized to the cerebral hemispheres. The surrounding brain tissue usually shows marked edemas. The supratentorial white matter is the most common location. GBMs have a significant variability in size from only a few centimeters to lesions that replace a hemisphere. Infiltration beyond the visible tumor margin is always present. The microscopic appearance of GMBs is characterized by a heterogeneous composition of cells with various morphological features, including

astrocyte-like cells, fusiform cells, small anaplastic and pleomorphic multinuclear giant cells, with marked atypia and numerous mitoses. Necrosis and microvascular proliferation are often observed. Microvascular proliferation results in an abundance of new blood vessels. Two types of necrosis may be distinguished: large ischemic necrosis and small, often multiple, irregularly shaped ban-like or serpiginous foci of necrosis, typically surrounded by glioma cells in a pseudopalisading pattern [10].

GBMs have traditionally been divided into primary and secondary. The majority of GBMs (90%) arises de novo in elderly patients (primary GBMs), with no clinical or histological evidence of a previous lesion of lower malignancy, whereas secondary GMB form develops from a pre-existing lower grade gliomas (low-grade diffuse astrocytoma or anaplastic astrocytoma), usually occurring in younger patients below 45 years of age [11]. Histologically and morphologically, primary and secondary GBMs are not distinguishable, but they differ in their genetic and epigenetic profile. Primary GBMs are almost invariably IDH wild-type. Secondary GBMs are often IDH mutant, associated with a hypermethylation phenotype, a mutation shared by over 80% of grade II and III astrocytomas [12-14].

Molecular characterization of glioblastomas

Several approaches alternative to histopathologic one were employed in GBMs classification, starting from large-scale profiling studies based on gene or protein expression the molecular profile studied in the different GMB subtypes to identify transcriptional or proteomic signatures, in an attempt to better understand GBM biology and to identify new clinically relevant markers. Verhaak et *al*. used the data obtained by The Cancer Genome Atlas (TCGA) to correlate gene expression-based GBM subtypes with alterations in DNA sequences and copy numbers. They

identified 840 genes differentially expressed in GMB samples and have thereby established a classification of GBM into Classical, Mesenchymal, Proneural and Neural subtypes demonstrating that these subtypes are associated with specific genomic alterations (Figure 3). The Classical subtype is characterized by Epidermal Growth Factor Receptor (EGFR) amplification and the absence of p53 mutations. The Proneural subtype is characterized by IDH1 and tumor protein (TP53) mutations and Platelet Derived Growth Factor A (PDGFR-A) amplification. The Neural subtype was typified by the expression of neuron markers such as neurofilament light chain gene (NEFL), Gamma-Aminobutyric Acid Type A Receptor (GABRA1), Synaptotagmin 1 (SYT1) and Solute Carrier Family 12 Member 5 (SLC12A5). Finally, the Mesenchymal subtype is characterized by deletions or mutation of the Neurofibromin 1 gene (NF1) [15]. By comparing these subtypes with their response to therapy, it was possible to correlate the classification with the response to treatment, increasing the importance of this molecular classification.

Interestingly, using a proteomic approach based on unsupervised hierarchical clustering obtained without forcing a predetermined number of classes, Brennan et al. showed that gliomas can be divided into three main subtypes associated with EGFR activation, PDGFR activation and NF1 loss [16], and having close relationships with the classes identified by Verhaak et al. (Figure 4). Such integrated work has revealed that GBMs can be classified into a few major subtypes on the basis of a small number of molecular aberrations, also identified by using IHC-based techniques [17, 18].

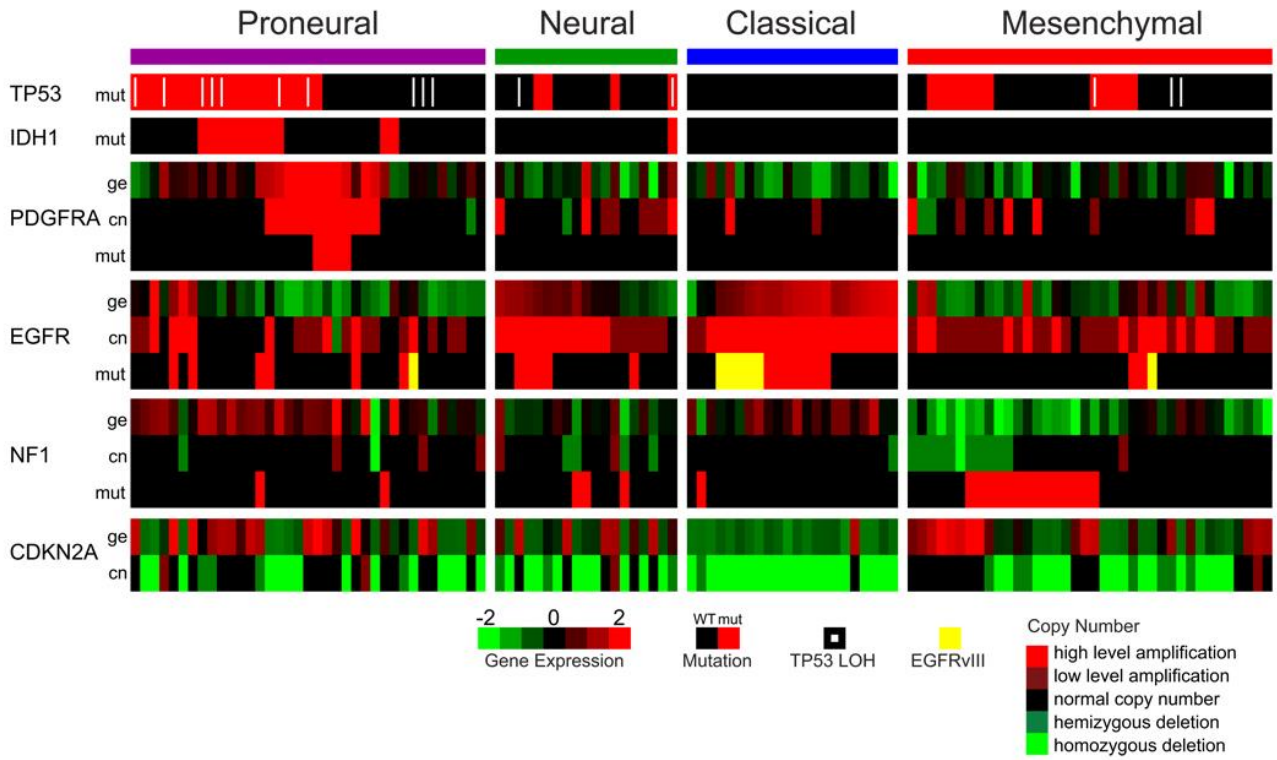

Figure 3

Integrated view of gene expression and genomic alterations across glioblastoma subtypes identified by Vheraak and al. from TGCA gene expression data [15].

Gain of gene expression or amplification in receptor tyrosine kinases (RTKs) such as EGFR and PDGFR resulted in constitutively activated receptor signaling in cancer cells [19]. EGFR (ErbB1, HER1) is a transmembrane tyrosine kinase on chromosome 7p12 whose downstream signaling pathways modulate a wide range of cellular activities, including growth, migration, and survival [20]. It belongs to the HER superfamily, together with ErbB2 (HER2, *neu* in rodents), ErbB3 (HER3) and ErbB4 (HER4). These receptors are structurally related single chain transmembrane glycoproteins, consisting of an extracellular ligand-binding ectodomain, a transmembrane domain, a short juxtamembrane section, a tyrosine kinase domain and a tyrosine-containing C-terminal tail. Binding of soluble ligand to the ectodomain of the receptor promotes homo- and heterodimer formation between receptors, that activate the intracellular tyrosine kinase

domain and the phosphorylation of the C-terminal tail [21]. Phosphotyrosine residues activate, either directly or through adaptor proteins, downstream components of signaling pathways including Ras/Raf/Mitogen Activated Protein Kinase (MAPK), Phospholipase C (PLCγ1), Phosphoinositide 3-kinase/Protein kinase B (PI(3)kinase/Akt), and Signal Transducer and Activator of Transcription (STAT) pathways [22].

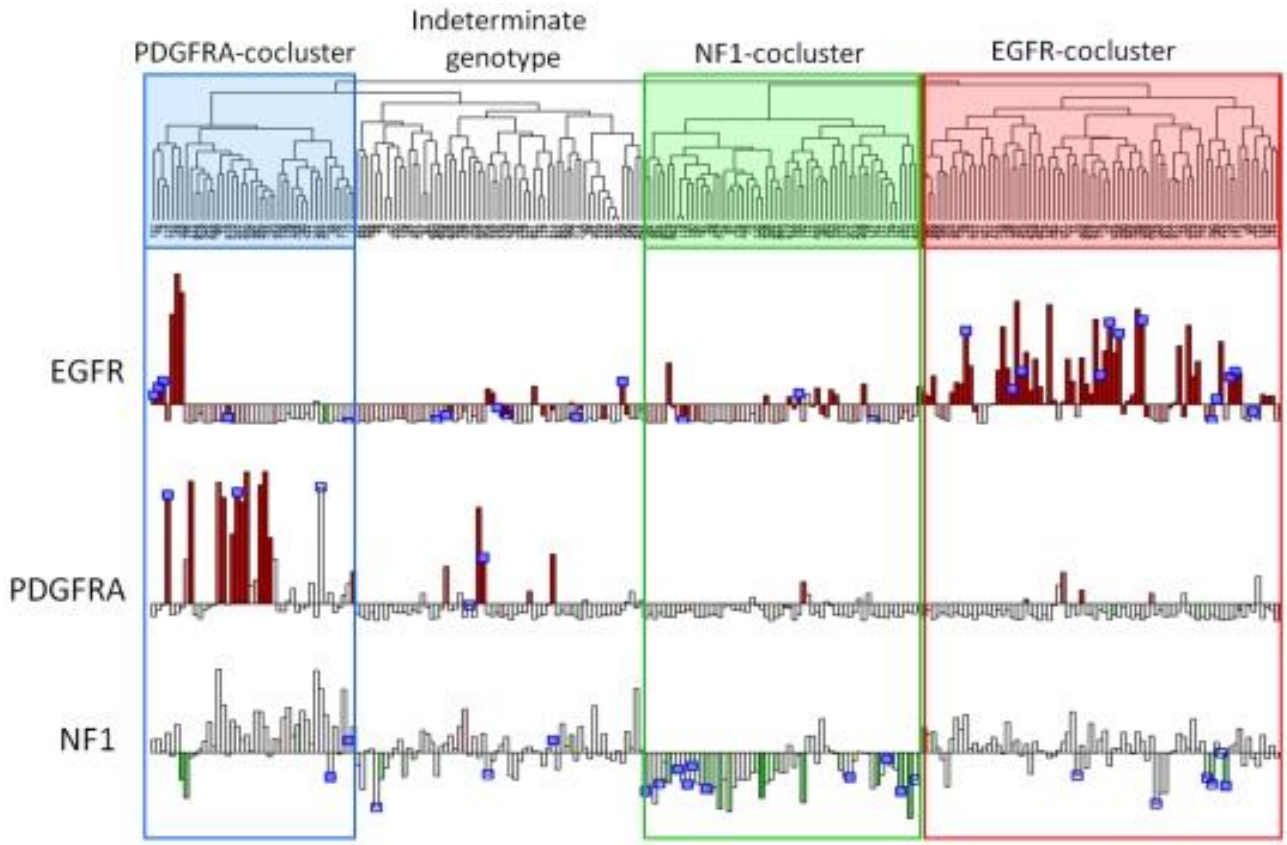

Figure 4

Unsupervised hierarchical clustering of gene expression from 243 GBM samples in The Cancer Genome Atlas analyzed by Brennan et al. revealed four transcriptomal clusters, three of which are enriched for alterations of PDGFRA, NF1, and EGFR respectively. A fourth cluster lacks clear enrichment for any specific mutation or CNA.

EGFR gene amplification occurred in about 40% of patients with GBM, it is expressed at very low levels in health brain [23]. EGFR amplification is more common in primary as compared to

secondary GBMs [14, 24]. In GBMs, EGFR signaling promotes cell division, tumor invasiveness, and resistance to RT and chemotherapy [25, 26].

Alteration of the EGFR gene, results in over-expression of varied mutations, including the most common mutation, EGFR variant III (EGFRvIII), as well as wild-type EGFR [27, 28]. EGFRvIII is the most common mutation among EGFR amplified GBMs and has been described in 60–70% of these tumors [29, 30], and in 20-30% of all GBMs [31]. EGFRvIII exhibits the deletion of exons 2-7, lacking a portion of the extracellular ligand-binding domain and resulting in a constitutively autophosphorylated receptor [32]. EGFRvIII has not been found in any normal tissue [33], and its over-expression was found to be a strong predictor of poor prognosis in presence of EGFR amplification [34]. Accumulating evidences have implicated EGFR signaling as a pivotal player in the initiation and recurrence of GBMs, identifying it as attractive target for molecular therapy [35].

The most common ligands for HER2 receptors are the transforming growth factor alpha and those belonging to the epidermal growth factor family. Interestingly, there are not known ligands for HER2, which is believed to undergo ligand-independent activation [36]. HER2 is expressed in a fraction of gliomas, variably from 15 to 80% depending on the technology employed for receptor detection [37-39], whereas it is not expressed in adult NCS in healthy conditions [40]. IN GBMs, HER2 expression increases with the level of anaplasia and has been associated with poor survival [38, 41, 42].

Platelet-derived Growth Factors (PDGF) constitute a family of six subunits assembled into heterodimer and homodimer ligands and tyrosine kinase receptors, which are enrolled in physiological embryogenesis, hematopoiesis, neuroprotection and glial cell development besides of being identified as part of the GBM molecular panel. Overexpression/hyperactivity of

PDGF ligands and receptors are frequent events in human gliomas of all grades [43-45], and their expression pattern in tumors suggests the presence of autocrine and paracrine stimulatory loops [46]. Amplification of PDGF and PDGFR genes is not as common as the amplification of EGFR [47] and occurs only in 11% of GBs.

Retinoblastoma (RB) and TP53 pathways, which regulate the cell cycle mainly at the level of the G1/S checkpoint, are main targets of inactivating mutations in GBM.

Aberration in Cyclin Dependent Kinase Inhibitor 2A (CDKN2A), p16-Cyclin Dependent Kinase 4 ($p16^{INK4A}$) and 6-RB pathway are common in GBMs and are reported to be critical in gliomagenesis (Ichimura et al, 1996). P16 is able to bind CDK4, preventing its association with cyclin D. CDK4 and cyclin D form a complex which, among others, is able to phosphorylation of critical substrates necessary for G1/S phase transition. P16 subtracts CDK4 by this association, inhibiting cell progression. The TGCA project showed that this pathway is altered in about 80% of primary GBMs. Nevertheless, several studies showed that the alteration of this pathway is not sufficient to induce cellular transformation, suggesting that other cell cycle regulation pathways integrate its activities in avoiding gliomagenesis [48].

TP53 is a well-known tumor suppressor gene that has been widely studied over these past decades in many cancers. The gene encodes a 393-amino acid tumor suppressor protein (p53), that is involved in cell cycle regulation and prevents the proliferation of genetically damaged cells. Mutation of the TP53 gene has been found in 60% to 70% of secondary GBMs, 25% to 30% of primary GBMs and occurs more frequently in younger patients [14]. Besides, p53 activation is regulated p14ARF, an alternate reading frame protein product of the CDKN2A locus, that neutralizes mouse double minute 2 MDM2 protein. MDM2 is an E3 ubiquitin ligase responsible for the ubiquitination and degradation of p53. Loss of p14ARF expression was often observed

in GBMs, and it correlates with homozygous deletion or promoter hypermethylation of p14ARF locus.

NF1 is a tumor suppressor gene encoding a negative regulator of Ras and mammalian target of rapamycin (mTOR) signaling in astrocytes. Genetic alterations of NF1 such as deletions and inactivating mutations were observed in GBMs. NF1 loss results in increased cells proliferation and migration, due to Ras mediated hyperactivation of mTOR.

Finally, approximately 70% to 80% of secondary GBMs have somatic mutation in the isocitrate dehydrogenase 1 (IDH1) gene, which are absent in primary GBMs [49]. Mutations in IDH1 associated with GBMs map to the highly conserved residue R132 in the enzyme active site. Somatic mutations in the corresponding codon (codon R172) of the IDH2 gene was observed in a minor extent of GBMs. Five genes encode for three human IDH catalytic isozymes: IDH1, IDH2, and IDH3. The IDH1 and IDH2 proteins act in the cytosol and mitochondria, respectively, generating reduced nicotinamide adenine dinucleotide phosphate (NADPH) from NADP+ by catalyzing the oxidative decarboxylation of isocitrate to alpha-ketoglutarate outside of the Kreb cycle [50]. IDH mutations seem to be early events in gliomagenesis, followed by acquisition of *TP53* mutations [13].

Glioblastoma prognosis and current therapies

Due to its fast and infiltrative pattern, the outcome for patients with GBM is poor, with a median survival period of less than 15 months. Only a few patients reaching long-term survival status of 2.5 years and less than 5% of patients survive 5 years post diagnosis [51], despite aggressive multimodality therapy.

GBM has a poor prognosis with quite low relative survival estimates [2, 52]. The relative survival for the first year after diagnosis is 35% and it falls in the second year post diagnosis (13.7%) and thereafter [2, 53]} (Figure 5). A population based study found that the first quarter of the second year post-diagnosis is considered to be the peak incidence of mortality and the risk of death decreases to half of its rate at 2.5 years [52]. Patients surviving past 2 years from diagnosis have a relatively favorable conditional probability of survival into the future compared to newly diagnosed patients [54, 55].

One of the causes leading to low survival of patients is cancer own localization. The brain is an organ extremely delicate, which undergoes important damage by only pressure from tumor mass. Moreover, tumor is poorly accessible, so tumor is difficult to remove by surgery.

Advances in imaging, neuronavigation and fluoroscopic guidance have increased diagnostic accuracy, improved safety and decreased deficits associated with surgery, allowing for extent of tumor resection, with more accurate surgical margins [56]. However, about 90% of GBM patients develop tumor recurrence following resection.

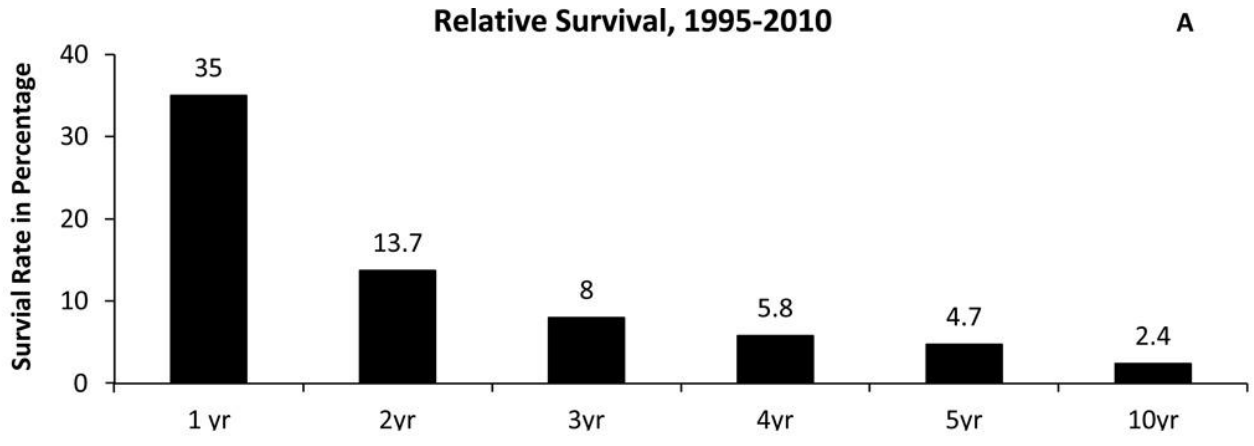

Figure 5

Relative Survival Rates for Glioblastoma, estimated by CBTRUS using SEER Program, 1995–2010 [53].

GBM is also isolated by most of macromolecules and hydrophilic molecules, due to the blood brain barrier (BBB), hindering the use of many classes of drugs including much of the biological ones.

Despite the knowledge about the molecular nature of gliomas has increased extremely in recent years and we are able to separate them into many different subtypes, the current clinical therapy is rather backward: the most common treatment is the removal of the tumor mass, when it is possible, and the subsequent treatment with radiotherapy and chemotherapy using temozolomide (TMZ [57]). TMZ is an alkylating agent with not specific targeting of tumor cells. It is toxic for all the cells in active replication. The main advantage of TMZ is its ability to cross the blood brain barrier. The effect of TMZ is significant, albeit mild: as regards GBMs, temozolomide combined with radiotherapy increases the survival median of 2.5 months with respect to alone radiotherapy, extending life expectancy from 12 months to 14.5 [57].

An advantage acquired by the molecular analysis of GBMs was obtained by studying the correlation between the presence of mutation in the O6-methylguanine-DNA methyltransferase (MGMT) gene and the response to TMZ. MGMT is involved in DNA repair of O06-alkylating agents, such as TMZ. The MGMT promoter is methylated in approximately 50% of newly diagnosed glioblastomas overall and more commonly in secondary glioblastoma [58]. MGMT promoter methylation has prognostic and predictive significance in patients with GBM, with longer survival rates in newly diagnosed patients treated with radiotherapy and subsequent adjuvant temozolomide [59].

Although the introduction of anti-angiogenic therapies, with bevacizumab being the lead drug in class, initially appeared to be a striking approach, successive clinical trial experience has been

disappointing. Bevacizumab is a humanized monoclonal antibody directed against Vascular endothelial growth factor (VEGF). Initial studies for recurrent GBM demonstrated that treatment with bevacizumab was associated with higher response rates, clinical improvement, and longer time to progression than historical controls employing chemotherapy [60]. Two randomized prospective trials in which bevacizumab was used in combination with the standard chemo-radiation followed by adjuvant TMZ failed in demonstrating a benefit in overall survival for the bevacizumab arm [61, 62]. Phase 2 trials evaluating bevacizumab in combination with cytotoxic chemotherapies then failed to demonstrate an advantage in overall survival with the combination therapy, compared to bevacizumab alone [63]. Currently, outside of clinical trials, the role of bevacizumab in the treatment of GBM is in treating patients with neurologic symptoms and signs related to the size of the tumor or the surrounding edema. This benchmark for overall survival with bevacizumab is only eight to nine months [60].

Imatinib is a kinase inhibitor od PDGFR, of mast/stem cell growth factor receptor (SCFR) and of the oncogene fusion protein breakpoint cluster region/Abelson gene (BCR/ABL). Imatinib monotherapy against malignant glioma seems to have only minimal activity. In a phase II study in recurrent BGM with patients stratified by their PDGFR expression, a 6-months progression free survival rate of only 3% of patients was reported [64]. Several other multicenter trials failed to show efficacy of imatinib in GBM treatment [65].

These single agent tyrosine kinase inhibitors for recurrent GBM, as imatinib or bevacizumab, have proved to be insufficient to induce significant inhibition and, although efficient, they are not able to reach their target in a sufficient concentration, due to intratumoral pressure o efflux pumps and BBB obstruction. More, the inhibition developed by these agents is overtaken by the

activation of downstream pathways. Nevertheless, ongoing trials are applying insights into mechanisms of resistance and better understanding of driver mutations.

Translational clinical trial approaches for recurrent and newly diagnosed GBM include other molecular targeted therapeutics, immunotherapies, and somatic gene therapy [66].

Monoclonal antibodies directed towards EGFR and EGFRvIII have been developed as therapy against GBM. The most used is the unconjugated antibody cetuximab, which works preventing signal transduction mediated by EGFR, interfering with ligand binding end receptor extracellular dimerization [67]. The observed effects of EGFR inhibitors in the treatment of patients with GBM are generally weak. Better results could possibly be achieved by stratification of patients by presence of overexpression or specific mutations of EGFR in their tumor tissue [68]. For example, while cetuximab alone has limited clinical efficacy among GBM therapies, data suggest that it may be more promising agent for patients harboring specific EGFR mutations [69].

After a generation of persistent investigation by immunologists in the face of multiple negative trials, discoveries elucidating the mechanisms of tumor-induced immunosuppression in the tumor microenvironment have been translated into the clinic [70]. The first immunomodulatory drug trials in solid tumors have focused on the immunosuppressive signals Programmed cell death protein 1 (PD1), Programmed death-ligand 1 (PDL-1), Cytotoxic T-Lymphocyte Antigen 4 (CTLA4) and indoleamine 2,3-dioxygenase (IDO). PD-1 inhibitors and CTLA-4 inhibitors have been FDA approved for melanoma and non-small-cell lung cancer trials. Nivolumab, pembrolizumab, and ipilimumab are humanized monoclonal antibodies with molecular weight and lipid/water solubility characteristics that likely limit penetration into the tumor microenvironment, especially in regions neighboring tumor mass where the blood–brain barrier is almost intact. Targeting PD-1 may not require intratumoral drug delivery, since PD-1 is expressed on T cells

rather than tumor cells. Ongoing trials of these checkpoint inhibitors in recurrent GBM have reported encouraging preliminary data [71-73]. However, in a clinical trial, nivolumab did not meet the primary endpoint for overall survival compared to bevacizumab alone. Trials of checkpoint inhibitors, single drugs and combinations, are currently under phase I trial for newly diagnosed GBMs.

Antitumor vaccines have been developed with the aim to eradicating tumor cells while limiting toxicity. Numerous studies of vaccines for recurrent and newly diagnosed GBMs have been recently completed or are ongoing. Current vaccine strategies include different combination of autologous vaccines generated from the patient's tumor at resection, peptide-based vaccines, and a new generation of vaccines using dendritic cells exposed to tumor cell RNA [74, 75].

Definitely, additional investigations aimed to better define the clinical and biologic subtypes of glioblastoma and an improved disease control are necessary to identify new biomarkers and potential therapeutic targets.

Oncolytic virotherapy

Oncolytic virotherapy is a promising new therapeutic approach for cancer treatment. Oncolytic virotherapy uses the virus itself as an active drug reagent, employing viruses with a genetically engineered or a natural ability to selectively replicate in and kill tumor cells avoiding the healthy tissues. In the last three decades, advances in understanding of tumor biology and virology have increased the possibilities and the interest in using oncolytic viruses for cancer therapy (Figure 6),

Replication-competent oncolytic viruses have the striking capacity to induce tumor lysis through the release of viral progeny, which can subsequently infect nearby tumor cells. Among

replication-competent oncolytic viruses, Herpes Simplex Virus-1 (HSV-1) is perhaps the best studied and one of the most promising for cancer therapy. It is a double-stranded DNA virus, natural pathogen of humans that can cause serious, and on rare occasions, lethal disease, such as encephalitis in the brain [76]. HSV-1 has a large (>150 kb), fully sequenced and well characterized genome, with multiple nonessential genes amenable for genetic engineering and making it attractive for cancer therapy. HSV-1 does not integrate in the host genome, and is actually cytotoxic, killing cells through varied mechanisms at low multiplicities of infection. Moreover, effective antiviral drugs, such as acyclovir of ganciclovir, are available to treat unexpected replications, improving the safety profile of the virus when used in clinical trials [77].

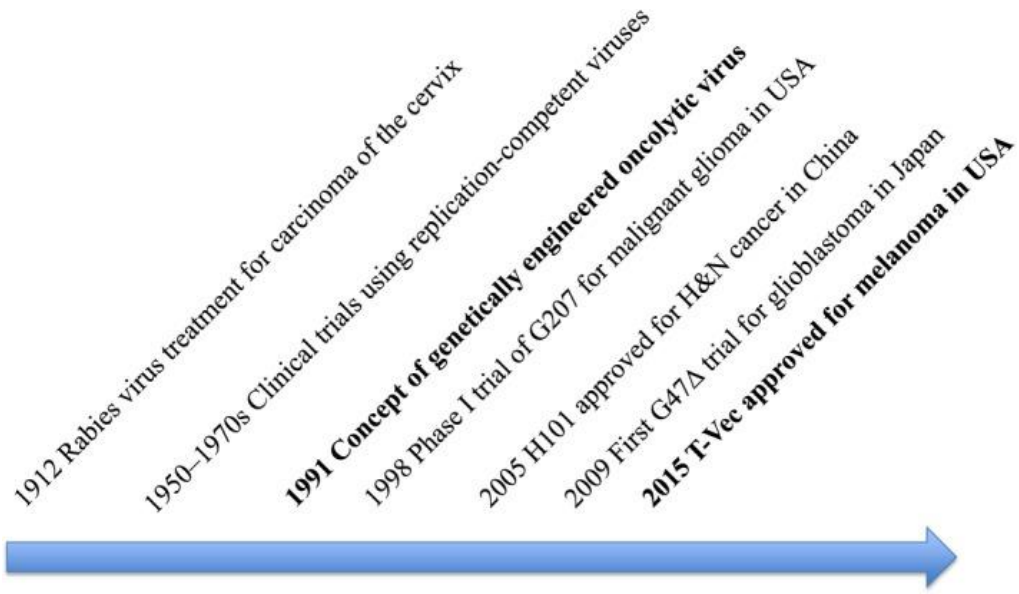

Figure 6

Breakthroughs in oncolytic virotherapy development [78].

The first generations of genetically engineered oncolytic HSV-1 (oHSV) for the treatment of high grade glioma have been developed by using engineering strategies to reduce neurotoxicity while retaining the ability to infect and lyse actively dividing tumor cells. These attenuating mutations involve deletion of both copies of γ134.5 an essential gene for neurovirulence, or

disruption of UL39, encoding the large subunit of ribonucleotide reductase, which is essential for DNA replication in postmitotic cells such as the neuron [77].

Three oHSVs (G207, 1716 and G47Δ) have entered clinical trials for GBM; all contain deletions of both copies of the γ34.5 gene, as well as an inhibitor of interferon-induced host protein synthesis shut-off [79]. Following encouraging results of murine and nonhuman primate studies [80-82], 3 early-phase trials have been completed using G207 alone or in combination with radiation [83-85]. In parallel, HSV1716 has been evaluated by a group in the UK [86]. A further HSV was built from G207 by the deletion of the α47 gene [87], enhancing major histocompatibility complex class I presentation and viral replication. The results of a phase I/II Japanese study in recurrent and progressive GBM (JPRN-UMIN000002661) are pending.

Oncolytic herpes simplex virus (oHSV) has been shown to be safe when administered intratumorally to glioblastoma patients. However, studies on virus deleted in γ34.5 gene showed that the lack of response to the virus in some tumors was subsequently ascribed to tumor heterogeneity in Protein Kinase R (PKR) activation, as a function of MEK (MAP/ERK kinase) levels. A low MEK activity, typical of normal cells, leads to high PKR activity thus preventing replication and oncolytic activity of the HSV deleted in γ34.5 gene. In xenografts, a virus deleted in γ34.5 gene infected, selectively replicated, and inhibited tumor growth in cells with a high MEK activity, either endogenous or after gene transduction, but the virus was rapidly lost when tumor cells expressed a dominant negative form of MEK and this occurred even following intratumoral administration. Accordingly, the heterogeneity of MEK status poses a serious limitation to strategies based on viruses deleted in γ34.5 gene and various alternative approach have been developed to restore late viral protein synthesis [88].

A third advance in the oncolytic virotherapy with oHSVs has been the employment of viruses that express foreign genes to enhance the antitumor immune response. Genetically engineered, attenuated HSV expressing trans-genes coding for cytokines have been shown to provide a survival benefit in murine brain tumor models via combination of oncolytic effects and immunologic effects mediated by T cells [89]. A phase I clinical trial is currently enrolling at the University of Alabama Birmingham (NCT02062827) evaluating the safety of M032, a second generation oHSV conditionally replicative by the deletion of both γ134.5 gene copies and armed with an expression cassette encoding human IL-12.

oHSV	Parental strain	Mutated/deleted HSV genes	Transgenes/inserted genes	In clinical use
1716	17+	*γ34.5*	N	Y
R3616	F	*γ34.5*	N	N
C134	F	*γ34.5*	HCMV *IRS1*	N
hrR3	KOS	*ICP6*	*LacZ*	N
R7041	F	*US3*	N	N
G207	F	*γ34.5* and *ICP6*	*LacZ*	Y
MGH1	F	*γ34.5* and *ICP6*	*LacZ*	N
3616UB	F	*γ34.5* and *UNG*	*LacZ*	N
DM33	McKrae	*γ34.5* and *LAT*	*GFP*	N
rHsvQ1	F	*γ34.5* and *ICP6*	*GFP*	N
Δ68H-6	17+	*γ34.5* (BBD) and *ICP6*	*LacZ*	N
rQnestin34.5	F	Endogenous *γ34.5* , *ICP6*	Nestin promoter-driven *γ34.5*, *G*	N
KeM34.5	F	Endogenous *γ34.5* , *ICP6*	Musashi promoter-driven *γ34.5*	N
G47Δ	F	*γ34.5* , *ICP6* , *α47*	*LacZ*	Y
MG18L	F	*US3* and *ICP6*	*LacZ*	N
R-LM113	F	*gD*	*scFv* anti-HER2	N

HCMV: Human cytomegalovirus; HSV: Herpes simplex virus; oHSV: Oncolytic herpes simplex virus; N: No; Y: Yes.

Table 1

Oncolytic herpes simplex viruses used for brain tumor therapy [90].

Other different strategies were employed to engineer oHSVs, and viruses used in preclinical brain tumor models (Table 1). To gain tumor specificity preserving the full lytic ability typical of wild-type oHSVs, a retargeting approach to specific receptors was employed. The safety of

attenuated viruses is achieved at the expense of potency. These viruses are characterized by much lower replication and killing capacity than wild-type viruses, as well as non-stringent specificity of entry into tumor cells. To overcome these limits, the virus tropism can be modified and the viruses can be detargeted from their natural receptors and retargeted to receptors specifically overexpressed in tumor cells.

The glycoprotein gD mediates the binding of wild-type HSV-1 and the two entry receptor Nectin-1 and HVEM, present on the surface of cells (herpesvirus entry mediator) and triggers the virion-to-cell fusion [91]. The basis for tropism retargeting is the genetic engineering of recombinants oHSV in which gD is fused to a heterologous ligand able to interact with the tumor-specific receptor. In the first series of experiments, the targeted tumor-specific receptor was IL-13Rα2, expressed in malignant gliomas [92]. Another receptor of interest is uPAR, targeted with two different strategy in R5181 and R5182 recombinant virus [93]. A further receptor indicated for tropism retargeting is HER2, since it is expressed in a large fraction of HGGs [37-39]. HER2 is an orphan receptor, without available natural ligand. The selected ligand for the retargeting toward HER2 of an oHSV, named R-LM113, was a single-chain antibody. The glycoprotein gD tolerated the scFv insertion and could mediate virus entry into cells expressing HER2. For detargeting the HVEM tropism was readily abolished by deletion of the most N-terminal region and overall access through the Nectin-1 binding site was simply hindered by the large insert [94]. Several oHSVs entered clinical trial in the past decades, but now the rationale in cancer therapy is that no single drug or treatment will cure definitively cancer, hence research is rather moving towards combination therapies [95], and it is realistic to consider combining oncolytic virotherapy with current or novel therapies, which by themselves often fail.

EGFRvIII and PDGF driven Glioma mouse models: genomic characterization and comparison

The research on gliomas, as well as oncological research in general, requires the establishment of reliable disease models, making possible to study its biology and to find new effective therapies. Glioma models can result from subcutaneous or orthopedic grafts of tumor cells derived from patients in immunodeficient mice, or can be induced directly into the animal by unspecific carcinogens (alkylating agents, radiations) or by cell type-specific modulation of the expression of oncogenes or oncosuppressor genes. During the last years, syngeneic modeling increased in complexity. Modeling gliomas with well-defined genetic summarizes the biological mechanisms in human tumors and may validate the causes of genetic disorders occurring in gliomagenesis [96].

Over the years, several mouse high grade glioma models have been developed based on human genetic alteration, with the hypothesis that genetic aberrations responsible for gliomagenesis play an important role in tumor maintenance too. By modeling cancer with defined genetics, it is thus possible to identify causative mutations and relationships between them.

Among them, EGFR gene amplification and overexpression are a striking feature of in high grade glioma. Enhanced activation of EGFR can occur through a variety of different mechanisms, both ligand-dependent and ligand-independent. Numerous evidence has suggested that EGFR is overexpressed in most of primary glioblastomas and some of the secondary glioblastomas and is characteristic of more aggressive glioblastoma phenotypes. Mutations of EGFR occur in roughly one-third of all classical tumors and often in mesenchymal, proneural and neural glioblastomas as well [15].

In murine models, it was provided that transgenic mice overexpressing an active homolog of the EGFR (v-erbB), develop low-grade oligodendogliomas, without requiring a tumor suppressor loss. However, EGFR over-activation induces gliomas only when it is combined with the loss of p53 or the INK4a/ARF locus [97]. When v-erbB overexpression occurs together with loss of Ink4a/Arf or p53, it resulted in a shorter tumor latency and increased tumor grade and penetrance [98].

In a model elaborated by Holland and colleagues, gliomas were induced by transfer of EGFRvIII gene, a cancer specific mutation making the receptor constitutively active, in Ink4a/Arf deficient Gt-a or Ntv-a transgenic mice [99]. They noticed that EGFRvIII induced lesions, occurred in these background and having many similarities to human gliomas, appeared more frequently with gene transfer to Ntv-a mice than to Gtv-a mice, suggesting that, since in this context tumors arise more efficiently from immature cells in the glial lineage, glial progenitors may be generally more prone to malignant transformation.

However, it was reported that the transduction of Ink4a/ARF -/- astrocytes with EGFRvIll induced high-grade gliomas too [100], identifying astrocytes as permissive compartments for gliomagenesis, similarly to progenitors of Ntv-a mice.

Furthermore, mice derived from a transgenic mouse astrocytoma model established by using the GFAP promoter to express RAS in astrocytes were crossed with a population expressing EGFRvIll under the control of the GFAP promoter. The double transgenic mice developed aggressive oligodendroglial or mixed gliomas, although GFAP-EGFRvIll single transgenic mice did not exhibit tumor growth. This observation indicates that astrocyte-specific expression of EGFRvill alone is not sufficient for gliomagenesis, but contributes to glioma progression in the context of existing predisposing genetic changes [101].

These studies highlight the importance of cell lineage in gliomagenesis together with genetic alteration required for glioma development.

As first demonstrated by Uhrbom and colleagues, in vivo PDGF overexpression in neonatal mouse neural stem cells efficiently induces the formation of gliomas [102-104].

In our laboratory, a murine model of induced gliomagenesis was developed by overexpression of the platelet-derived growth factor B (PDGF-B) in neural progenitor cells. The injection of replication deficient Moloney Murine Leukemia Virus (MMLV) expressing PDGF-B into lateral telencephalic ventricles of mouse embryos at mid neurogenesis led to development of tumors in 100% of mice [105, 106]. Tumors showed the typical features of high-grade gliomas: widespread necrosis, massive neovascularization, hemorrhagic regions and cells often arranged into pseudopalisades around necrotic foci. Noteworthy, despite transducing such a highly heterogeneous progenitor population, able to generate all mature cell types in central nervous system, PDGF-B overexpression led to the formation of pure oligodendrogliomas and, importantly, the homogeneity of the tumors induced by PDGF-B at embryonic stages was defined by its fate specification activity [105].

A different strategy to obtain PDGF-B induced glioma model exploits neural precursor cells (NPCs) explanted at embryonic day 14, namely the same time of in vivo injection, that are transduced in vitro with retroviruses encoding PDGF-B [107]. When transplanted in adult mouse brains, this cells population able to generate tumors resembling human high grade gliomas, in terms of molecular markers expression, histological phenotype and tumorigenic potential and maintaining their tumorigenic features after in vitro culture.

Materials and methods

Animal Procedures

Mice were handled in agreement with the guidelines conforming to current Italian regulations for the protection of animals used for scientific purposes (D.lvo 27/01/1992, no. 116). Procedures were approved by the Ethical Committee for Animal Experimentation of the National Institute of Cancer Research and by the Italian Ministry of Health. The experiments were performed with the BALB/c mouse strain, both wild-type and p16/p19 knock-out.

Anesthetized animals were injected by means of a stereotaxic apparatus. Up to 2 µl of suspension, containing 2e4 cells, were injected using a Hamilton syringe (Bregma coordinates: anterior-posterior, 1.0 mm; lateral, 1.5 mm left and 2.5 mm below the skull surface). Resorbable suture was used before awakening the animals. Animals were monitored daily after transplant, and killed at first sign of neurological distress. Their brains were then explanted and photographed under a Leica fluorescence stereomicroscope (Wetzlar, Germany). Survival curves were determined using Kaplan–Meier survival between groups.

Cell cultures and transfection

mHGG^{pdgf} and mHGG^{egfrvIII} brain tumors expressing DsRed fluorescent reporter were obtained as follows. Embryonic neural precursors were obtained from embryonic day (E14) mouse embryos as described [107]. Cells were plated at a density of 3e5 cells/cm^2 onto Matrigel matrix (1:200; BD Biosciences, Franklin Lakes, NJ) coated 24-well plates in DMEM-F12 added with B27 supplement, human bFGF and EGF (10 ng/ml). Immediately after plating, cells were transduced with pCAG:DsRed-EGFRvIII and pCAG:DsRed-PDGF retroviral vectors already described [108-

110]. After 7 days 2x104 transduced cells were intracranially inoculated in adult BALB/c mice. Tumor cell cultures derived from explanted mHGG^{pdgf} and mHGG^{egfrvIII} brain tumors were maintained in the medium described above.

Immunostainings

For histological analyses, brains were fixed with 4% paraformaldehyde, cryoprotected in 20% sucrose and sectioned with a Leica CM3050 S cryostat. Immunostainings were performed using the following antibodies: mouse monoclonal antibodies against nestin (1:100, BD Pharmingen, San Diego, CA, USA), GFAP (1:100, Sigma-Aldrich, Milano, Italy); rabbit polyclonal antibodies against Olig2 (1:500, Sigma-Aldrich, Milano, Italy), Ng2 (1:200, Chemicon, ThermoFisher Scientific, Waltham, MA, USA) and EGFR (1:500, Santa Cruz Biotechnology, Santa Cruz, CA, USA). Binding of primary antibodies was revealed with appropriate secondary anti-rabbit IgG Dylight 488-conjugated (1:500, Jackson Immunoresearch, Milano, Italy), cy2-conjugate anti-mouse IgG (1:100, Jackson Immunoresearch, Milano, Italy). Nuclei were stained through 10 min incubation in Hoechst 33342 solution (1 µg/ml, Sigma-Aldrich, Milano, Italy).

Microarray and RNA sequencing analyses

RNA extracted from cultured cells from 2 mHGG^{pdgf} and 4 mHGG^{egfrvIII} tumors were hybridized on Affymetrix GeneChip Mouse Genome 430 2.0 Array (GEO Accession Number GSE108955) by AROS Applied Biotechnology (Aarhus,Denmark). Data from transcriptome database for murine astrocytes, neurons, and oligodendrocytes [111] and from data of wide gene expression profile of cells from sub ventricular zone (SVZ, [112]) and murine adult olfactory bulb stem cells [113], performed on the same microarray platform were obtained from literature and analyzed with the same procedures of our samples.

Data were analyzed using the R3.4.2 software and BioConductor version 3.5 35. Expression values were extracted from raw data files using the RMA method built in the affy 1.54.0 library package. Differentially expressed genes were ranked by using RankProd 3.2.0 library. The entire dataset was eventually quantile normalized [114].

For whole-exome sequencing, dissociated cells from 3 mHGG^{pdgf} and 3 mHGG^{egfrvIII} secondary tumors were sorted for DsRed with FACSAria II in Trizol (Invitrogen) directly, where they were harvested in for RNA extraction. at least 0.01 µg RNA derived from three ex-vivo primary tumor sample, sorted by FACS for DsRed reporter and harvested in Trizol, was send to BGI genomics (BGI, Shenzhen, China) and sequenced on BGISEQ-500 RS generating 50 base-pair single-end reads. Data from Glia, Neurons, and Vascular Cells of the Cerebral Cortex transcriptome database present in the literature [115] were obtained as fastq files and analyzed in parallel with our data. The high-quality clean tags were mapped to reference genome (mm10) using STAR [116]. To quantify the gene expression level, RSEM analysis was carried out [117], acquiring expected read count of each gene of each sample, based on the mapping results and used for successive analyses. Normalization, data trimming and differential expression analysis were performed by edgeR [118]. Genes were ranked by their fold enrichment in each cell type of neuronal/glia database and successively confronted with data from mHGG^{pdgf} and mHGG^{egfrvIII} tumors. Raw and processed data are available on GEO Dataset (Accession number GSE109614).

Results

Mice transplanted with mHGG^{pdgf} and mHGG^{egfrvIII} cells developed high grade gliomas.

The mHGG^{pdgf} model was generated by transplanting in adult BALB/c mouse brains 2e5 murine neural progenitor cells explanted at embryonic day 14 (E14) and transduced with a PDGF-B overexpressing retroviral vector as described [119].

To generate the mHGG^{egfrvIII} model, murine neural progenitor cells from p16/p19 knock-out mouse were explanted at embryonic day 14 (E14). Cell obtained were infected in vitro with replication-deficient retroviruses carrying both EGFRvIII and DsRed coding sequences. After ten days, we orthotopically transplanted 2e5 cells in syngeneic adult BALB/c mice. The same procedure was used to overexpress PDGF-B in NPCs derived from p16/p19 knock-out mice too (mHGG^{pdgf}-ko).

Neurological symptoms appeared in all mice (n=17) injected with mHGG^{pdgf} cells between 15 and 169 days after transplant, and in all mice (n=20) injected with mHGG^{egfrvIII} between 27 and 196 days after transplant (Fig. 1a). All mice (n=5) injected with mHGG^{pdgf}-ko cells developed signs of neurological distress within 26 days after transplant. Tumor cells from these tumors were not used in the successive steps of the study.

Mice were killed as soon as they showed the first hint of symptoms. Brains were explanted and showed invariably large DsRed positive tumor masses. Cell derived from microdissectection mHGG^{pdgf} and mHGG^{egfrvIII} tumors were systematic transplanted in adult BALB/c mice (2.5e5 cells/mouse). All mice transplanted with mHGG^{pdgf} cells showed symptoms of neurological distress within 39 days (n=11). Masses of DsRed-positive cells were observed in all the brains from this cohort after explantation. On the contrary, not all mice transplanted with mHGG^{egfrvIII}

(n=37) developed neurological symptoms. Anyhow, all mice were killed within 161 days after transplant and the analysis of explanted brains showed 70% (n=26) of the to be DsRed-positive cells free (Fig. 1b).

HGG obtained from transplant of mHGG^{pdgf} and mHGG^{egfrvIII} cells histologically closely resemble each other and human HGGs. They are characterized by a compact structure and wide necrotic areas. Highly proliferating cells forms pseudopalisades structures around necrotic foci. Immunoistochemical characterization of PDGF-B-driven HGG was provided [105, 120]. Here, immunofluorescence analysis showed that mHGG^{egfrvIII} primary tumors express progenitor/stem cells marker Nestin as well as oligodendroglial maker Olig2, together with EGFR. In contrast, they express low levels of astroglial marker GFAP (Fig. 1c).

Molecular profiling of mHGG^{pdgf} and mHGG^{egfrvIII} cells maintained in culture revealed close similarity between the two models and OPCs.

Cells obtained from both mHGG^{pdgf} and mHGG^{egfrvIII} primary and secondary tumors were maintained in culture in a serum-free medium optimized for the growth and in vitro differentiation of neural stem cells. Primary tumor cells were tested to generate secondary tumors after up to 15 passages in culture (data not showed).

Gene-expression profiling was performed by microarray analysis starting from biological replicates of cells grown in vitro derived from mHGG^{pdgf} (n=2) or mHGG^{egfrvIII} (n=4) different tumors. Differential expression analysis revealed a strong similarity between the two groups. A gene annotation enrichment analysis on BP-GOTERM, based on differentially expressed genes between the two models (identified by RankProduct using as cutoff pfp=0.05) highlighted the functional class of cellular response to interferon-beta, enriched in mHGG^{egfrvIII} (fold change

3.7E1), suggesting that this class of tumor could be more immunogenic than mHGG^{pdgf}, but failed to identify other strong enriched functional clusters.

Therefore, in order to correlate data obtained from our tumors and genome profiling of cells derived from several neural-glial lineages, we took advantage of a transcriptome database for murine astrocytes, neurons, and oligodendrocytes [111] and from data of wide gene expression profile of cells from sub ventricular zone (SVZ, [112]) and murine adult olfactory bulb stem cells [113], performed on the same microarray platform.

We achieved a principal component analysis (PCA) on all samples, based on most differently expressed genes between astrocytes, neurons, oligodendrocytes, SVZ and OB cells. The first two components were able to explain the 65% of the differences between samples. In the PCA representation, mHGG^{pdgf} and mHGG^{egfrvIII} tumor cells appeared to be closest to oligodendrocyte progenitor cells (OPCs). After OPCs, the group most contiguous to our sample was represented by SVZ and OB cells. These classes of cells, however, are farer than HGGs cells from OPCs. We validated mRNA levels observed in several genes mildly differentially expressed in mHGG^{pdgf} and mHGG^{egfrvIII}, by comparing them with murine NPCs (data not shown). This analysis showed that expression profile of NPCs is very close to that of SVZ and OB cells. This suggests that mHGG^{pdgf} and mHGG^{egfrvIII} tumors are more similar to OPCs than wild-type NPCs.

The heat map generated from unsupervised hierarchical gene clustering of samples (taking count of the most differently expressed genes between astrocytes, neurons, oligodendrocytes, SVZ and OB cells) confirmed and highlighted that both mHGG^{pdgf} and mHGG^{egfrvIII} tumor cells clustered together with OPCs. Interestingly, OPCs expression profile was more correlated to that of murine HGG cells than to the profile of adult neural stem cells.

RNA-seq analysis from ex-vivo samples confirmed that our models clustered with OPCs.

Because of murine tumor cells underwent to some passages in culture before being collected for genome-expression analyses, we speculated on if the high similarity revealed between mHGG^{pdgf} and mHGG^{egfrvIII} profiles was due to biases related to culture conditions and did not reflect the real composition of tumor transcriptomes.

Thus, we collected cells from ex-vivo samples of three mHGG^{pdgf} and three mHGG^{egfrvIII} primary tumors to obtained a more realistic genome-wide transcriptional profiling. Brain tumors were dissociated and cancer cells were separated by fluorescence activated cell sorting (FACS), based on the expression of the fluorescent reporter DsRed. RNA from purified cell populations was extracted and RNA-Seq was performed with the BGISEQ-500 RS platform, obtaining 41.3±3.7 million 50bp reads. We decided to analyze our samples by Next Generation Sequencing (NGS) approach due to its higher sensitivity and more extended dynamic range compared to microarray technology [121-123]. A first unsupervised hierarchical clustering of our transcriptome data showed two different clusters belonging to the two classes of tumors. We compared again transcriptome profiling of our murine tumor samples with that of the major cell classes present in the brain, take advantage of transcriptome database present in the literature [115]. Dendrogram and unsupervised hierarchical clustering heat map constructed starting from most differentially expressed genes between the different classes of brain cells confirmed us that both mHGG^{pdgf} and mHGG^{egfrvIII} tumor cells are mostly similar to OPCs. Furthermore, we performed PCA analysis on these samples. The first three components were able to explain the

86% of the differences between samples. PCA analysis showed us a strong closeness between OPCs, mHGG^{pdgf} and mHGG^{egfrvIII} cells.

Conclusions

In recent years, extensive molecular profiling has afforded an increasing understanding of the genomic landscape of high grade gliomas. Whole genome analyses have provided new data on molecular changes in gene expression, copy number, somatic mutations, and epigenetic signatures in high grade gliomas [124, 125]. Based on signature genome-wide gene expression changes, coupled with somatic mutations and copy number changes, high grade gliomas were classified into four subtypes: proneural, mesenchymal, classical, and neural subtypes [15, 125]. In addition to exhibiting characteristic mutational and gene expression profiles, mutations in EGFR are prevalent in the classical subtype, mutations in NF1 in the mesenchymal subtype and alteration of PDGFR-A and IDH1 in the proneural subtype. These subtypes are also found to bear resemblance with gene expression profiles of normal brain cells, with proneural tumours enriched for the oligodendrocyte development signature.

A variety of animal models have been developed that incorporate signature mutations found in human patients. Genetically engineered mouse models are powerful tools in investigating glioma origins and development and also as preclinical models, although most of the existing animal systems mimic just one of the human molecular classes, known as "proneural" [103, 105]. HGGs induced by overexpression of PDGF-B in neural progenitors is a well characterized model, used in many studies worldwide. Here, we generate PDGF-B driven HGG by overexpressing that growth factor in neural precursor cells (NPC) immediately after explant from BALB/c embryos at embryonic day 14, and transplanting them in brain of adult BALB/c mice after ten days from

transduction. Tumors obtained were compared with gliomas generated with the same protocol, but induced by overexpression of EGFRvIII. This receptor alone, however, is not sufficient to induce malignant transformation in NPCs. Therefore, we transduced EGFRvIII in NPCs derived from p16/p19 knock-out BALB/c mice. These cells, when orthotopically transplanted in wild-type BALB/c mice, are able to give rise to tumor resembling human glioblastoma.

Interestingly, the features of PDGF-B and EGFRvIII driven models are highly similar, although the penetrance of secondary $HGG^{egfrvIII}$ is lower. The similarity is very striking when considering data obtained from microarray and the NGS analyses. The resemblance observed between the cells derived by the two models is not due to adaptation to culture condition. It was observed, indeed, both in samples from culture and in samples analyzed immediately after the tumor explant. The comparison between gene expression profiles of our tumors with published datasets from neural cell types shows a strong similarity between oligodendrocyte progenitor cells (OPCs) and $HGG^{egfrvIII}$ tumor cells which maps close to HGG^{pdgf} tumors but further from neural stem cells.

While the similarity between HGG^{pdgf} gliomas and OPCs fits with the role of PDGF-B in oligodendrocyte lineage specification, EFGR is less clearly connected with such cell lineages thus our results suggest a deeper and more general connection between OPC-like phenotype and gliomas.

Figures

Fig 1.1

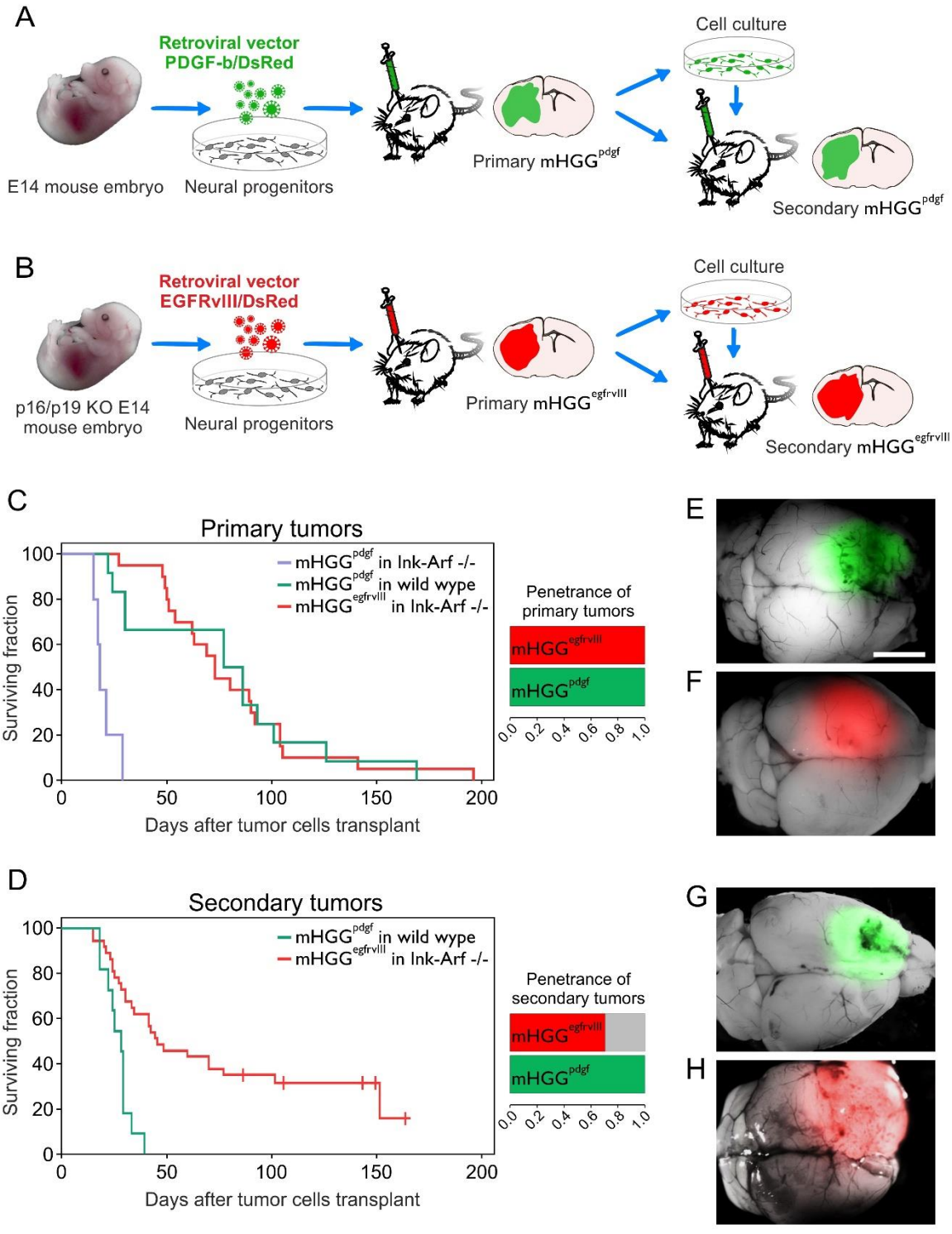

Figure 1.1

(A,B) Experimental design of generation of mHGG^{pdgf}(A) and mHGG^{egfrvIII} (B). (C) Kaplan-Meyer survival curves of mice transplanted with primary mHGG^{pdgf} (green line), mHGG^{pdgf}-ko (purple line) or mHGG^{egfrvIII} (red line) cells. Mice from mHGG^{pdgf} and mHGG^{egfrvIII} arms invariably developed tumors, with similar median survival. Tumors from mHGG^{pdgf}-ko developed tumor masses that lead mice to death much faster. (D) Kaplan-Meyer survival curves of mice transplanted with secondary mHGG^{pdgf} (green line) or mHGG^{egfrvIII} (red line) cells, showing differences in overall penetrance and in median survival. (E-H) Representative dorsal images of brains from mice bearing primary (E,F) or secondary (G,H) tumors after mHGG^{pdgf} (E,G) or mHGG^{egfrvIII} (F,H) cell transplant. In micrographs the DsRed fluorescent reporter expressed by mHGG cells is represented in the red channel for HGG^{egfrvIII} and in green channel for mHGG^{pdgf} tumors.

Fig 1.2

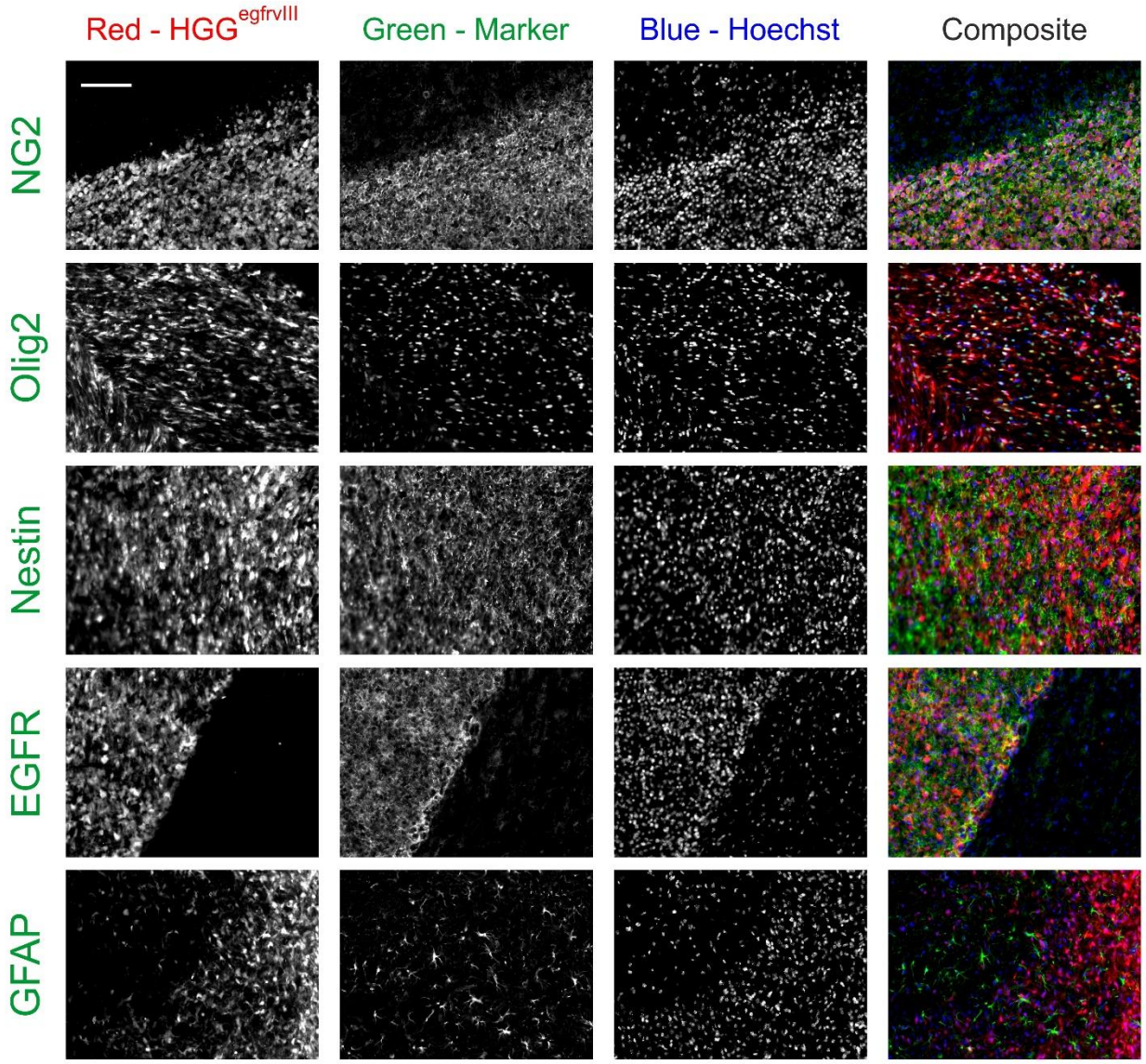

Figure 1.2

Immunofluorescence stainings of brain section of mice that developed mHGG^{egfrvIII} tumors.

High presence of EGFR, stemness marker and OPC marker were observed. On the contrary, mHGG^{egfrvIII} express low levels of GFAP.

Fig. 1.3

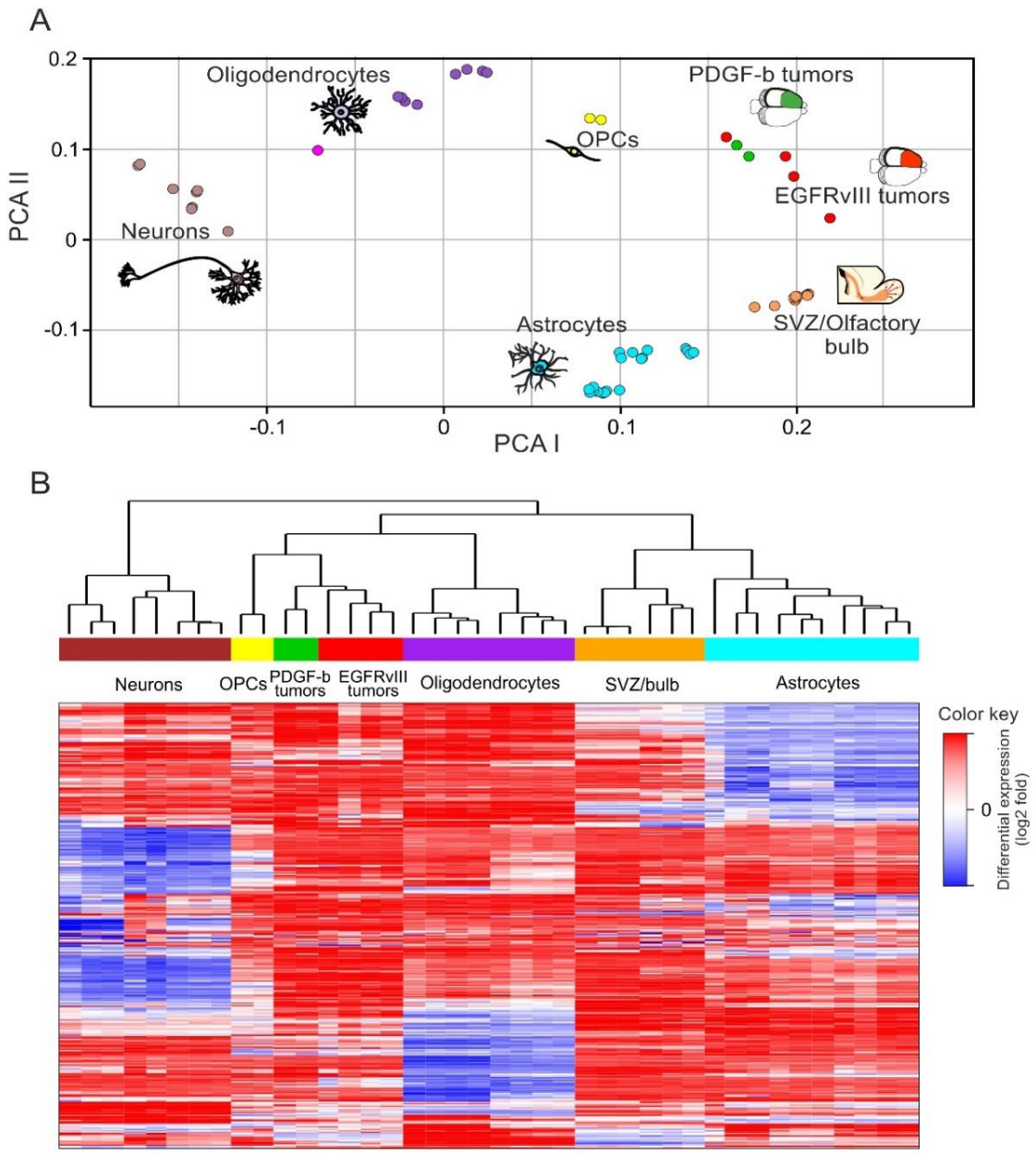

Figure 1.3

(A) Principal component analysis (PCA) plot of the mRNA data that characterizes the trends exhibited by the expression profiles of purified CNS cell types and cultured cells from our mHGGs, showing a strong similarity between oligodendrocyte progenitor cells (OPCs) and HGG^{egfrvIII} tumor cells which maps closer to HGG^{pdgf} tumors than from neural stem cells. (B) Dendrogram, sample clustering and expression of the top type-specific genes (for CNS cells) of purified CNS cell types

and cultured cells of mHGGs. Hierarchical clustering reveals the high similarity between our tumors and the OPCs. Each individual gene expression level was normalized and plotted on a log2 color scale, with blue representing low expression and red representing high expression. Color bar and sample labels describe each individual sample type (brown, neurons; yellow, OPCs; green, mHGG^{pdgf}; red, mHGG^{egfrvIII}; purple, oligodendrocytes; orange, neural stem cells; cyan, astrocytes).

Fig. 1.4

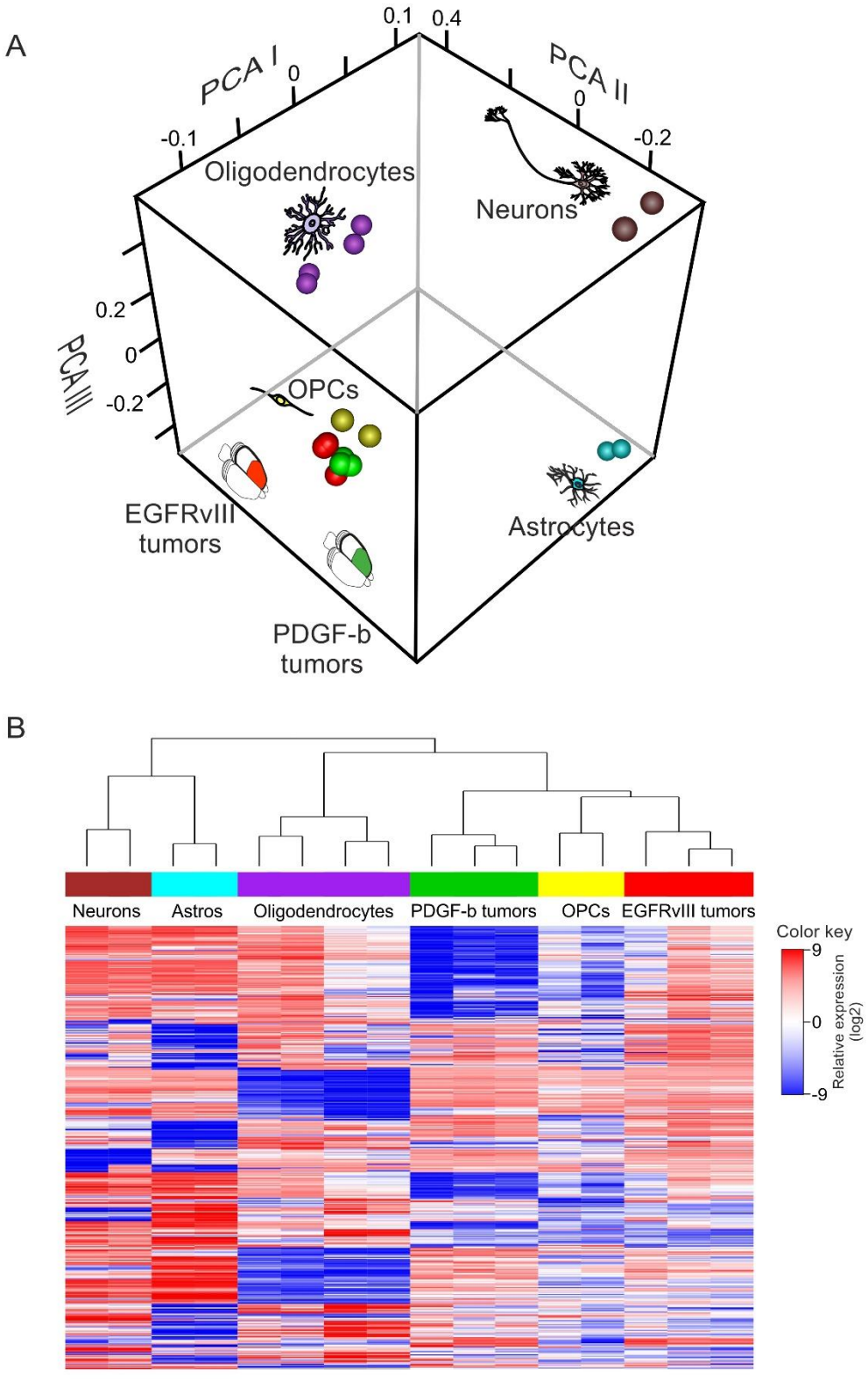

Figure 1.4

(A) 3-D PCA plot of the transcriptome NGS data that characterizes the trends exhibited by the expression profiles of purified CNS cell types and our mHGGs from ex-vivo samples, confirming the extreme similarity between oligodendrocyte progenitor cells (OPCs) and HGG^{egfrvIII} tumor cells. (B) Dendrogram, sample clustering and expression of the top type-specific genes (for CNS cells) of purified CNS cell types and mHGGs from ex-vivo samples, analyzed by RNA-seq. Hierarchical clustering confirms the similarity between our tumors and the OPCs. Each individual gene expression level was normalized and plotted on a log2 color scale, with blue representing low expression and red representing high expression. Color bar and sample labels describe each individual sample type (brown, neurons; cyan, astrocytes; purple, oligodendrocytes; green, mHGG^{pdgf}; yellow, OPCs; red, mHGG^{egfrvIII}).

Noninvasive Monitoring of Glioma Growth in the Mouse

Malignant gliomas are among the hardest challenge of modern oncology. Despite all the efforts of scientific community, only modest improvements have been achieved in the last decades. To break the current deadlock, an important tool is represented by in vivo models of gliomas. To be reliable, these models have to grow orthotopically inside the brain of animals, and this make their development not easy to monitor. The available options to monitor the orthotropic growth of gliomas are NMR [126], microPET [127] and bioluminescence analysis on tumors engineered to express a luciferase [128]. All these methods are generally time consuming, expensive and, most importantly, extremely invasive, requiring risky procedures for anesthesia and substrates administration. This greatly limits the frequency of measurements, preventing a reliable analysis of tumor growth dynamic.

A possible alternative to the aforementioned methods is the employment of reporter proteins secreted in liquid fluids, which can be measured frequently over the time, therefore providing a large amount of data with minimally invasive procedures.

Secreted alkaline phosphatase (SEAP) and Gaussia luciferase (Gluc) are the most used liquid fluid reporters. These enzymes can be exploited for different applications and have been used to monitor several processes, including the growth of tumor masses in inaccessible locations [129-131].

Gluc is one of the smallest luciferase (19.9 kDa), isolated from the copepod *Gaussia princeps*. Unlike the first generation of luciferases, like *Photinus pyralis* luciferase (Fluc) and *Renilla reniformis* luciferase (Rluc), Gluc is naturally secreted by cells. Moreover, Gluc activity does not require ATP and, in vitro, is linear with the number of cells [132]. Gluc has a flashing kinetics and

its activity tends to rapidly decrease when reacting with its substrate celenterazine [133]. This disadvantage is, however, largely compensated by its initial activity per mole, that is about 100 times higher than that of Rluc and 1000 times higher than that of Fluc [134-136]. This makes Gluc an excellent choice as body fluid reporter, since its assay is extremely sensitive, about 20,000-fold higher than that of SEAP [137]. Few microliters of blood taken from the mouse tail tip are sufficient to obtain an accurate measurement, making possible to perform daily assays.

A few studies have already reported the use of Gluc as biomarker to monitor neoplastic cell proliferation in various tumor models including intracranial gliomas [132, 138, 139]. However, the extent of the correlation between Gluc levels in blood and tumor burden has not been thoroughly analysed.

The aim of this work is to test the efficiency of Gluc as a blood reporter system to dynamically estimate the tumor size and to monitor the intracranial growth of gliomas in both immunodeficient and immunocompetent mice.

We found that the assay of Gluc in the blood of immunodeficient mice allows the detection of a tumor graft as early as ten days from transplant, and, in average, 60 days before mice showed the first hint of neurological symptoms. We also observed a good correlation between Gluc activity and tumor size evaluated with morphometric and weight analyses. In immunocompetent mice, however, the use of Gluc is limited by the development of immune response that inhibits Gluc activity, impairing its correlation with tumor size.

Materials and Methods

Animal procedures

Mice were handled in agreement with guidelines conforming to current Italian regulations for the protection of animals used for scientific purposes (D.lvo 27/01/1992, no. 116). Procedures were approved by the Ethical Committee for Animal Experimentation of the IRCCS San Martino-IST and by the Italian Ministry of Health. The experiments were performed on the Nod/Scid and BALB/c mouse strains. Anesthetized animals were injected by way of a stereotaxic apparatus. Up to 5 µl of suspension, containing from $4x10^4$ to 10^5 cells preparations, were injected using a Hamilton syringe (Bregma coordinates: anterio-posterior, 1.0 mm; lateral, 1.5 mm left and 2.5 mm below the skull surface). Resorbable suture was used before awakening the animals. Animals were then monitored daily and killed at first sign of neurological symptoms or, in some instance, before it, as soon as they reached planned levels of Gluc activity. Their brains were then explanted and photographed under a Leica fluorescence stereomicroscope (Wetzlar, Germany).

Gluc assays were carried on twice a week, by collecting about 5 µl of blood from the tail tip of mice in tube containing 0.5M EDTA. Mice sera were obtained by centrifuging at 500 RCF blood samples preincubated without EDTA at 37°C for 30 minutes.

To estimate the volume of the tumors inside the brains, the apparent feret diameters of the tumor were calculated from two pictures taken from the dorsal- (upper feret) and from the ventral- (lower feret) side of the brain. We then approximated the tumor volume to that of a sphere with a diameter equal to the average between the upper and lower feret diameter.

Survival curves were determined using Kaplan–Meier analysis and survival between groups was assayed by log-rank test.

Retroviral Vectors

pCAG:DsRed-EGFRvIII and pCAG:DsRed retroviral vectors were previously described [108].

pCAG:mGFP-Gluc vector was obtained as follows. The coding sequence of Gaussia luciferase from the pCMV-GLuc 2 Control Plasmid (New England BioLabs, Hitchin, UK) was cloned into the pCAG:GFP vector (kindly provided by Dr. M. Goetz) upstream the IRES-GFP region. GFP sequence was replaced with a mutated, non-fluorescent, GFP (mGFP) that is detectable by immunostaining techniques. mGFP was obtained by substitution of three nucleotides inducing the mutations T66A and Y67A by PCR.

Cell cultures and Transduction Procedures

Human glioma initiating cells (hGIC) L0306, kindly provided by Dr. R. Galli [140], were engineered with pCAG:DsRed and oCAG:mGFP-Gluc and maintained as spheres in Neurocult Medium supplemented with NeuroCult NS-A (StemCell Technologies, Vancouver, British Columbia, CA), human recombinant fibroblast growth factor 2 (10 ng/ml; PeproTech, Rocky Hill, USA), epidermal growth factor (20 ng/ml; PeproTech, Rocky Hill, USA) and Heparin (2µg/ml, Sigma-Aldrich, Milano, Italy).

mHGG^{egfrvIII}-7 cells were obtained from INK4a/ARF knock-out BALB/c mice intracranially injected with syngeneic neural progenitor cells transduced with pCAG:DsRed-EGFRvIII as previously described [107]. Cells were maintained in Dulbecco's modified Eagle's medium-F12 (Invitrogen, Carlsbad,CA) with B27 supplement (Invitrogen, Carlsbad,CA), human basic fibroblast growth factor (10 ng/ml, Peprotech, London, UK) and epidermal growth factor (10 ng/ml, Peprotech,

London, UK) and plated on Matrigel (1:200; BD Biosciences, Franklin Lakes, NJ). Cultures from tumors were established microdissecting DsRed-positive areas under a fluorescence microscope and trypsinizing them for 20 minutes. Cells were maintained in the medium described above.

Gaussia luciferase assay

Gluc activity was evaluated in a reaction set up obtained by combining 5µl of blood sample with a buffer constituted by 17.5 µl of Stop & Glo® Buffer (Promega, Milano, IT) supplemented with coelentherazine , and 17.5 µl of a buffer containing HEPES 75mM; DTT 20 mM, EDTA 100 µM, pH 8.0. The luminometer (Promega Glomax 20/20n) was set to acquire a series of 40 consecutive measures with an integration time of 1 second. Data analysis was performed in R environment 3.4.2 [118] with software built in house.

Results

Gluc expression does not alter cell proliferation rate and tumor latency of different glioma models

To be employed as tool for monitor glioma growth, a reporter gene should not induce alterations on cell behavior. A recent report addressed specifically this point on a model of glioma expressing firefly luciferase [141] showing not gross alteration on cell proliferation and *in vivo* growth. To assess whether also Gluc expression does not perturb glioma cells, we compared the doubling time of the human glioma initiating cells L0306, with that of L0306 transduced with pCAG:mGFP-Gluc construct expressing Gluc (L0306-Gluc). This analysis showed

that Gluc does not grossly alter glioma proliferation rate, since the doubling time of L0306 was 3.8±1.3 days before transduction and 3.1±0.6 days after transduction.

Most significantly, the median survival time of Nod/Scid mice following intracranic transplantation of L0306-Gluc (81 days, Figure 2.1A) did not significantly differed from that of mice transplanted with non-transduced L0306 cells (78 days). Similar results were obtained with one population from the mouse glioma model induced by EGFRvIII overexpression (mHGG^{egfrvIII}-7), as previously described, where the median survival time was 42 days for Gluc-transduced- (Figure 2.1A) and 41 days for untransduced-mHGG^{egfrvIII}-7 cells.

Correlation between glioma growth and Gluc activity

To evaluate the reliability of Gluc quantification as a method to monitor the growth of intracranic gliomas in mice, 10^5 L0306-Gluc cells were orthotopically transplanted in 18 Nod/Scid mice. Starting from two days after transplant, 5 µl of blood were collected twice a week from the tail tip and assayed for Gluc activity.

Since Gluc has a flashing kinetics, its activity (herein referred as [Gluc]) under substrate excess conditions changes rapidly during time. An analysis of our experimental data showed that [Gluc], which value is proportional to the luminescence, decreases over time following the relation:

$$[Gluc](\mathrm{t}) = \{[Gluc]_{T0}^{(1-\alpha)} + (\alpha - 1)\ k\ \ t\}^{\frac{1}{1-\alpha}}$$

To standardize the way of measuring [Gluc] in all blood samples, a series of measurements of luminescence over time was recorded for each sample and used to extrapolate by linear regression from the former relationship the starting activity of Gluc ($[Gluc]_{To}$; Figure 2.1B). This method allows fully exploiting the initial activity of the enzyme, thus making the assay very

sensitive compared to methods relying on stabilization of the luciferase activity, which lowers it of one or more order of magnitude.

In 40% of the mice, the level of Gluc activity crossed the detection threshold already at the first experimental point, and the levels became detectable in all mice within 43 days after transplant. By plotting $[Gluc]_{T0}$ values versus time after transplant, we obtained exponential curves (Figure 2A), suggesting that the tumors were expanding at an exponential rate, with a doubling time of 113±19 hours.

To measure the correlation between $[Gluc]_{T0}$ and tumors burden, mice were killed when showing different levels of $[Gluc]_{T0}$. Brains were photographed under an epifluorescence stereomicroscope that allows the visualization of the tumor mass thanks to the DsRed reporter gene expressed by L0306-Gluc cells. A morphometric analysis was then performed to estimate the volume of the tumors. Additionally, tumors were microdissected and weighted. These two independent measurements were combined to obtain an estimated tumor burden and to analyse its correlation with $[Gluc]_{T0}$. This analysis showed that tumor burden is linearly related to $[Gluc]_{T0}$ and the regression has a R^2 of 0.79 (Figure 2.2B) independently from the localizations of the tumor that varied from mostly dorsal- to mostly ventral-localization and even partly extraencephalic (Figure 2.2B). This suggests that the localization of the tumor has a minor impact on the level of Gluc activity found in the blood. It should be noticed that the estimation of tumor burden is invariably affected by an error due to the variable tumor cell density inside the tumor masses. This may explain why the trend line of the logarithm of $[Gluc]_{T0}$ over the time in each animal shows a better correlation coefficient (R^2=0.97±0.03; Figure 2.2A) than that between $[Gluc]_{T0}$ and the estimated tumor burden in different animals.

Similar results were obtained using a different line of hGIC transplanted in NOD/Scid mice.

Gluc activity assay in immunocompetent mice

We then tested the suitability of Gluc assay in immunocompetent mice, by using the murine glioblastoma stem cells mHGG^{egfrvIII}-7, induced by the overexpression of EGFRvIII and the DsRed reporter gene in p16/p19 knock-out neural progenitor cells and orthotopically transplanted in syngeneic adult BALB/c mice. Such a model is more aggressive than the L0306 in Nod/Scid mice, and the median survival time of transplanted animals is about 41 days. In contrast to the L0306 transplants, not all the mHGG^{egfrvIII}-7 transplants resulted in the development of a glioma and the overall penetrance was about 75%.

We therefore transplanted a pool of 24 mice with $4x10^4$ mHGG^{egfrvIII}-7 cells engineered to express Gluc (mHGG^{egfrvIII}-7-Gluc). During the first 4 weeks from transplant, 9 animals showed growing levels of $[Gluc]_{To}$, consistent with a doubling time of the tumor mass of 51±20 hours, which reflected the higher aggressivity of the model. Thanks to the very dense series of measurements, in five additional animals we had the possibility to observe irregular patterns of Gluc levels, which underwent to a sudden decrease following a previous phase of growth. The remaining mice did not show any detectable level of Gluc (Figure 2.3A). From day 27, mice displaying higher Gluc levels started to develop neurological symptoms and were therefore killed. Mice were found to harbor large gliomas expressing DsRed reporter gene (Figure 2.4A). Unexpectedly, however, from day 36 some animals with low levels of $[Gluc]_{To}$ also started to display neurological symptoms. Four of them belonged to the group of animals with irregular pattern of Gluc activity, two showed a slight increase of $[Gluc]_{To}$ just before developing symptoms, and other two never showed any detectable level of Gluc. When analyzed, all these animals showed DsRed-expressing tumor masses similar in size to those found in the animals

displaying high-level of $[Gluc]_{To}$ (Figure 2.4B). Since this phenomenon was only seen in immunocompetent animals, we speculated that an immune response of the host occurred, selectively depleting the Gluc expressing population from the tumors. To test this hypothesis, we dissociated and cultured cells from tumor masses explanted from two animals displaying no detectable levels of Gluc in their blood and assayed their Gluc expression in vitro. Surprisingly, the supernatants from both cultures were found to contain an amount of Gluc not far from that of $mHGG^{egfrvIII}$-7-Gluc population prior to the transplant, ranging from one half to one third of the original level. These results indicate that the fall of Gluc levels in those mice cannot be explained by a decrease of Gluc expressing cells. We therefore hypothesize that the decrease of $[Gluc]_{To}$ could be due to the rise of a neutralizing antibody against Gluc, as suggested by Tannous [131], but in contrast to what reported by other authors [142]. To test this possibility, we incubated a defined amount of Gluc with sera derived from mice having displayed low or irregular pattern of $[Gluc]_{To}$ over the time and found that 7 out of the 8 tested sera were able to dramatically inhibit Gluc activity (Figure 2.3B-C). On the contrary, sera derived either from non-transplanted mice or from mice that did not develop gliomas following $mHGG^{egfrvIII}$-7 transplant, were not able to significantly inhibit Gluc activity. Moreover, the further addition of 0.1M glycine in samples where Gluc was inhibited by serum restored the Gluc activity, as expected if the inhibition would depend on neutralizing antibodies (Figure 2.3B-C). The addition of 0.1M glycine was also able to unmask Gluc activity in sera of mice displaying barely detectable levels of Gluc but harbouring large tumor masses (Figure 2.3D). Taken together these results indicate that immunocompetent mice tends to develop neutralizing antibody that can perturb the Gluc activity. Accordingly with this view, $[Gluc]_{To}$ was not correlated to tumor size even in those animals displaying exponentially growing $[Gluc]_{To}$ levels, as shown by the Pearson correlation

coefficient lower than 0.5 (data not shown), suggesting the presence of Gluc antibodies even in these animals. The luciferase monitoring immunocompetent animals can be therefore used as qualitative method to determine whether tumor successfully grafted but cannot be used as a quantitative method to establish the tumor size.

Conclusions

Tumor growth is not easily monitored when the tumor mass is located in inaccessible locations as in the case of gliomas. A precise assessment of the tumor dynamic, however, would be important to evaluate the effects of experimental treatments and may guide the establishment of new treatments. An essential characteristic of a method designed to frequently monitor tumor growth should be a minimal invasiveness, and this criterion is not fulfilled by the currently used methods, which need anesthesia and long acquisition times. Gluc assay allows to monitor tumor growth in Nod/Scid mice at least twice a week, with a rapid and non-invasive procedure. By exploiting the initial burst of activity of Gluc, our method is highly sensitive allowing to detect the tumor at very early stages. Data collected here allowed for the first time a thorough analysis of the correlation between [Gluc]To and tumor burden, determined directly by weight and morphometric assay. The analysis showed this correlation is good and thus we deem that Gluc assay represents an excellent tool to monitor gliomas in vivo. The Gluc assay is, however, not suitable in immunocompetent animals, due to the onset of an immune response against the luciferase.

Figures

Fig. 2.1

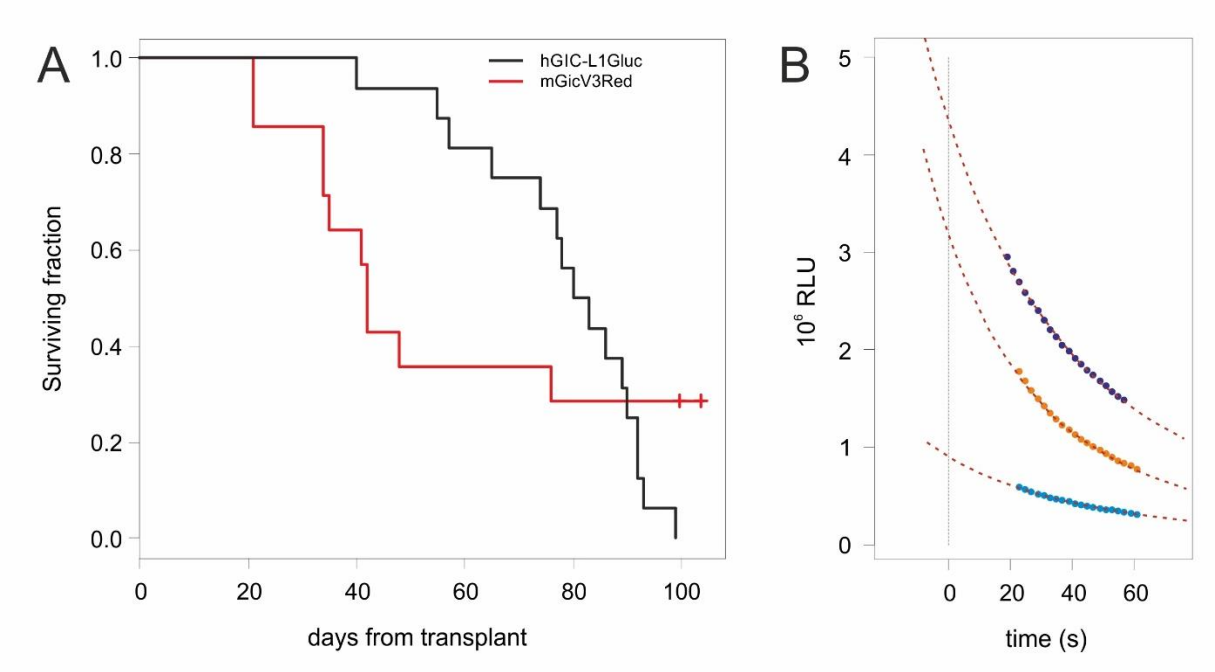

Figure 2.1 (A) Kaplan-Meyer survival curves of Nod/Scid mice transplanted with L0306-Gluc (black) and BALB/c mice transplanted with mHGG^{egfrvIII}-7 (red). (B) Gluc has a flashing kinetic and its activity dramatically decreases over the time when incubated with the substrate. The curves represent three examples of regression curves obtained from measured values of luminescence over the time (colored dot) to extrapolate the starting activity ([Gluc]T0), determining a value that is time-independent.

Fig.2.2

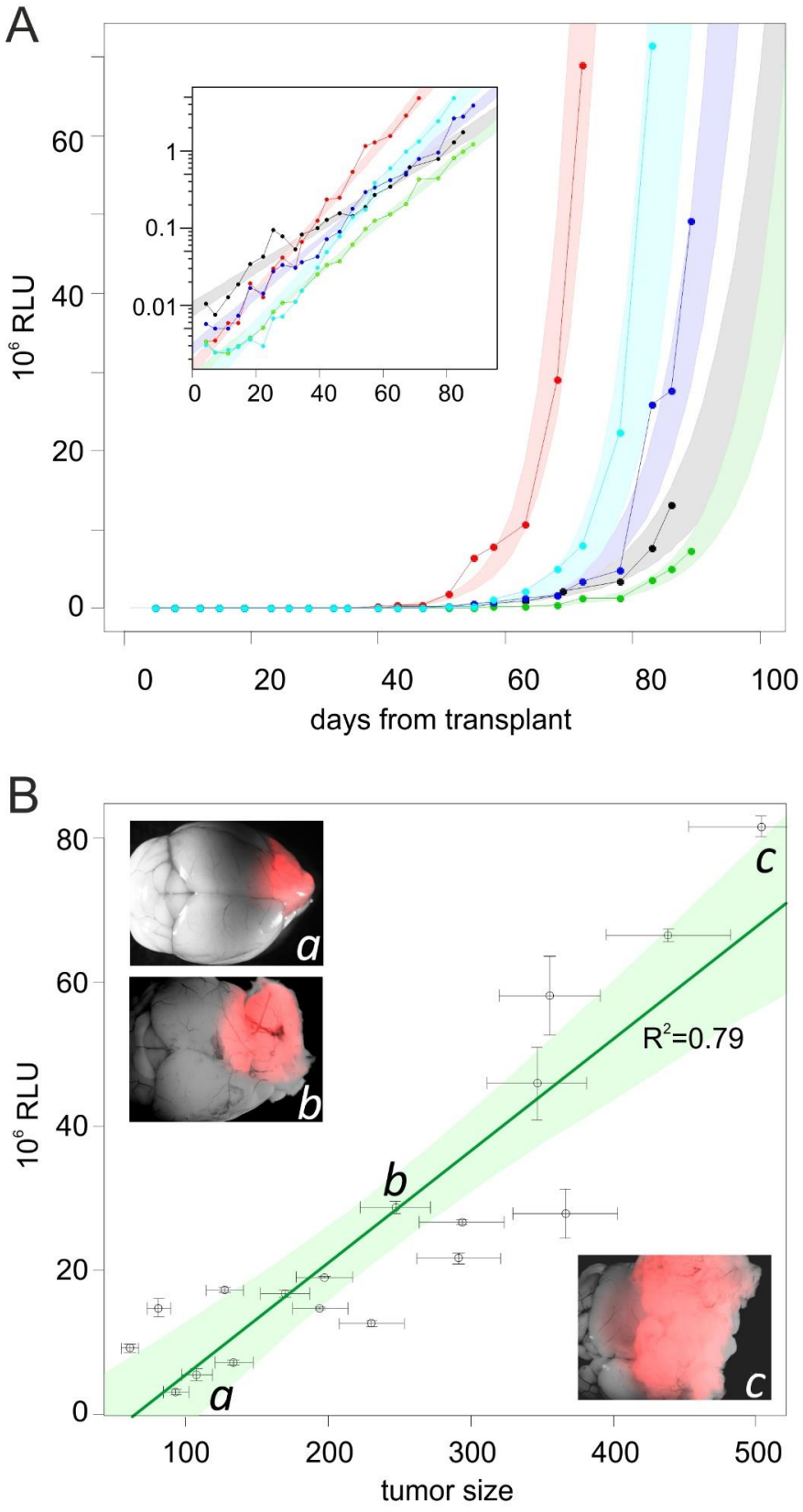

Figure 2.2 (A) Increase of [Gluc]To over the time from tumor transplant. The plot shows the levels of [Gluc]To from blood samples collected starting from 2 days after transplant, up to the end of the experiment in five representative mice. In the inset, the same curves are shown in logarithmic scale. Colored areas represent the 90% confidence interval of each regression curve. (B) Correlation between [Gluc]To and glioma size. The plot represents the [Gluc]To from mouse blood samples versus the size (estimated as described in the text) of L0306-Gluc tumors harbored by the mice. Green area represents the 90% confidence interval of the regression line (in dark green). Examples of brains harboring tumors (in red) from three mice with low (a), medium (b) and high (c) [Gluc]To are shown in inset pictures.

Fig. 2.3

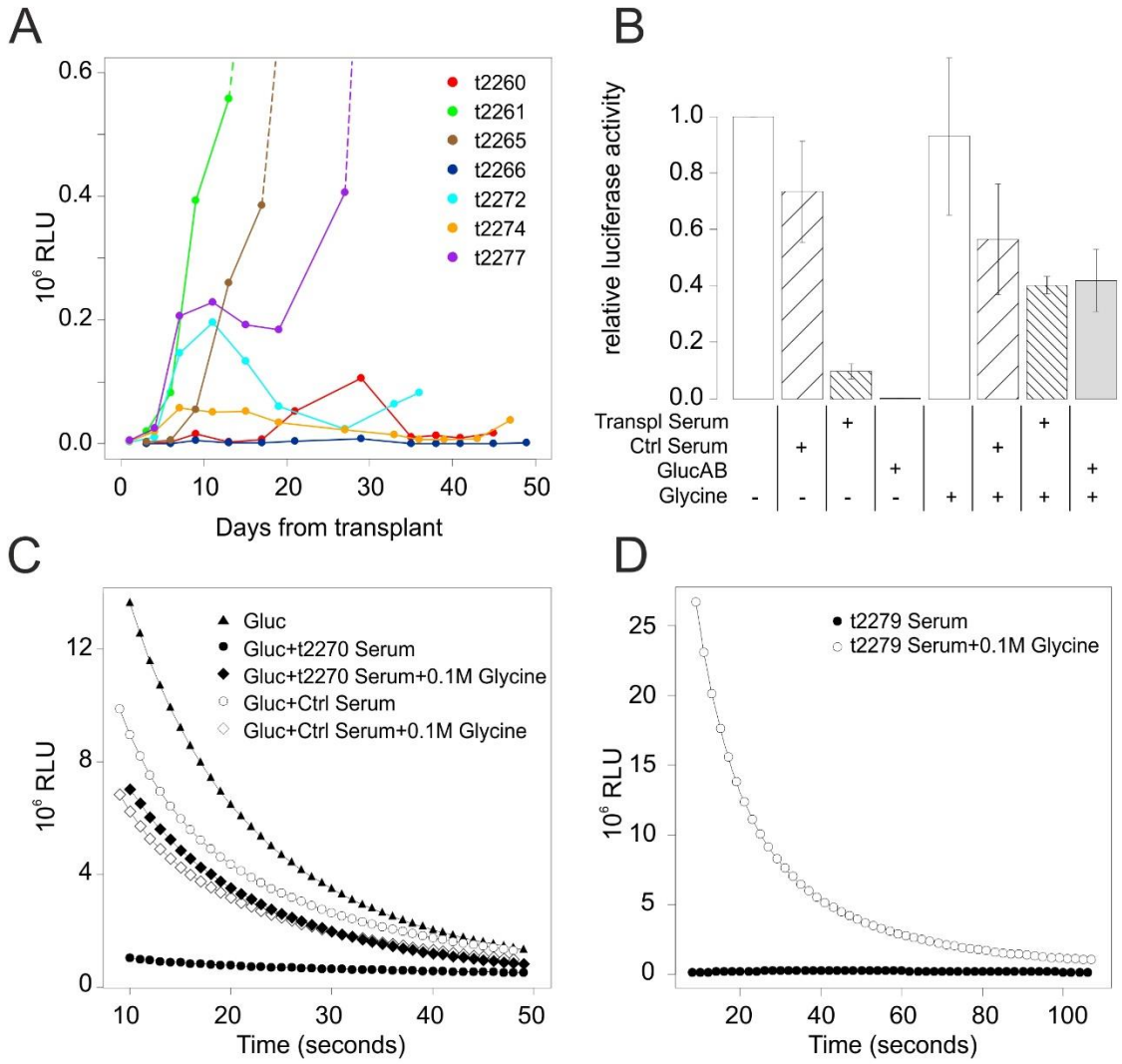

Figure 2.3 (A) Levels of [Gluc]To in blood samples over the time in a representative sample of BALB/c mice transplanted with mHGG^{egfrvIII}-7-Gluc cells. (B) Effects on Gluc activity of sera derived from BALB/c mice displaying irregular patterns of Gluc levels over the time (Transpl Serum) following transplantation with mHGG^{egfrvIII}-7-Gluc cells. Purified anti-Gluc antibody (GlucAB) and sera from non-transplanted BALB/c mice (Ctrl Serum) were included as positive and negative controls respectively. Glycine 0.1M was used, as control, to inhibit antibody binding. (C) The plot shows how the kinetic of Gluc reaction is modified by the incubation in the specified conditions. Ctrl serum and t2270 serum derived respectively from a non-transplanted mouse and a mouse transplanted with mHGG^{egfrvIII}-7-Gluc 33 days before. (D) The plot shows the effects of 0.1M Glycine on the activity of Gluc in a transplanted mouse which displayed irregular pattern of Gluc activity over the time.

Fig. 2.4

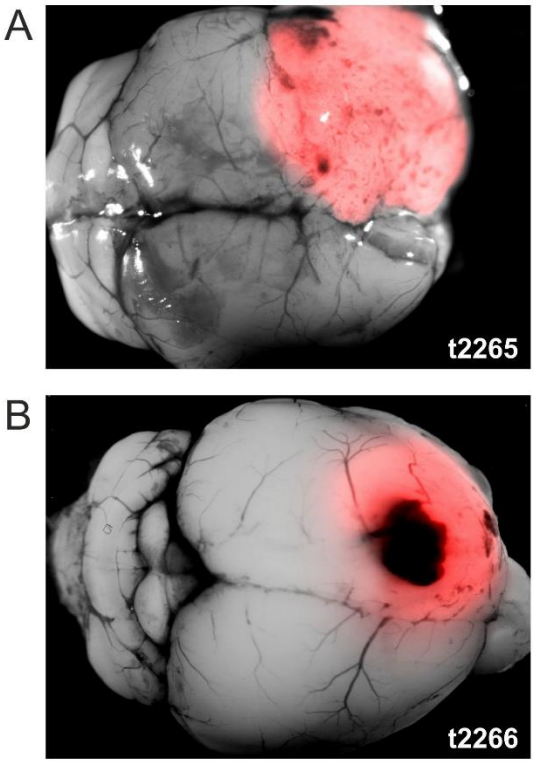

Figure 2.4 Example mHGG^{egfrvIII}-7 tumors of similar size derived from two BALB/c mice displaying very different [Gluc]To levels. [Gluc]To never reached a detectable level in the blood of t2266, while it exponentially grew in t2265.

IL-12 armed retargeted herpes simplex virus as therapy for a high-grade glioma preclinical model

Herpes Simplex Virus 1 (HSV-1) is among the most studied oncolytic viruses for treating several types of cancers. HSV-1 has relevant characteristics as therapeutic agent: it has a large genome that can accommodate exogenous genes, it does not integrate into the host genome and is not oncogenic [88, 143, 144]. Moreover, anti-HSV-1 drugs are available to shut off virus replication in case of uncontrolled infection. Oncolytic HSVs (oHSVs) are emerging as one of the effective therapies to fight malignant neoplasms lacking effective therapeutic alternatives. Clinical trials are ongoing to test the safety and the efficacy of oHSVs against colorectal, breast and non-resectable pancreatic cancers [145-147]. Recently, T-VEC, an oHSV with tumor-selective replication which expresses GM-CSF (granulocyte monocyte colony stimulating factor), has been approved as therapy for non-resectable metastatic melanoma [148, 149].

A noteworthy potential target for oHSVs therapy is glioblastoma [84], the most aggressive form of brain tumors, and one of the most lethal types of human cancer, classified by WHO as grade IV glioma [150]. The life expectancy of glioblastoma patients has not substantially changed in the past 50 years. When treated with the standard of care protocol, patients may survive for up to 15 months; only 10% of them survives for more than five years from diagnosis [51]. Challenging properties of glioblastoma are its tendency to infiltrate the healthy brain parenchyma and its high radio- and chemo-resistance. As a consequence, the incidence of recurrence after surgical resection is high. Oncolytic virotherapy may represent a breakthrough since viral spread could potentially hit disseminating cells. Oncolytic viruses have the advantage that they can spread

among cancer cells and kill them. In addition, they stimulate the immune system so as to break the tolerance against the tumor.

Although for a long time the central nervous system (CNS) has been considered a privileged site of immunity, now this paradigm is disputed and there is growing evidence that activated T cells are able to recognize their targets even when they are located within the CNS parenchyma [151, 152]. oHSVs offer the possibility to be armed with immunostimulatory molecules. In recent years, evidence has been provided that the expression of mIL-12 increases the effectiveness of oncolytic viruses by activating the immune response, thus potentiating the clearance of cancer cells through an immunotherapeutic effect. Preclinical trials were conducted on oHSVs armed with mIL-12 for ovarian cancer [153], breast cancer brain metastases [154] and also glioblastoma [155]. An HSV armed with IL-12 is currently under phase 1 clinical trial [156].

The above studies exploited HSV recombinants attenuated by genetic manipulation in order to achieve cancer-specific replication. As an alternative approach, we recently assayed the safety and the efficacy of a replication-competent retargeted oHSV, fully virulent in its target cells, named R-LM113. R-LM113 is retargeted to the human receptor tyrosine-protein kinase erbB-2 (hHER2), a receptor expressed in a number of tumors, including a large fraction of human high-grade gliomas (HGGs) [37-39]. In a murine model developed in our laboratory, R-LM113 counteracted high-grade glioma [119, 120]. Of note, the retargeted oHSVs are intrinsically safer than the attenuated ones, replicate to higher yields, and can be readily engineered so as to target different cancer-specific receptors [157].

Here we report on the efficacy of a fully virulent, retargeted oHSV-1, armed with mIL-12, (R-115; L. Menotti, et al., unpublished manuscript) in counteracting glioma. The effects of treatment

were tested against established orthotopic HGGs in a syngeneic glioma model in BALB/c mouse strain.

Materials and methods

Animal procedures

Mice were handled in agreement with the guidelines conforming to current Italian regulations for the protection of animals used for scientific purposes (D.lvo 27/01/1992, no. 116). Procedures were approved by the Ethical Committee for Animal Experimentation of the National Institute of Cancer Research and by the Italian Ministry of Health. The experiments were performed with the BALB/c mouse strain.

Tumors were implanted by injecting a suspension of $2x10^4$ cells in adult mouse brains using a Hamilton syringe (Bregma coordinates: anterior-posterior, 1.0 mm anterior; lateral, and 2.5 mm below the skull surface). 21 days after tumor implantation, 5µl oHSV preparation, containing $2 \cdot 10^6$ PFU of either R-115 or R-LM113 or gamma irradiated R-LM113 were injected at the same stereotaxic coordinates. Animals were monitored daily and were killed at first signs of neurological symptoms or at the predetermined time point. Their brains were photographed by fluorescence stereomicroscope (Wetzlar, Germany).

Survival curves were determined using Kaplan–Meier survival between groups and was compared by log-rank test.

Up to 0.3 ml of blood was withdrawn 20 days after treatment with oHSV. In addition, we took blood from long surviving mice, 4 days after the transplantation of $mHGG^{pdgf}$-hHER2 in the contralateral hemisphere. Heparinized capillaries were used for retro-orbital bleeding

procedure. Samples were incubated for 6h at 60°C with heparin. Cells were removed from serum by centrifugation (10 minutes at 2,000 g with refrigerated centrifuge).

Cell cultures and infection

Platelet-derived growth factor B (PDGF-B)-induced brain tumors expressing DsRed fluorescent reporter were obtained as previously described [120]. Cells derived from primary tumors were maintained onto plates coated with Matrigel matrix (1:200; BD Biosciences, Franklin Lakes, NJ) in DMEM-F12 added with B27 supplement, human bFGF and EGF (10 ng/ml). mHGG^{pdgf} cells were transduced with RAVI-hHER2 retroviral vectors and sorted by FACS based on the expression of the receptor.

The construction and production of the recombinant oHSVs R-LM113 and R-115, retargeted to hHER2, was described elsewhere [94, 158]. Cells were infected with R-115 or R-LM113, at the indicated multiplicity of infection estimated on the basis of titer determined in SK-OV-3 cells. The efficiency of infection was monitored under inverted microscope (EVOS FL Cell Imaging System, ThermoFisher Scientific, Waltham, MA, USA) by means of enhanced green fluorescent protein (EGFP) expression for both viruses. The percentage of infected cells was evaluated by loading them on a hemocytometer and acquiring pictures/imaging with a motorized epifluorescence microscope (Axio Imager.M2, Zeiss, Oberkochen, Germany). Images were automatically analyzed with an ImageJ plug-in (Rasband, W.S., ImageJ; US National Institutes of Health, Bethesda, MD, http://rsb.info.nih.gov/ij/, 1997–2007), which allows to measure and plot area and fluorescence intensity of each cell.

mIL-12 was quantified from the supernatants of mHGG^{pdgf}-hHER2 cells infected at 0.1, 0.3 or 1 PFU/cell with R-LM113 or R-115, using the Mouse IL-12 (p70) ELISA Plate kit (ThermoFisher Scientific, Waltham, MA, USA).

Immunostaining and flow cytometry

For flow cytometry and cell sorting, mHGG^{pdgf}-hHER2 cells were stained in suspension with mouse monoclonal antibody against hHER2 (1µg/10^6 cells; Santa Cruz Biotechnology, Santa Cruz, CA, USA). Binding of primary antibody was revealed with secondary anti-mouse Cy^{TM}2-conjugated, (1:50; Jackson Immunoresearch, Milano, Italy).

To detect antibodies in murine plasma, tumor cells and NIH/3T3 cells (in ratio 1:1.5) were incubated for 1 hour at 4°C with plasma diluted in saline solution (1:5). After washing in PBS, cells were incubated for 30 min with a secondary anti-mouse IgG antibody (Cy^{TM}2 conjugated, Jackson Immunoresearch, Milano, Italy) and analyzed by flow cytometry (CyAn ADP, Beckman Coulter, Indianapolis, IN, USA). Positive control consisted of mouse monoclonal antibody against hHER2 and secondary anti-mouse Cy^{TM}2-conjugated. The proportion of DsRed-positive mHGG^{pdgf}-hHER2 cell above a threshold on the FITC-fluorescence axis among the cells were normalized to the mean of the proportion of cells above the same threshold among the DsRed-negative in all samples.

For histological analysis, brains were fixed with 4% paraformaldehyde, cryoprotected in 20% sucrose and sectioned with a Leica CM3050 S cryostat. Immunostainings on brain sections or cultured cells were performed using mouse monoclonal antibody against CD4 (1:500, BD Pharmingen, San Diego, CA, USA) or CD8 (1:200, Novus Biological, Littleton, USA). Binding of primary antibody was revealed with secondary anti-rat Alexa 488-conjugated (1:500; Jackson

Immunoresearch, Milano, Italy). The shapes of the sections, of tumor masses and positions of CD4 and CD8 were acquired by epifluorescence microscope (Axio Imager.M2, Zeiss, Oberkochen, Germany) by using AxioVision Rel. 4.8 (Zeiss, Oberkochen, Germany) and Slide Explorer2 plug-in of Micromanager [159]. A set scripts for R 3.4.0 developed in house (available on request) were used to produce the overlay between pictures and acquired positions of lymphocytes and to calculate their distances from the tumor edges.

RNA sequencing

For whole-exome sequencing, at least 0.01 µg RNA derived from three ex-vivo primary tumor sample, sorted by FACS for DsRed reporter and harvested in Trizol, was send to BGI genomics (BGI, Shenzhen, China) and sequenced on BGISEQ-500 RS generating 50 base-pair single-end reads. The high-quality clean tags were mapped to reference genome (mm10) using STAR [116]. To quantify the gene expression level, RSEM analysis was carried out [117], acquiring read count of each gene of each sample, based on the mapping results. Normalization and data trimming were performed by edgeR [118]. Raw and processed data are available on GEO Dataset (Accession number GSE109614).

Results

Mouse PDGF-driven glioma cells show hallmarks of human glioblastoma and are poorly immunogenic

To study the effects of the mIL-12-armed hHER2-retargeted oHSV (R-115) on HGGs, we took advantage of a model of HGG based on the transduction of Platelet Derived Growth Factor-B

(PDGF-B) in neural progenitor cells derived from BALB/c mice, a mouse strain sensitive to HSV infection. The HGG model was generated by transplanting in adult mouse brains murine neural progenitor cells explanted at embryonic day 14 (E14) and transduced with a PDGF-B overexpressing retroviral vector as described [119]. The generated HGGs, hereinafter referred to as mHGG^{pdgf}, express markers typical of oligodendroglial progenitor cells (OPCs) and exhibit histological features typical of human HGGs, as previously described [120]. Here, mHGG^{pdgf} were further characterized by RNA sequencing carried on three independent tumor specimens (raw data are available on GEO Dataset. Accession number GSE109614). The analysis showed that mHGG^{pdgf} cells express OPC markers such as Olig2, PDGFR-alpha and NG2, and stem cell markers, including Sox2, Stat3 and Nestin (Figure 3.1A). mHGG^{pdgf} cells showed very low levels of mRNAs for immune system co-stimulatory molecules CD40 and CD80, and IL-12 and IL15 cytokines. Low levels of expression were also observed for the co-stimulatory molecule CD86. On the contrary, the immunosuppressive gene CD73 [160] was highly expressed. This pattern is consistent with mHGG^{pdgf} being poorly immunogenic, as typically seen in human glioblastomas.

Primary mHGG^{pdgf} were microdissected, cultured and engineered to express hHER2 receptor. hHER2-transduced cells (hereinafter referred to as mHGG^{pdgf}-hHER2) maintained the tumorigenic potential exhibited by the parental mHGG^{pdgf} cells, and were able to consistently generate tumor masses after intracranic transplantation of $2 \cdot 10^4$ cells in adult immunocompetent mice leading them invariably to death.

R-115 efficiently infects hHER2-positive murine glioma cells in vitro, and mediates mIL-12 secretion

To assess if mHGG^{pdgf}-hHER2 are susceptible to R-115 infection in vitro and to compare R-115 with R-LM113, whose efficiency was reported earlier [120], we infected mHGG^{pdgf}-hHER2 cells with R-115 or R-LM113 at the multiplicity of infection (MOI) of 0.5 plaque-forming units (PFU) per cell, as titrated in SK-OV-3 cells. Viral infection was scored as expression of the EGFP reporter gene inserted in the virus genome. After 30 hours, we observed an equivalent percentage of infected cells in the R-115- and R-LM113-infected cultures (Figure 3.1 B and C). To ensure that R-115 exhibited the specific hHER2 tropism typical of the parental R-LM113, the control hHER2-negative mHGG^{pdgf} monolayers were inoculated with R-115. No EGFP-positive infected cells were detected up to 96 hours after exposure to the virus (Figure 3.1D). mHGG^{pdgf}-hHER2-expressing cells infected with R-115 and monitored for 72 h after infection produced and secreted mIL-12 in the medium, in a MOI-dependent fashion (Figure 3.1E). In addition, we monitored the time course of R-115 infection in mHGG^{pdgf}-hHER2 cell monolayers, after infection at low MOI (0.01 PFU/cell, as titrated in SK-OV-3 cells). The collected images showed that R-115 progeny was able to efficiently spread in culture (Figure 3.1F).

Inhibition of tumor growth *in vivo* by R-115 in immunocompetent mice and induction of cancer-specific immune memory

R-115 efficacy in counteracting gliomas was analyzed as ability to inhibit the progressive growth of established mHGG^{pdgf}-hHER2 tumors *in vivo*. Mice bearing tumors induced by orthotopic transplantation of mHGG^{pdgf}-hHER2 cells in the left cranial hemisphere were randomized and treated by intracranic injection of $2{\cdot}10^6$ PFU of R-115 (R-115 arm), or the same amount of R-LM113

(R-LM113 arm), 21 days after tumor implantation. The control group was injected with an equivalent volume of gamma-irradiated R-LM113 (control arm). The animals that did not survive intracranial injection procedure and died within 3 days from virus injection were excluded from the experiment (n=1). In total, we analyzed 14 surviving mice in the R-115 arm, 12 mice in the R-LM113 arm and 6 mice in the control arm.

The median survival time of animals in the control arm was 15 days from the treatment. Mice belonging to the R-LM113 and R-115 arms showed a median survival time of 35 and 33 days from the treatment, respectively. Both figures are significantly different from that in the control arm (Rank-test $p<0.001$ both for R-LM113 and R-115; Figure 3.2A). No difference in term of median survival time was detected between the two different oHSVs. However, a dramatic difference between the R-LM113 and R-115 arms was evident in terms of long survivors. While in the R-LM113 arm all mice died within 48 days from treatment, in the R-115 arm 29% of mice (n=4) were still alive 100 days after the virus treatment. Two of them were sacrificed and resulted tumor-free (Figure 3.2B). The other two mice were implanted with additional $2 \cdot 10^4$ mHGG^{pdgf}-hHER2 cells in the contralateral hemisphere relative to the first injection. In parallel, the same amount of cells was injected into the right hemisphere of three control mice. The animals belonging to the control set died within 26 days after transplantation. Conversely, the two mice that had undergone mIL-12 expressing oHSV administration were still alive 220 days after the transplant in the contralateral hemisphere (Figure 3.2C), demonstrating that they acquired resistance to the tumor, likely due to immune memory.

R-115 elicits production of antibodies and the infiltration of CD4 and CD8 positive cells in the tumor

To provide direct evidence that R-115 elicits a tumor-specific response, we transplanted 14 additional mice with mHGG^{pdgf}-hHER2 cells. After 21 days, 6 mice were injected with R-115 and 5 with R-LM113 ($2{\cdot}10^6$ PFU/mouse). After further 20 days, we took the blood from the retro-orbital sinus to check whether the mice had developed antibodies targeting mHGG^{pdgf}-hHER2 antigens. Blood was also drawn from the two long-surviving mice from the R-115 arm of the previous experiment, from two non-transplanted mice (naïve), from three mice transplanted with mHGG^{pdgf}-hHER2 cells and not treated with virus. The plasma samples were assessed for the presence of antibodies against mHGG^{pdgf}-hHER2 cells, by checking their reactivity with mHGG^{pdgf}-hHER2 cells. The plasma samples were incubated with a cell mixture constituted by DsRed-labeled mHGG^{pdgf}-hHER2 cells and unlabeled murine fibroblasts (NIH/3T3), as internal negative control. Following incubation with a FITC-conjugated anti-mouse IgG secondary antibody, the increase in FITC fluorescence of DsRed-labeled cells was measured (Figure 3.3A). This analysis showed that no antibodies were detectable in the plasma of naïve (non tumor-transplanted) mice, nor in those of mice receiving tumor cells but no virus injection. In contrast, immunoreactivity was clearly detectable in the plasma of 2 out of 5 animals from the R-LM113 group, and in 5 out of 6 animals from the R-115 group. Immunoreactivity was also detected in the plasma of both long surviving mice. To evaluate the specificity of immunoreactivity of plasma samples, we took advantage of the internal negative control, which allowed to discriminate between specific and unspecific FITC signal. To do so, we normalized the fraction of mHGG^{pdgf}-hHER2 cells above a fixed FITC threshold to the fraction of NIH/3T3 cells above the

same FITC threshold (i.e. unspecific signal; Figure 3.3B, C). This analysis allowed to test by one way Anova followed by a TukeyHSD post-hoc test the levels of immunoreactivity in the three groups. The analysis confirmed that there was a significant difference (Anova $p<0.05$) and the difference was between R-115 and the control group.

Next, we carried out the same assay with the parental hHER2-negative mHGG^{pdgf} cells. The reactivity was much lower than that against mHGG^{pdgf}-hHER2, suggesting that the immune response elicited by oHSV infection was mainly targeting the xenogeneic hHER2 receptor. However, three plasma samples exhibited a higher reactivity, those drown from the two long survivor mice from the R-115 arm of the first experiment, and one of the mice that had received R-115 (Figure 3.3D).

Beside the humoral immune response, IL-12 is known to activate T-cell response [161]. An increase in the number of T-lymphocytes a few days after oHSVs armed with mIL-12 was reported [162]. We analyzed the brains of 11 mice treated with R-LM113 or R-115 at 22 days after virus administration. The brains were analyzed for the presence of CD4- and CD8-positive cells by immunostaining. While the overall number of CD4- and CD8-positive cells did not significantly differ between animals treated with R-LM113 or with R-115, we observed a striking difference in their intratumoral distribution, depending on the injected oHSV. Thus, CD4- and CD8-positive cells accumulated at the edge of the tumors treated with R-LM113, while they deeply infiltrated the tumor masses in the animals treated with the mIL-12 expressing R-115 (Figure 3.4A-D). A quantification of the distances of CD4- and CD8-positive cells inside the tumor masses from the nearest edge of the tumor was performed on 5 independent tumors for each treatment (Figure 3.4E,F). T-test confirmed a significant difference between R-LM113 and R-115 groups for both CD4 and CD8 cells tumor localization ($p<10^{-12}$), arguing that the mIL-12 armed oHSV strongly

promoted CD4- and CD8-positive infiltration of the tumors masses which, otherwise, tend to exclude lymphocytes.

Discussion

To our knowledge, this is the first study where a retargeted, fully virulent oHSV armed with mIL-12 has been tested on orthotropic high-grade gliomas. The murine glioma employed here (mHGG^{pdgf}) is highly invasive, shows 100% penetrance after intracranic transplantation in immunocompetent mice, and exhibits an immunosuppressive gene expression profile, similar to that of human glioblastomas. Like human glioblastomas, it is rather resistant to a number of treatments, including chemotherapy and experimental gene therapy [163], and it invariably leads to animal death. In our experience, all the different treatments tested (temozolomide administration, peptide immunotherapy, oHSVs) on mHGG^{pdgf} harboring mice led, at best, to an improvement in the median survival time [119, 120, 163]. So far, one of the most effective treatments was that with the fully virulent retargeted oHSV (R-LM113) [119] of which R-115, employed in this work, represents an evolution, by the insertion of mIL-12 expression cassette (L. Menotti, et al., unpublished manuscript). In the present work, $2{\cdot}10^6$ PFU of R-115 was administered in a single injection session in animal harboring already established tumors. The timing for treatment was selected based on the survival curves previously determined for mHGG^{pdgf}-hHER2 to be shortly before the first animals exhibited disease symptoms. Strikingly, about 30% of the R-115 treated animals underwent permanent and complete remission and resulted even resistant to a distant re-challenge with the same tumor cells. In our experience, this is the first time that a complete tumor eradication is achieved in this tumor model, as reliably established by the lack of any fluorescently (DsRed) labelled cells.

The overall median survival time of mice treated with R-115 was doubled in comparison to that of the mock treated animals, although it was not significantly different from that of the animals treated with the non-armed version of the oHSV (R-LM113). Current findings differ from the reported efficacy study on mIL-12-armed *versus* non-armed versions of attenuated oHSVs, based on the deletion of the $\gamma_1$34.5 virulence gene [155, 162]. The main difference between our results and the former lies in the higher efficacy of R-LM113 on the overall survival time: indeed, unlike attenuated oHSVs, fully virulent R-LM113 was, by itself, already capable to double the median survival time even when injected in large neoplastic masses.

Noteworthy, the effect on overall survival and eradication was obtained with a single administration of low amount of R-115 on grown tumors, in close proximity to the time in which they would have exhibited neurological symptoms, as it can be deduced from the survival curves of the control arm mice. It is therefore conceivable that protocol employed in earlier studies, consisting of repeated sessions of injections or earlier treatments [155], would result in higher R-115 efficacy. Recently, higher percentages of experimental glioma eradication in immunocompetent mice have been obtained with mIL-12 expressing attenuated oHSV [164]. However, that result was obtained only when the IL-12-expressing oHSV was employed in combination with two immune checkpoint inhibitors (anti CTLA-4 and anti PD1 antibodies); this protocol cannot be readily translated to clinical practice due to toxicity of the antibodies in trials [165].

Our observations show that the mIL-12 expressing hHER2 retargeted R-115 enhanced the production of antibodies targeting the transplanted glioma cells. The immunoreactivity was mostly directed to the exogenous human receptor hHER2, expressed by mHGG^{pdgf}-hHER2.

However, a subset of animals (about 1/3, among which the long survivors) showed immunoreactivity also against the parental mHGG^{pdgf} cells, lacking hHER2.

Beside an enhanced humoral response, it is well known that T-cell response is activated by mIL-12 [161]. We investigated CD4 and CD8 positive population in brain sections. Our analysis did not highlight differences in terms of the total amount of CD4 and CD8 positive cells in the long term. However, a striking difference in the distribution of these cells was evident 20 days after virus injection. In mice treated with R-LM113, CD4 and CD8 positive cells appeared confined at the tumor edges, as observed in cold (i.e. excluded) tumors [166], while they were able to infiltrate deeply the entire tumor masses in mice treated with R-115, arguing that mIL-12 influenced the immune cell landscape within the immunosuppressive tumor microenvironment.

This study provides a proof of concept of the benefits of a retargeted, fully virulent, oHSVs over attenuated oHSVs to counteract high-grade gliomas by overexpressing mIL-12, and suggests they are the fully eligible candidates for oHSV-based glioblastoma treatment.

Figures

Fig. 3.1

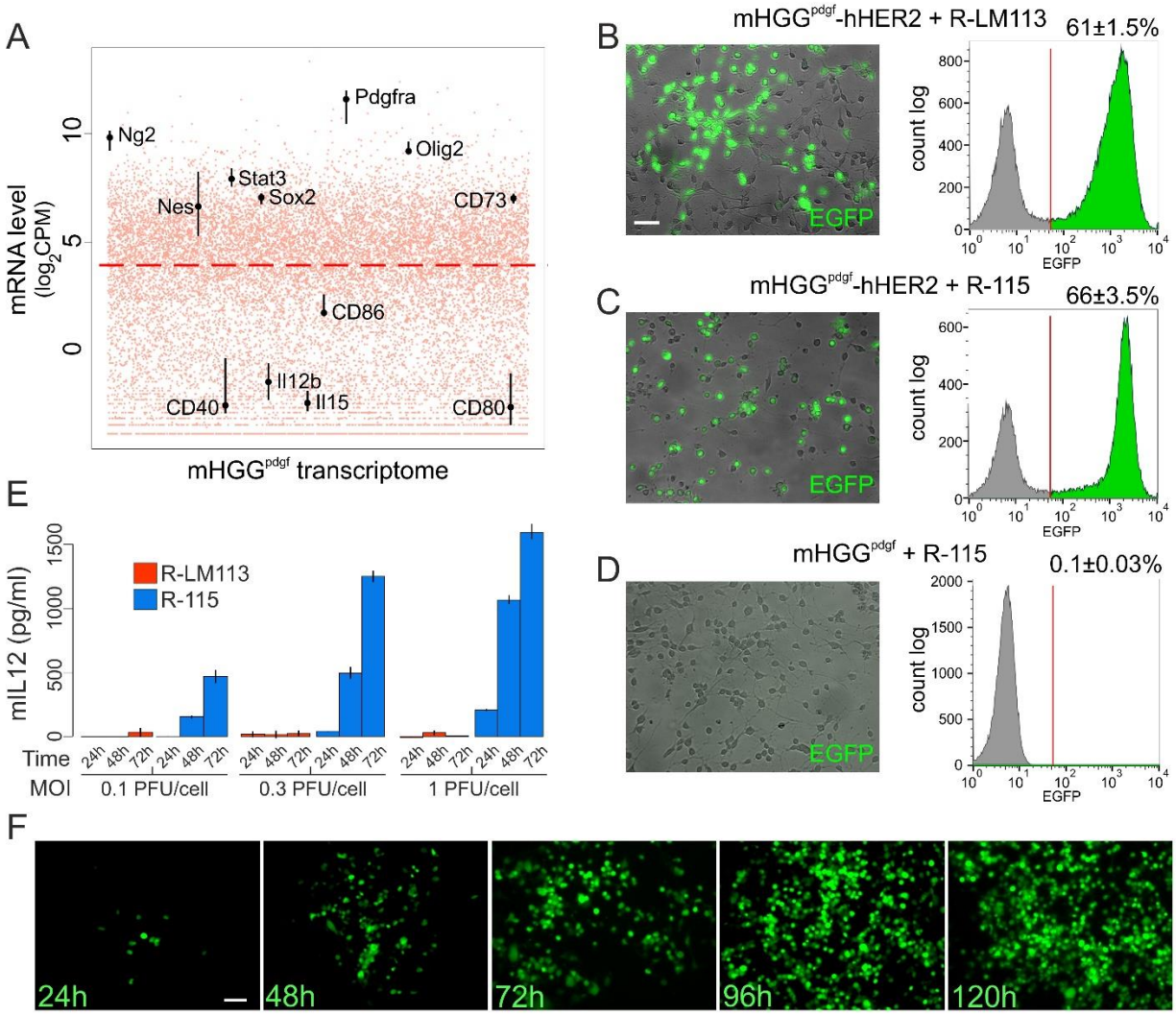

Figure 3.1

(A) Expression levels of the whole transcriptome of mHGG^{pdgf} cells as determined by RNA-seq analysis from three independent tumors. Genes of interest are highlighted and the level of their expression is represented as a bar summarizing the results from the 3 samples. Black dots represent the median. Dashed red line represents the overall median expression level across the whole transcriptome. The arrangement of the genes along the x axis is randomized. This analysis shows that mHGG^{pdgf} cells express OPC markers Olig2, PDGFR-alpha and NG2 and stem cell markers Sox2, Stat3 and Nestin. mRNAs for CD40, CD80 and CD86, IL-12 and IL15 are expressed at low levels, while

CD73 gene is highly expressed. This pattern is consistent with mHGG^{pdgf} poor immunogenicity, similar to that of human glioblastomas. (B-D) Infection of mHGG^{pdgf}-hHER2 cells with 0.5 PFU/cell of R-LM113 (B) or R-115 (C), or of the parental mHGG^{pdgf} cells with 0.5 PFU/cell of R-115 (D). Pictures were taken at 30 hours after infection. Histograms show the corresponding cytofluorimetric quantifications of the cells expressing the EGFP reporter expressed by the viral genome. The insertion of the mIL-12 expression cassette in R-LM113 genome, resulting in R-115 recombinant, did not impair the efficiency of infection and the specificity of retargeting. (E) ELISA quantification of mIL-12 concentration in supernatants of mHGG^{pdgf}-hHER2 cells infected with R-LM113 (red bars) or R-115 (blue bars) at the indicated MOI and times after infection. Error bars indicate standard deviation. (F) Time course of R-115 infection in mHGG^{pdgf}-hHER2 monolayers (input MOI 0.01 PFU/cell). Scale bars 50µm.

Fig. 3.2

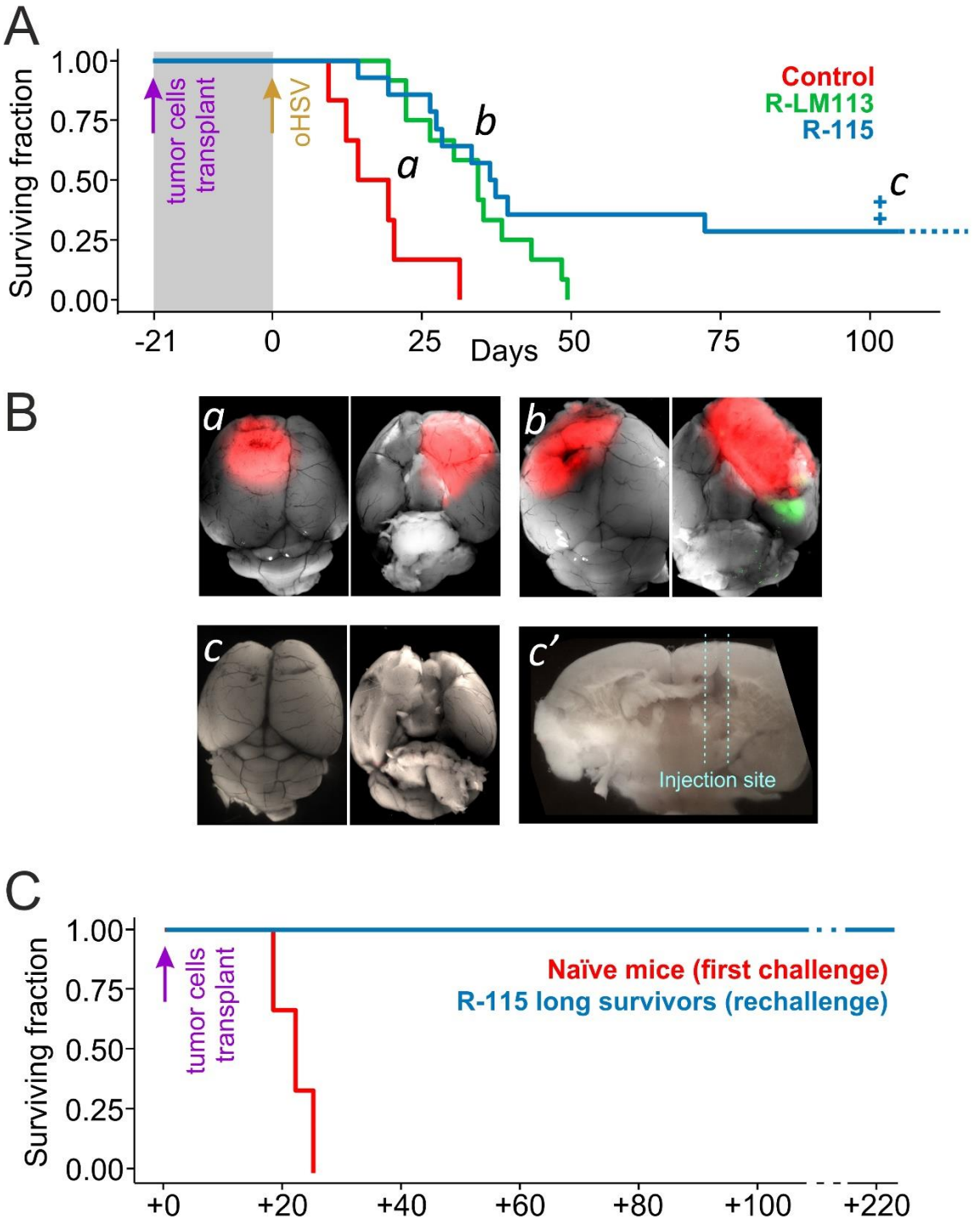

Figure 3.2

(A) Kaplan-Meyer survival curves of mice transplanted with mHGG^{pdgf}-hHER2 and treated after 21 days with R-LM113 (green line), R-115 (blue line) and gamma-irradiated R-LM113 (control; red line).

Rank-test p<0.001 both for R-LM113 arm and R-115 arm, compared to the control arm. About 30% of mice were still alive 100 days after treatment with R-115. (B) Representative dorsal and ventral images of brains from mice of the control arm (a), the R-115 arm (b) and a long surviving mouse from R-115 arm, found to be tumor free (c). In all micrographs the red channel shows the DsRed fluorescent reporter expressed by mHGG^{pdgf}-hHER2 cells, the green channel shows the viral reporter EGFP. c': coronal section of the brain of panel in c at the level of injection site. (C) Kaplan-Meyer curves of the long surviving mice from R-115 arm rechallenged by a second transplantation of mHGG^{pdgf}-hHER2 in the contralateral hemisphere, 125 days after the first tumor transplantation (blue line), and control naïve mice transplanted with the same preparation of mHGG^{pdgf}-hHER2 cells (red line). Long surviving mice were still alive 220 days after rechallenged with mHGG^{pdgf}-hHER2 cells.

Fig. 3.3

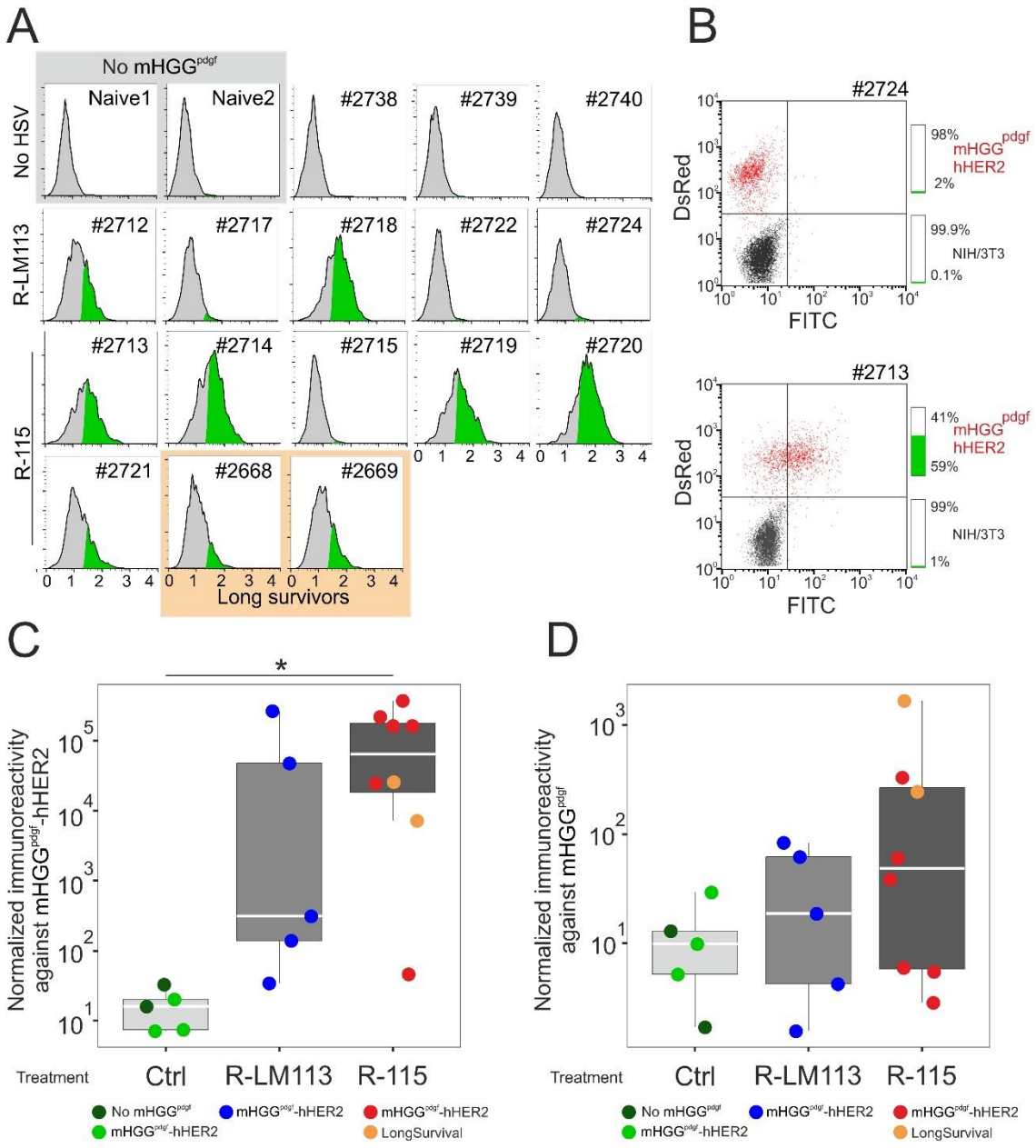

Figure 3.3

(A) Development of antibodies against mHGG^{pdgf}-hHER2 cells by mice treated with R-LM113 or R-115 oHSV. Plasma samples drawn from mice treated with the indicated virus were evaluated for their ability to label mHGG^{pdgf}-hHER2 cells. Green areas represent the events above the fluorescent intensity threshold determined from the negative control. (B) Evaluation of the specificity of the immunoreactivity of the plasma of two representative mice tested by evaluating the ability of plasma samples to specifically label mHGG^{pdgf}-hHER2 cells in a mixture containing both mHGG^{pdgf}-

hHER2 (labelled with DsRed) and unlabeled NIH/3T3 as negative control. (C) Ratio between (specifically) labelled mHGG^{pdgf}-hHER2 cells and the (unspecifically) labelled NIH/3T3, each normalized to the size of the respective population, calculated for all the plasma samples from control-, R-LM113- and R-115-arm, graphed as boxplot. Plasma samples from mice of R-115 arm appeared more immunoreactive than those from mice of control arm (Anova p<0.05). (D) The same assay was repeated using the parental mHGG^{pdgf} cells instead mHGG^{pdgf}-hHER2. The diagram shows that the plasma of three mice from R-115 arm (two of which are long survivors) displays immunoreactivity against the parental population.

Fig. 3.4

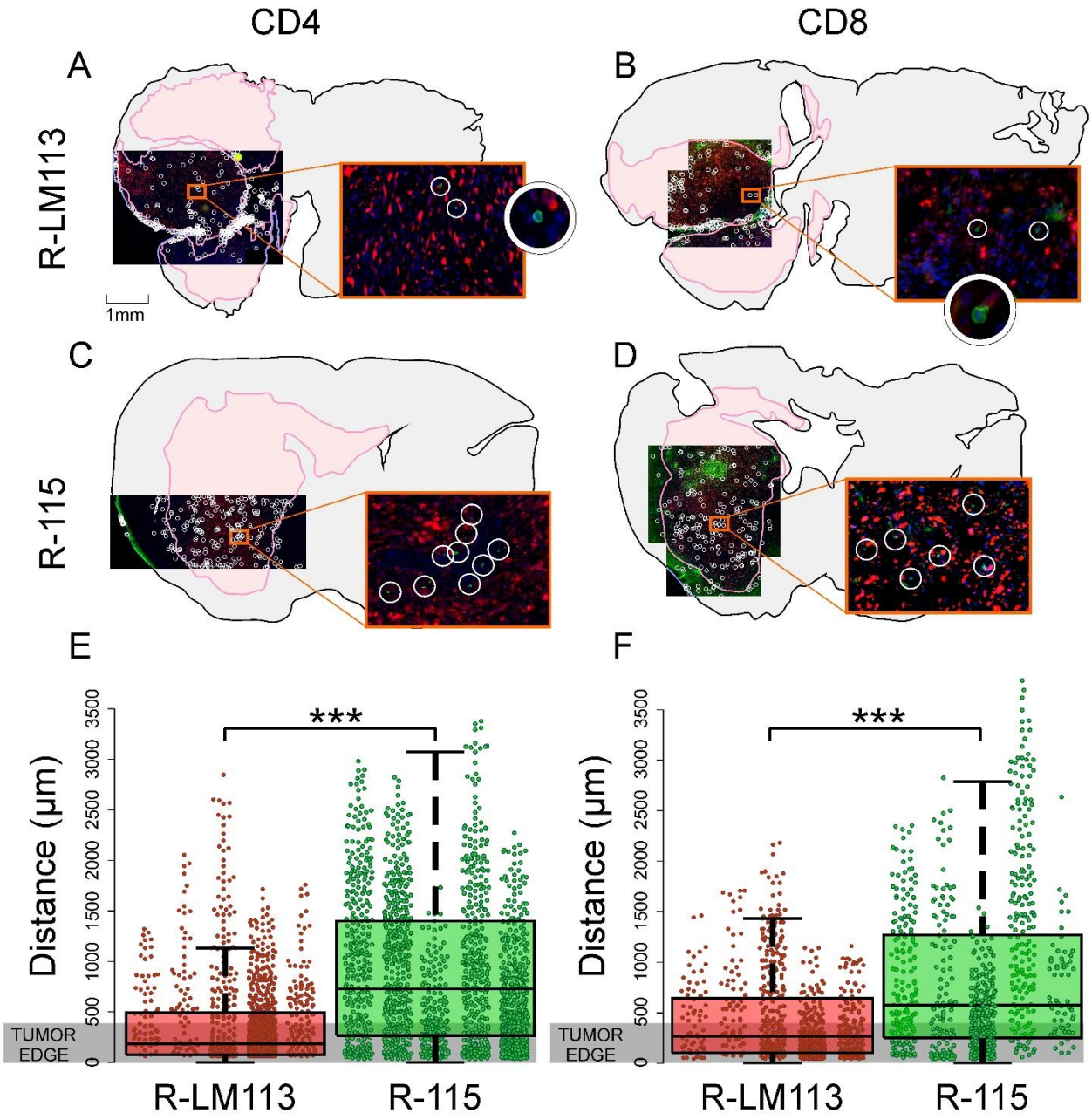

Figure 3.4

Brain sections of mice transplanted with mHGG^{pdgf}-hHER2 cells and treated with R-LM113 (A-B) or with R-115 (C-D) were immunostained for CD4 (A,C) or CD8 (B,D). Positive cells (green) were encircled in white as shown in the inserts. Both CD4 and CD8 lymphocytes were found at the edges of tumors in the animals treated with R-LM113 (A,B) while they strongly infiltrated the tumor masses in the animals treated with R-115 (C,D). Tumors are represented as pink areas. (E,F) The

distance from the nearest edge of the tumor mass of each CD4-positive cell (E) or CD8-positive cell (F) inside the tumor was measured in sections of 10 independent animals treated with R-LM113 or R-115. The results are depicted as bee swarm plots and cumulative box plots. The data confirm the difference of the distribution of both CD4 and CD8 lymphocytes between the treatment with the two different oHSVs (t-test p<10-12).

Efficacy of EGFR-vIII retargeted herpes simplex virus treatment in a preclinical model of human glioblastoma

The epidermal growth factor receptor (EGFR) induces proliferation and/or has a trophic effect on multiple cell types [167]. The EGFR is expressed at high levels in various types of cancer, suggesting a role in the pathogenesis of multiple cancer types [168]. In particular, EGFR gene amplification and overexpression are a striking feature of glioblastoma.

The most common EGFR mutant is its constitutively active form EGFRvIII, generated from a deletion of exons 2 to 7 of the gene, which results in an in-frame deletion of 267 amino acids from the extracellular domain of the receptor. Though low-level in nature, constitutive signaling downstream of EGFRvIII leads to increased glioblastoma cell survival in vivo through selective augmentation of various mitogenic factors, namely Akt and repression of apoptosis via enhanced Bcl2 family member expression [20].

The exclusive expression of EGFRvIII on tumor cells makes it an ideal target for patients with GBM. Among the promising approach that have been developed to specifically hit glioma cells, the employment of oncolytic viruses is extensively studied. We obtained a proof of concept of the feasibility and efficacy of an oncolytic therapy for a murine model of high grade glioma with a herpes virus retargeted to HER2 [119, 120], and a striking improvement by using a version of the same virus armed with interleukin-12 (see chapter 3).

Here, we tested a novel oncolytic virus, retargeted to the human receptor EGFRvIII on a xenotransplanted human glioblastoma model, by evaluating its efficacy in human tumor initiating cells derived from patients and endogenously expressing EGFRvIII.

Materials and methods

Animal procedures

Mice were handled in agreement with guidelines conforming to current Italian regulations for the protection of animals used for scientific purposes (D.lvo 27/01/1992, no. 116). Procedures were approved by the Ethical Committee for Animal Experimentation of the IRCCS San Martino-IST and by the Italian Ministry of Health. The experiments were performed on the Nod/Scid mouse strains. Anesthetized animals were injected by way of a stereotaxic apparatus. Up to 5 µl of suspension, containing from 10^5 cells preparations, were injected using a Hamilton syringe (Bregma coordinates: anterio-posterior, 1.0 mm; lateral, 1.5 mm left and 2.5 mm below the skull surface). Resorbable suture was used before awakening the animals. Animals were then monitored daily and killed at first sign of neurological symptoms Their brains were then explanted and photographed under a Leica fluorescence stereomicroscope (Wetzlar, Germany).

Gluc assays were carried on twice a week, by collecting about 5 µl of blood from the tail tip of mice in tube containing 0.5M EDTA.

Survival curves were determined using Kaplan–Meier analysis and survival between groups was assayed by log-rank test.

Cell cultures, transduction procedures and infection

Human glioma initiating cells (hGIC), included L0306, kindly provided by Dr. R. Galli [140], engineered with oCAG:mGFP-Gluc, were maintained as spheres in Neurocult Medium supplemented with NeuroCult NS-A (StemCell Technologies, Vancouver, British Columbia, CA),

human recombinant fibroblast growth factor 2 (10 ng/ml; PeproTech, Rocky Hill, USA), epidermal growth factor (20 ng/ml; PeproTech, Rocky Hill, USA) and Heparin (2µg/ml, Sigma-Aldrich, Milano, Italy).

Cultures from tumors were established microdissecting DsRed-positive areas under a fluorescence microscope and trypsinizing them for 20 minutes. Cells were maintained in the medium described above.

The construction and production of the recombinant oHSV R-LM613 was described elsewhere [158]. Cells were infected with R-LM613, at the indicated multiplicity of infection estimated on the basis of titer determined in SK-OV-3 cells. The efficiency of infection was monitored under inverted microscope (EVOS FL Cell Imaging System, ThermoFisher Scientific, Waltham, MA, USA) by means of enhanced green fluorescent protein (EGFP) expression for the virus. The percentage of infected cells was evaluated by loading them on a hemocytometer and acquiring pictures/imaging with a motorized epifluorescence microscope (Axio Imager.M2, Zeiss, Oberkochen, Germany). Images were automatically analyzed with an ImageJ plug-in (Rasband, W.S., ImageJ; US National Institutes of Health, Bethesda, MD, http://rsb.info.nih.gov/ij/, 1997–2007), which allows to measure and plot area and fluorescence intensity of each cell.

Western blot analysis

Protein extracts, separated by SDS-PAGE and transferred onto PVDF membranes, were probed with antibodies against EGFR (1:1000, Santa Cruz Biotechnology, Santa Cruz, CA, USA) or actin (1:5000, Chemicon, Billerica, MA). Proteins of interest were detected with HRP-conjugated sheep anti-mouse IgG antibody (1:5000, GE Healthcare, Uppsala, Sweden) and visualized with the ECL (EuroClone S.p.A., Milano, Itlay).

Gaussia luciferase assay

Gluc activity was evaluated in a reaction set up obtained by combining 5µl of blood sample with a buffer constituted by 17.5 µl of Stop & Glo® Buffer (Promega, Milano, IT) supplemented with coelentherazine , and 17.5 µl of a buffer containing HEPES 75mM; DTT 20 mM, EDTA 100 µM, pH 8.0. The luminometer (Promega Glomax 20/20n) was set to acquire a series of 40 consecutive measures with an integration time of 1 second. Data analysis was performed in R environment 3.4.2 [118] with software built in house.

Results

R-LM613 efficiently infects human glioma cells endogenously expressing EGFRvIII *in vitro*

Infection efficiency and specificity of R-LM613 had been previously tested on human glioma initiating cells (hGIC) derived from different patients and maintained in a serum-free medium optimized to preserve their stem features. EGFRvIII positive hTIC primary lines have been evaluated in EGFRvIII expression by rtPCR (data not shown). EGFRvIII positive hTICs have been infected in vitro with R-LM613, at the multiplicity of infection (MOI) of 0.5 plaque-forming units (PFU) per cell, as titrated in SK-OV-3 cells. As negative control, human neural stem cells (hNSCs) or EGFRvIII negative cells have been infected with the same amount of the virus. R-LM613 was able to efficiently infect EGFRvIII positive hTICs, but did not infect NSCs (Fig. 4.1A) or EGFRvIII negative cells (data not shown). Viral infection was scored as expression of the EGFP reporter gene inserted in the virus genome 48 hours after infection (Fig 4.1B).

The different hTIC lines, once transplanted into immunodeficient mice, develop tumors that have different rates of growth. Between hTIC lines we tested, one of them, named L0306 and kindly provided by Dr. R. Galli [140], have proved to grow faster in vivo, permitting us to carry on experiments in reliable times. Thus, them have been assayed for EGFRvIII expression by Western Blot (Fig. 4.1C). L0306 expressed high levels of EGFRvIII and thus we employed this hTIC line to performed the followiong experiments. We monitored the time course of viral infection in L0306 cells in the 120 hours after infection at low MOI (0.1 pfu/cells) of R-Lm613. The collected images showed that R-LM613 progeny was able to efficiently spread in culture (Fig.4.1D).

Oncolytic effect of R-LM613 on human gliomas endogenously expressing EGFRvIII *in vivo*

L0306 were transduced with Ravi:DsRed-Gluc construct expressing the fluorescent reporter DsRed and the Gaussia luciferase (L0306-Gluc), in order to monitor the development of tumor in vivo with a non-invasive assay, as previously described above (chapter 2). To assess the efficacy of R-LM613 in counteracting in vivo the development of human gliomas endogenously expressing EGFRvIII, we used at first an experimental approach designed to mimic the earliest possible treatment of the neoplasia, already used in previous studies [119, 120]. A cohort of 45 Nod/Scid mice, randomly allocated so that the possible confounding factors such as age, gender and weight, were intracranially transplanted in two independent sessions with human hTICs. A first group of animals (n=27, herein referred as to control arm) were injected with 1e5 of L0306-Gluc cells. A second group of animals (n=18, R-LM613 arm) were transplanted with the same number of L0306-Gluc cells and, in addition, with 1e5 cells infected in vitro 24 hours before with

RLM613 at 1 MOI. EGFP reporter expression was quantified before transplantation. 30% of positive cells were observed in this additional population of cells, so we can inferred that, at the moment of injection, 15% of cells have been previously infected by R-LM613.

Mice were monitored for more than 160 days. To dynamically estimate the tumor size during time, and to monitor the intracranial growth of gliomas, up to 10 µl of blood were withdrawn from the tip of the tail of the mice twice a week and Gaussia luciferase activity assay was performed [169]. In the control arm, we observed a volumetric increase of tumor masses from the first days after the transplant. On the contrary, in the mice belonging to the R-LM613 arm we observed a long period of latency before the onset of tumor growth (Fig. 4.2A)

The median survival time of animals of the control arm was 82 days. Survival time of mice belonging to the R-LM613 arm appeared significantly increased, showing a median survival time of 114 days (Rank-test $p<0.001$, Figure 4.2B). All the mice of the control arm showed neurological symptoms within 112 days after transplant, due to the development of larges DsRed positive tumor masses. Only a mouse belonging to the R-LM613 arm showed symptoms of neurological distress 50 days after tumor cell transplantation. The analysis of explanted brain of this mouse showed a DsRed tumor mass extensive infected by R-LM613. No other mice of R-LM613 arm showed neurological symptoms before 106 days after transplant, and more than 60% of this animals did not show any sign of distress before the last mouse in the control arm was killed, after the onset of neurological symptoms. Five mice of R-LM613 arm were killed without the onset of neurological symptoms from 114 to 152 days after transplant. The analyses of explanted brains of these animals revealed DsRed positive tumor masses with EGFP positive areas, indicating ongoing infection more than 114 days after treatment with the virus (Fig. 4.3C). The last three animals of the R-LM613 arm were killed in absence of symptoms of neurological

distress 167 days after tumor cell transplantation. Brains of these mice contained only a few DsRed tumor cells.

L0306 cells dissociated from tumor masses that had carried the animals to death despite treatment were tested for in vitro susceptibility to R-LM613. The virus is still able to infect them (Fig. 4.2D), showing that ability of the tumor cells to survive treatment is not due to the development of resistance to the virus and suggesting that a subsequent or longer treatment may further increase the survival of the animals.

Conclusions

Malignant brain tumors continue to be rapidly progressive and resistant to most treatments. A variety of antigens specifically enriched in brain tumors have been proposed to serve as targets for therapies. Among them, the constitutively active form of EGFR, EGFRvIII, which promotes ligand independent signaling, is expressed by 25% to 30% of high-grade gliomas, making it an interesting target for new therapies.

The employment of fully virulent, retargeted oHSVs for treatment of high grade gliomas has been proved in preclinical murine models. Here, the efficacy of an oHSV fully retargeted to EGFRvIII (named R-LM613) was evaluated in human glioma xenotransplanted in immunodeficient mice.

As first experiment on this model, we use an experimental scheme mimic the administration of the virus at the earliest possible (namely at the same time of glioma transplantation). The treatment with R-LM613 improved significantly the survival of mice, demonstrating the ability of the virus to inhibit the growth of glioma cells expressing endogenously the target molecule EGFRvIII. Importantly, the analysis of the brains revealed EGFP-expressing cells also in animals

dying very late. Thus, the ability of the tumor cells to survive to the treatment is not due to the development of resistance to the virus. This observation suggests the survival of the animals may increase more by using multiple or longer treatments.

Human glioma initiating cells were transduced with the Gaussia luciferase before transplant in mouse brains, in order to monitor tumor growth during time in a non-invasive manner, as described in chapter 2. This assay was demonstrating a suitable tool to study the impact of treatment on tumor growth. Curves obtained showed that the early infection with HSV R-LM613 causes a significant delay in the onset of the tumor mass inhibiting the tumor development for a long time. Data obtained, however, suggest that, when tumor find the way to escape from viral infection, growth rate is similar to that of untreated masse, leading to a rapid increase of the tumor mass.

This study provides the evidence that retargeted HSVs can increase animal survival of mice transplanted with human gliomas that express EGFRvIII endogenously, and therefore represents a step forward towards the possibility to treat human high grade gliomas with retargeted oHSVs.

Figures

Fig. 4.1

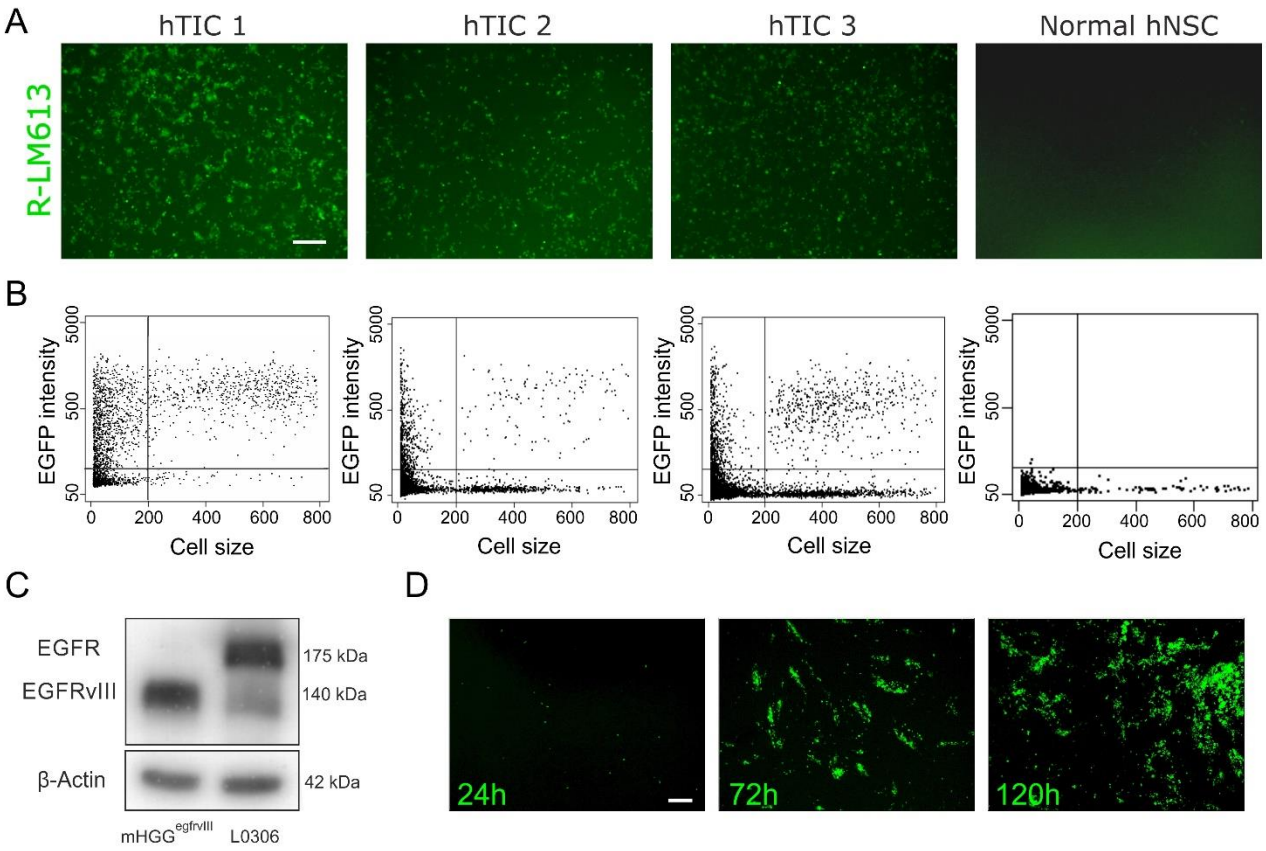

Figure 4.1

(A) Infection of EGFRvIII-positive human tumor initiating cells from several glioma patients or human normal neural stem cells with 0.5 PFU/cell of R-LM613. (B). Dot plots show the quantifications of the cells expressing the EGFP reporter expressed by the viral genome 48h after infection with R-LM613. The virus is specific for EGFRvIII positive cells. (E) Western blot analysis of protein extracts from L0306 or mHGG^{egfrvIII} cells and detected with anti-EGFR antibody. L0306 cells express the constitutively active receptor EGFRvIII. β-actin was used by normalize whole protein amount. (D) Time course of R-LM613 infection in L0306 monolayers (input MOI 0.01 PFU/cell). Scale bars 50μm.

Fig. 4.2

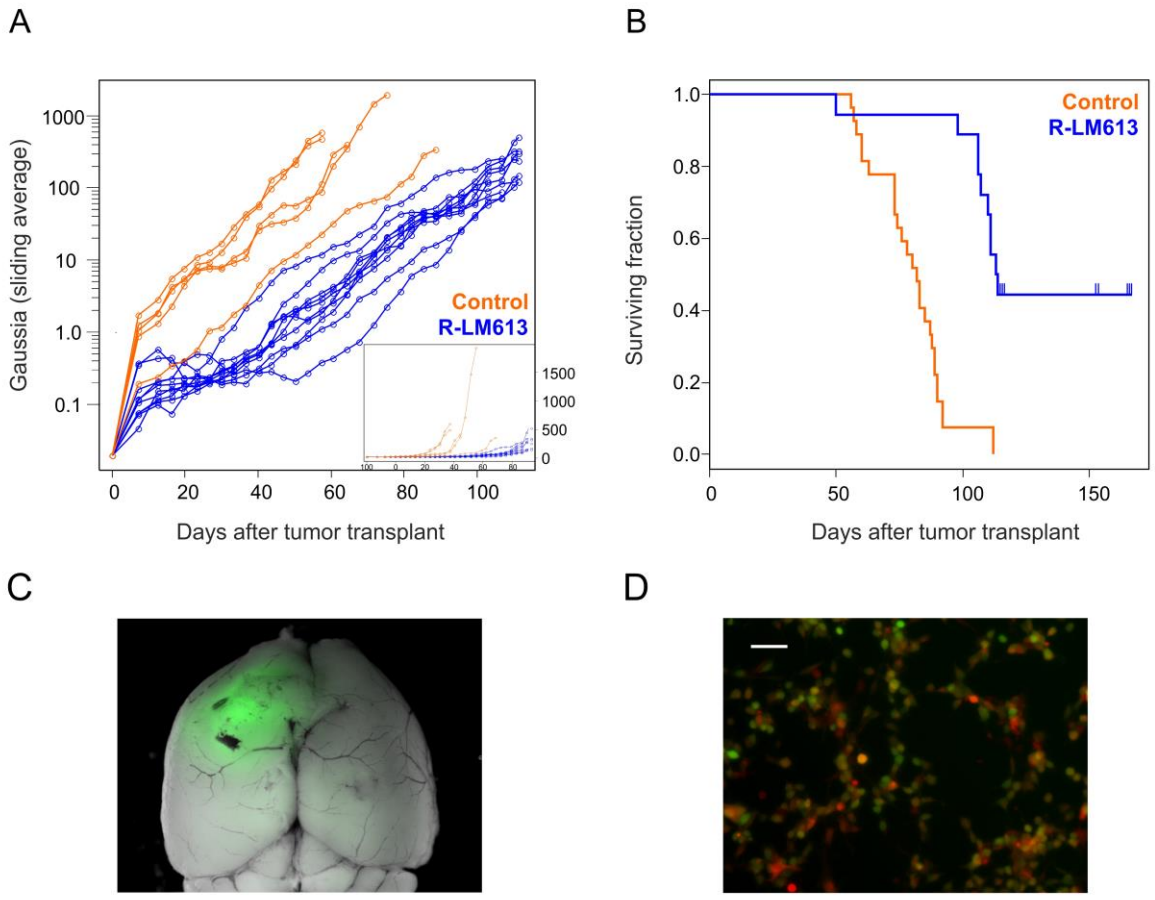

Figure 4.2

(A) Gaussia luciferase measurements over time from mice transplanted with L0306 cells (orange lines) or mice transplanted with the same preparation together with a fraction of L0306 cells (15%) pre-infected in vitro with R-LM613 (blue lines). The virus is able to delay the onset of tumor masses. (B) Kaplan-Meyer survival curves of mice receiving the early treatment (blue line) and of mice from control arm (orange line). Rank-test p<0.001. Mice treated with the virus survive significantly longer than the control ones. (C) Representative dorsal image of brains from mice of the R-LM613 arm, where the viral infection (green area) is clearly present more than 100 days after transplant. (D) Infection of cells explanted by a tumor from R-LM613 arm with the same R-LM613 virus. Tumor cells did not developed a resistance but are still susceptible to virus infection.

Acknowledgments

I would like to thank Dr Magdalena Götz (Institute of Stem Cell Research-Helmholtz Centre, Munich, Germany) for sharing plasmids, Dr Rossella Galli (IRCCS San Raffaele Scientific Institute, Milan, Italy) for providing L0306 cells, Dr Laura Menotti, Prof Maria Gabriella Campadelli and Dr Laura Avitabile (University of Bologna, Bologna, Italy) for providing retargeted viruses, Dr Daniele Reverberi (Ospedale Policlinico San Martino –IRCCS, Genova, Italy) for cell sorting.

References

1. Poppleton, H. and R.J. Gilbertson, *Stem cells of ependymoma.* British journal of cancer, 2007. **96**(1): p. 6-10.
2. Ostrom, Q.T., et al., *CBTRUS statistical report: Primary brain and central nervous system tumors diagnosed in the United States in 2006-2010.* Neuro-oncology, 2013. **15 Suppl 2**: p. ii1-56.
3. Louis, D.N., et al., *The 2007 WHO classification of tumours of the central nervous system.* Acta neuropathologica, 2007. **114**(2): p. 97-109.
4. Louis, D.N., et al., *The 2016 World Health Organization Classification of Tumors of the Central Nervous System: a summary.* Acta neuropathologica, 2016. **131**(6): p. 803-20.
5. Brat, D.J., et al., *Comprehensive, Integrative Genomic Analysis of Diffuse Lower-Grade Gliomas.* The New England journal of medicine, 2015. **372**(26): p. 2481-98.
6. Eckel-Passow, J.E., et al., *Glioma Groups Based on 1p/19q, IDH, and TERT Promoter Mutations in Tumors.* The New England journal of medicine, 2015. **372**(26): p. 2499-508.
7. Wen, P.Y. and S. Kesari, *Malignant gliomas in adults.* The New England journal of medicine, 2008. **359**(5): p. 492-507.
8. Wrensch, M., et al., *Epidemiology of primary brain tumors: current concepts and review of the literature.* Neuro-oncology, 2002. **4**(4): p. 278-99.
9. Pisapia, D.J., *The Updated World Health Organization Glioma Classification: Cellular and Molecular Origins of Adult Infiltrating Gliomas.* Archives of pathology & laboratory medicine, 2017. **141**(12): p. 1633-1645.
10. Reifenberger, G. and V.P. Collins, *Pathology and molecular genetics of astrocytic gliomas.* Journal of molecular medicine, 2004. **82**(10): p. 656-70.
11. Kleihues, P. and H. Ohgaki, *Phenotype vs genotype in the evolution of astrocytic brain tumors.* Toxicologic pathology, 2000. **28**(1): p. 164-70.
12. Kang, M.R., et al., *Mutational analysis of IDH1 codon 132 in glioblastomas and other common cancers.* International journal of cancer, 2009. **125**(2): p. 353-5.
13. Watanabe, T., et al., *IDH1 mutations are early events in the development of astrocytomas and oligodendrogliomas.* The American journal of pathology, 2009. **174**(4): p. 1149-53.

14. Ohgaki, H. and P. Kleihues, *The definition of primary and secondary glioblastoma.* Clinical cancer research : an official journal of the American Association for Cancer Research, 2013. **19**(4): p. 764-72.
15. Verhaak, R.G., et al., *Integrated genomic analysis identifies clinically relevant subtypes of glioblastoma characterized by abnormalities in PDGFRA, IDH1, EGFR, and NF1.* Cancer cell, 2010. **17**(1): p. 98-110.
16. Brennan, C., et al., *Glioblastoma subclasses can be defined by activity among signal transduction pathways and associated genomic alterations.* PloS one, 2009. **4**(11): p. e7752.
17. Huse, J.T., H.S. Phillips, and C.W. Brennan, *Molecular subclassification of diffuse gliomas: seeing order in the chaos.* Glia, 2011. **59**(8): p. 1190-9.
18. Le Mercier, M., et al., *A simplified approach for the molecular classification of glioblastomas.* PloS one, 2012. **7**(9): p. e45475.
19. Gao, Q., T. Lei, and F. Ye, *Therapeutic targeting of EGFR-activated metabolic pathways in glioblastoma.* Expert opinion on investigational drugs, 2013. **22**(8): p. 1023-40.
20. Nagane, M., et al., *A common mutant epidermal growth factor receptor confers enhanced tumorigenicity on human glioblastoma cells by increasing proliferation and reducing apoptosis.* Cancer research, 1996. **56**(21): p. 5079-86.
21. Linggi, B. and G. Carpenter, *ErbB receptors: new insights on mechanisms and biology.* Trends in cell biology, 2006. **16**(12): p. 649-56.
22. Scaltriti, M. and J. Baselga, *The epidermal growth factor receptor pathway: a model for targeted therapy.* Clinical cancer research : an official journal of the American Association for Cancer Research, 2006. **12**(18): p. 5268-72.
23. Nicholas, M.K., et al., *Epidermal growth factor receptor - mediated signal transduction in the development and therapy of gliomas.* Clinical cancer research : an official journal of the American Association for Cancer Research, 2006. **12**(24): p. 7261-70.
24. Benito, R., et al., *Primary glioblastomas with and without EGFR amplification: relationship to genetic alterations and clinicopathological features.* Neuropathology : official journal of the Japanese Society of Neuropathology, 2010. **30**(4): p. 392-400.
25. Chakravarti, A., et al., *The epidermal growth factor receptor pathway mediates resistance to sequential administration of radiation and chemotherapy in primary human glioblastoma cells in a RAS-dependent manner.* Cancer research, 2002. **62**(15): p. 4307-15.
26. Hatanpaa, K.J., et al., *Epidermal growth factor receptor in glioma: signal transduction, neuropathology, imaging, and radioresistance.* Neoplasia, 2010. **12**(9): p. 675-84.

27. Ekstrand, A.J., et al., *Amplified and rearranged epidermal growth factor receptor genes in human glioblastomas reveal deletions of sequences encoding portions of the N- and/or C-terminal tails.* Proceedings of the National Academy of Sciences of the United States of America, 1992. **89**(10): p. 4309-13.
28. Wong, A.J., et al., *Increased expression of the epidermal growth factor receptor gene in malignant gliomas is invariably associated with gene amplification.* Proceedings of the National Academy of Sciences of the United States of America, 1987. **84**(19): p. 6899-903.
29. Frederick, L., et al., *Diversity and frequency of epidermal growth factor receptor mutations in human glioblastomas.* Cancer research, 2000. **60**(5): p. 1383-7.
30. Schwechheimer, K., S. Huang, and W.K. Cavenee, *EGFR gene amplification--rearrangement in human glioblastomas.* International journal of cancer, 1995. **62**(2): p. 145-8.
31. Furnari, F.B., et al., *Malignant astrocytic glioma: genetics, biology, and paths to treatment.* Genes & development, 2007. **21**(21): p. 2683-710.
32. Kanu, O.O., et al., *Glioblastoma Multiforme Oncogenomics and Signaling Pathways.* Clinical medicine. Oncology, 2009. **3**: p. 39-52.
33. Nagane, M., et al., *Aberrant receptor signaling in human malignant gliomas: mechanisms and therapeutic implications.* Cancer letters, 2001. **162 Suppl**: p. S17-S21.
34. Shinojima, N., et al., *Prognostic value of epidermal growth factor receptor in patients with glioblastoma multiforme.* Cancer research, 2003. **63**(20): p. 6962-70.
35. Huang, P.H., A.M. Xu, and F.M. White, *Oncogenic EGFR signaling networks in glioma.* Science signaling, 2009. **2**(87): p. re6.
36. Hynes, N.E. and H.A. Lane, *ERBB receptors and cancer: the complexity of targeted inhibitors.* Nature reviews. Cancer, 2005. **5**(5): p. 341-54.
37. Duhem-Tonnelle, V., et al., *Differential distribution of erbB receptors in human glioblastoma multiforme: expression of erbB3 in CD133-positive putative cancer stem cells.* Journal of neuropathology and experimental neurology, 2010. **69**(6): p. 606-22.
38. Mineo, J.F., et al., *Low HER2-expressing glioblastomas are more often secondary to anaplastic transformation of low-grade glioma.* Journal of neuro-oncology, 2007. **85**(3): p. 281-7.
39. Nabika, S., et al., *Prognostic significance of expression patterns of EGFR family, p21 and p27 in high-grade astrocytoma.* Hiroshima journal of medical sciences, 2010. **59**(4): p. 65-70.
40. Press, M.F., C. Cordon-Cardo, and D.J. Slamon, *Expression of the HER-2/neu proto-oncogene in normal human adult and fetal tissues.* Oncogene, 1990. **5**(7): p. 953-62.

41. Gulati, S., et al., *Overexpression of c-erbB2 is a negative prognostic factor in anaplastic astrocytomas.* Diagnostic pathology, 2010. **5**: p. 18.
42. Hiesiger, E.M., et al., *Prognostic relevance of epidermal growth factor receptor (EGF-R) and c-neu/erbB2 expression in glioblastomas (GBMs).* Journal of neuro-oncology, 1993. **16**(2): p. 93-104.
43. Hermanson, M., et al., *Platelet-derived growth factor and its receptors in human glioma tissue: expression of messenger RNA and protein suggests the presence of autocrine and paracrine loops.* Cancer research, 1992. **52**(11): p. 3213-9.
44. Martinho, O., et al., *Expression, mutation and copy number analysis of platelet-derived growth factor receptor A (PDGFRA) and its ligand PDGFA in gliomas.* British journal of cancer, 2009. **101**(6): p. 973-82.
45. Nister, M., et al., *Expression of messenger RNAs for platelet-derived growth factor and transforming growth factor-alpha and their receptors in human malignant glioma cell lines.* Cancer research, 1988. **48**(14): p. 3910-8.
46. Lokker, N.A., et al., *Platelet-derived growth factor (PDGF) autocrine signaling regulates survival and mitogenic pathways in glioblastoma cells: evidence that the novel PDGF-C and PDGF-D ligands may play a role in the development of brain tumors.* Cancer research, 2002. **62**(13): p. 3729-35.
47. Fleming, T.P., et al., *Amplification and/or overexpression of platelet-derived growth factor receptors and epidermal growth factor receptor in human glial tumors.* Cancer research, 1992. **52**(16): p. 4550-3.
48. Uhrbom, L., et al., *Ink4a-Arf loss cooperates with KRas activation in astrocytes and neural progenitors to generate glioblastomas of various morphologies depending on activated Akt.* Cancer research, 2002. **62**(19): p. 5551-8.
49. Bleeker, F.E., et al., *The prognostic IDH1(R132) mutation is associated with reduced NADP+-dependent IDH activity in glioblastoma.* Acta neuropathologica, 2010. **119**(4): p. 487-94.
50. Pollard, P.J. and P.J. Ratcliffe, *Cancer. Puzzling patterns of predisposition.* Science, 2009. **324**(5924): p. 192-4.
51. Stupp, R., et al., *Effects of radiotherapy with concomitant and adjuvant temozolomide versus radiotherapy alone on survival in glioblastoma in a randomised phase III study: 5-year analysis of the EORTC-NCIC trial.* The Lancet. Oncology, 2009. **10**(5): p. 459-66.

52. Smoll, N.R., K. Schaller, and O.P. Gautschi, *Long-term survival of patients with glioblastoma multiforme (GBM).* Journal of clinical neuroscience : official journal of the Neurosurgical Society of Australasia, 2013. **20**(5): p. 670-5.
53. Thakkar, J.P., et al., *Epidemiologic and molecular prognostic review of glioblastoma.* Cancer epidemiology, biomarkers & prevention : a publication of the American Association for Cancer Research, cosponsored by the American Society of Preventive Oncology, 2014. **23**(10): p. 1985-96.
54. Johnson, D.R., et al., *Conditional probability of long-term survival in glioblastoma: a population-based analysis.* Cancer, 2012. **118**(22): p. 5608-13.
55. Porter, K.R., et al., *Conditional survival of all primary brain tumor patients by age, behavior, and histology.* Neuroepidemiology, 2011. **36**(4): p. 230-9.
56. Zhao, S., et al., *Intraoperative fluorescence-guided resection of high-grade malignant gliomas using 5-aminolevulinic acid-induced porphyrins: a systematic review and meta-analysis of prospective studies.* PloS one, 2013. **8**(5): p. e63682.
57. Stupp, R., et al., *Radiotherapy plus concomitant and adjuvant temozolomide for glioblastoma.* The New England journal of medicine, 2005. **352**(10): p. 987-96.
58. Weller, M., et al., *MGMT promoter methylation in malignant gliomas: ready for personalized medicine?* Nature reviews. Neurology, 2010. **6**(1): p. 39-51.
59. Aldape, K., et al., *Glioblastoma: pathology, molecular mechanisms and markers.* Acta neuropathologica, 2015. **129**(6): p. 829-48.
60. Norden, A.D., J. Drappatz, and P.Y. Wen, *Antiangiogenic therapy in malignant gliomas.* Current opinion in oncology, 2008. **20**(6): p. 652-61.
61. Chinot, O.L., et al., *AVAglio: Phase 3 trial of bevacizumab plus temozolomide and radiotherapy in newly diagnosed glioblastoma multiforme.* Advances in therapy, 2011. **28**(4): p. 334-40.
62. Gilbert, M.R., et al., *A randomized trial of bevacizumab for newly diagnosed glioblastoma.* The New England journal of medicine, 2014. **370**(8): p. 699-708.
63. Curry, R.C., et al., *Bevacizumab in high-grade gliomas: past, present, and future.* Expert review of anticancer therapy, 2015. **15**(4): p. 387-97.
64. Wen, P.Y., et al., *Phase I/II study of imatinib mesylate for recurrent malignant gliomas: North American Brain Tumor Consortium Study 99-08.* Clinical cancer research : an official journal of the American Association for Cancer Research, 2006. **12**(16): p. 4899-907.

65. Reardon, D.A., et al., *Multicentre phase II studies evaluating imatinib plus hydroxyurea in patients with progressive glioblastoma.* British journal of cancer, 2009. **101**(12): p. 1995-2004.
66. Seystahl, K., W. Wick, and M. Weller, *Therapeutic options in recurrent glioblastoma--An update.* Critical reviews in oncology/hematology, 2016. **99**: p. 389-408.
67. Weiner, L.M., R. Surana, and S. Wang, *Monoclonal antibodies: versatile platforms for cancer immunotherapy.* Nature reviews. Immunology, 2010. **10**(5): p. 317-27.
68. Gajadhar, A.S., et al., *In situ analysis of mutant EGFRs prevalent in glioblastoma multiforme reveals aberrant dimerization, activation, and differential response to anti-EGFR targeted therapy.* Molecular cancer research : MCR, 2012. **10**(3): p. 428-40.
69. Cho, J., et al., *Glioblastoma-derived epidermal growth factor receptor carboxyl-terminal deletion mutants are transforming and are sensitive to EGFR-directed therapies.* Cancer research, 2011. **71**(24): p. 7587-96.
70. Kamran, N., et al., *Recent advances and future of immunotherapy for glioblastoma.* Expert opinion on biological therapy, 2016. **16**(10): p. 1245-64.
71. Preusser, M., et al., *Prospects of immune checkpoint modulators in the treatment of glioblastoma.* Nature reviews. Neurology, 2015. **11**(9): p. 504-14.
72. Sahebjam, S., et al., *Assessing Response of High-Grade Gliomas to Immune Checkpoint Inhibitors.* Cancer control : journal of the Moffitt Cancer Center, 2017. **24**(2): p. 180-186.
73. Tan, A.C., A.B. Heimberger, and M. Khasraw, *Immune Checkpoint Inhibitors in Gliomas.* Current oncology reports, 2017. **19**(4): p. 23.
74. Ahn, B.J., I.F. Pollack, and H. Okada, *Immune-checkpoint blockade and active immunotherapy for glioma.* Cancers, 2013. **5**(4): p. 1379-412.
75. Lin, Y. and H. Okada, *Cellular immunotherapy for malignant gliomas.* Expert opinion on biological therapy, 2016. **16**(10): p. 1265-75.
76. Roizman, B. and B. Taddeo, *The strategy of herpes simplex virus replication and takeover of the host cell*, in *Human Herpesviruses: Biology, Therapy, and Immunoprophylaxis*, A. Arvin, et al., Editors. 2007: Cambridge.
77. Parker, J.N., et al., *Oncolytic viral therapy of malignant glioma.* Neurotherapeutics : the journal of the American Society for Experimental NeuroTherapeutics, 2009. **6**(3): p. 558-69.
78. Fukuhara, H., Y. Ino, and T. Todo, *Oncolytic virus therapy: A new era of cancer treatment at dawn.* Cancer science, 2016. **107**(10): p. 1373-1379.

79. Mohr, I., *To replicate or not to replicate: achieving selective oncolytic virus replication in cancer cells through translational control.* Oncogene, 2005. **24**(52): p. 7697-709.
80. Hunter, W.D., et al., *Attenuated, replication-competent herpes simplex virus type 1 mutant G207: safety evaluation of intracerebral injection in nonhuman primates.* Journal of virology, 1999. **73**(8): p. 6319-26.
81. Mineta, T., et al., *Attenuated multi-mutated herpes simplex virus-1 for the treatment of malignant gliomas.* Nature medicine, 1995. **1**(9): p. 938-43.
82. Sundaresan, P., et al., *Attenuated, replication-competent herpes simplex virus type 1 mutant G207: safety evaluation in mice.* Journal of virology, 2000. **74**(8): p. 3832-41.
83. Markert, J.M., et al., *Phase Ib trial of mutant herpes simplex virus G207 inoculated pre-and post-tumor resection for recurrent GBM.* Molecular therapy : the journal of the American Society of Gene Therapy, 2009. **17**(1): p. 199-207.
84. Markert, J.M., et al., *Conditionally replicating herpes simplex virus mutant, G207 for the treatment of malignant glioma: results of a phase I trial.* Gene therapy, 2000. **7**(10): p. 867-74.
85. Markert, J.M., et al., *A phase 1 trial of oncolytic HSV-1, G207, given in combination with radiation for recurrent GBM demonstrates safety and radiographic responses.* Molecular therapy : the journal of the American Society of Gene Therapy, 2014. **22**(5): p. 1048-55.
86. Rampling, R., et al., *Toxicity evaluation of replication-competent herpes simplex virus (ICP 34.5 null mutant 1716) in patients with recurrent malignant glioma.* Gene therapy, 2000. **7**(10): p. 859-66.
87. Todo, T., et al., *Oncolytic herpes simplex virus vector with enhanced MHC class I presentation and tumor cell killing.* Proceedings of the National Academy of Sciences of the United States of America, 2001. **98**(11): p. 6396-401.
88. Campadelli-Fiume, G., et al., *Rethinking herpes simplex virus: the way to oncolytic agents.* Reviews in medical virology, 2011. **21**(4): p. 213-26.
89. Parker, J.N., et al., *Engineered herpes simplex virus expressing IL-12 in the treatment of experimental murine brain tumors.* Proceedings of the National Academy of Sciences of the United States of America, 2000. **97**(5): p. 2208-13.
90. Kanai, R. and S.D. Rabkin, *Combinatorial strategies for oncolytic herpes simplex virus therapy of brain tumors.* CNS oncology, 2013. **2**(2): p. 129-42.
91. Campadelli-Fiume, G., et al., *The multipartite system that mediates entry of herpes simplex virus into the cell.* Reviews in medical virology, 2007. **17**(5): p. 313-26.

92. Zhou, G., et al., *Engineered herpes simplex virus 1 is dependent on IL13Ralpha 2 receptor for cell entry and independent of glycoprotein D receptor interaction.* Proceedings of the National Academy of Sciences of the United States of America, 2002. **99**(23): p. 15124-9.
93. Kamiyama, H., G. Zhou, and B. Roizman, *Herpes simplex virus 1 recombinant virions exhibiting the amino terminal fragment of urokinase-type plasminogen activator can enter cells via the cognate receptor.* Gene therapy, 2006. **13**(7): p. 621-9.
94. Menotti, L., et al., *Construction of a fully retargeted herpes simplex virus 1 recombinant capable of entering cells solely via human epidermal growth factor receptor 2.* Journal of virology, 2008. **82**(20): p. 10153-61.
95. Al-Lazikani, B., U. Banerji, and P. Workman, *Combinatorial drug therapy for cancer in the post-genomic era.* Nature biotechnology, 2012. **30**(7): p. 679-92.
96. Hu, X. and E.C. Holland, *Applications of mouse glioma models in preclinical trials.* Mutation research, 2005. **576**(1-2): p. 54-65.
97. Huse, J.T. and E.C. Holland, *Genetically engineered mouse models of brain cancer and the promise of preclinical testing.* Brain pathology, 2009. **19**(1): p. 132-43.
98. Weiss, W.A., et al., *Genetic determinants of malignancy in a mouse model for oligodendroglioma.* Cancer research, 2003. **63**(7): p. 1589-95.
99. Holland, E.C., et al., *A constitutively active epidermal growth factor receptor cooperates with disruption of G1 cell-cycle arrest pathways to induce glioma-like lesions in mice.* Genes & development, 1998. **12**(23): p. 3675-85.
100. Bachoo, R.M., et al., *Epidermal growth factor receptor and Ink4a/Arf: convergent mechanisms governing terminal differentiation and transformation along the neural stem cell to astrocyte axis.* Cancer cell, 2002. **1**(3): p. 269-77.
101. Ding, H., et al., *Oligodendrogliomas result from the expression of an activated mutant epidermal growth factor receptor in a RAS transgenic mouse astrocytoma model.* Cancer research, 2003. **63**(5): p. 1106-13.
102. Uhrbom, L., et al., *Induction of brain tumors in mice using a recombinant platelet-derived growth factor B-chain retrovirus.* Cancer research, 1998. **58**(23): p. 5275-9.
103. Dai, C., et al., *PDGF autocrine stimulation dedifferentiates cultured astrocytes and induces oligodendrogliomas and oligoastrocytomas from neural progenitors and astrocytes in vivo.* Genes & development, 2001. **15**(15): p. 1913-25.

104. Hesselager, G., et al., *Complementary effects of platelet-derived growth factor autocrine stimulation and p53 or Ink4a-Arf deletion in a mouse glioma model.* Cancer research, 2003. **63**(15): p. 4305-9.
105. Appolloni, I., et al., *PDGF-B induces a homogeneous class of oligodendrogliomas from embryonic neural progenitors.* International journal of cancer, 2009. **124**(10): p. 2251-9.
106. Calzolari, F., et al., *Tumor progression and oncogene addiction in a PDGF-B-induced model of gliomagenesis.* Neoplasia, 2008. **10**(12): p. 1373-82, following 1382.
107. Appolloni, I., et al., *Six3 controls the neural progenitor status in the murine CNS.* Cerebral cortex, 2008. **18**(3): p. 553-62.
108. Appolloni, I., et al., *A cadherin switch underlies malignancy in high-grade gliomas.* Oncogene, 2015. **34**(15): p. 1991-2002.
109. Appolloni, I., et al., *Antagonistic modulation of gliomagenesis by Pax6 and Olig2 in PDGF-induced oligodendroglioma.* International journal of cancer. Journal international du cancer, 2012. **131**(7): p. E1078-87.
110. Terrile, M., et al., *PDGF-B-driven gliomagenesis can occur in the absence of the proteoglycan NG2.* BMC cancer, 2010. **10**: p. 550.
111. Cahoy, J.D., et al., *A transcriptome database for astrocytes, neurons, and oligodendrocytes: a new resource for understanding brain development and function.* The Journal of neuroscience : the official journal of the Society for Neuroscience, 2008. **28**(1): p. 264-78.
112. Chen, Y.H., et al., *Mouse low-grade gliomas contain cancer stem cells with unique molecular and functional properties.* Cell reports, 2015. **10**(11): p. 1899-912.
113. Nieto-Estevez, V., et al., *A global transcriptome analysis reveals molecular hallmarks of neural stem cell death, survival, and differentiation in response to partial FGF-2 and EGF deprivation.* PloS one, 2013. **8**(1): p. e53594.
114. Bolstad, B.M., et al., *A comparison of normalization methods for high density oligonucleotide array data based on variance and bias.* Bioinformatics, 2003. **19**(2): p. 185-93.
115. Zhang, Y., et al., *An RNA-sequencing transcriptome and splicing database of glia, neurons, and vascular cells of the cerebral cortex.* The Journal of neuroscience : the official journal of the Society for Neuroscience, 2014. **34**(36): p. 11929-47.
116. Dobin, A. and T.R. Gingeras, *Mapping RNA-seq Reads with STAR.* Current protocols in bioinformatics, 2015. **51**: p. 11 14 1-19.
117. Li, B. and C.N. Dewey, *RSEM: accurate transcript quantification from RNA-Seq data with or without a reference genome.* BMC bioinformatics, 2011. **12**: p. 323.

118. Robinson, M.D., D.J. McCarthy, and G.K. Smyth, *edgeR: a Bioconductor package for differential expression analysis of digital gene expression data.* Bioinformatics, 2010. **26**(1): p. 139-40.
119. Gambini, E., et al., *Replication-competent herpes simplex virus retargeted to HER2 as therapy for high-grade glioma.* Molecular therapy : the journal of the American Society of Gene Therapy, 2012. **20**(5): p. 994-1001.
120. Reisoli, E., et al., *Efficacy of HER2 retargeted herpes simplex virus as therapy for high-grade glioma in immunocompetent mice.* Cancer gene therapy, 2012. **19**(11): p. 788-95.
121. Fu, X., et al., *Estimating accuracy of RNA-Seq and microarrays with proteomics.* BMC genomics, 2009. **10**: p. 161.
122. Marioni, J.C., et al., *RNA-seq: an assessment of technical reproducibility and comparison with gene expression arrays.* Genome research, 2008. **18**(9): p. 1509-17.
123. Zhao, S., et al., *Comparison of RNA-Seq and microarray in transcriptome profiling of activated T cells.* PloS one, 2014. **9**(1): p. e78644.
124. *Comprehensive genomic characterization defines human glioblastoma genes and core pathways.* Nature, 2008. **455**(7216): p. 1061-8.
125. Brennan, C.W., et al., *The somatic genomic landscape of glioblastoma.* Cell, 2013. **155**(2): p. 462-77.
126. Cho, H.R., et al., *Malignant glioma: MR imaging by using 5-aminolevulinic acid in an animal model.* Radiology, 2014. **272**(3): p. 720-30.
127. Nedergaard, M.K., et al., *The use of longitudinal 18F-FET MicroPET imaging to evaluate response to irinotecan in orthotopic human glioblastoma multiforme xenografts.* PloS one, 2014. **9**(2): p. e100009.
128. Sun, A., et al., *Firefly luciferase-based dynamic bioluminescence imaging: a noninvasive technique to assess tumor angiogenesis.* Neurosurgery, 2010. **66**(4): p. 751-7; discussion 757.
129. Kitamura, M. and N. Hiramatsu, *Real-time monitoring of ER stress in living cells and animals using ESTRAP assay.* Methods in enzymology, 2011. **490**: p. 93-106.
130. Lewandrowski, G.K., et al., *Simultaneous in vivo monitoring of regulatory and effector T lymphocytes using secreted Gaussia luciferase, Firefly luciferase, and secreted alkaline phosphatase.* Methods in molecular biology, 2014. **1098**: p. 211-27.
131. Tannous, B.A., *Gaussia luciferase reporter assay for monitoring biological processes in culture and in vivo.* Nature protocols, 2009. **4**(4): p. 582-91.

132. Wurdinger, T., et al., *A secreted luciferase for ex vivo monitoring of in vivo processes.* Nature methods, 2008. **5**(2): p. 171-3.
133. Tannous, B.A., et al., *Codon-optimized Gaussia luciferase cDNA for mammalian gene expression in culture and in vivo.* Molecular therapy : the journal of the American Society of Gene Therapy, 2005. **11**(3): p. 435-43.
134. Branchini, B.R., et al., *Red- and green-emitting firefly luciferase mutants for bioluminescent reporter applications.* Analytical biochemistry, 2005. **345**(1): p. 140-8.
135. Matthews, J.C., K. Hori, and M.J. Cormier, *Purification and properties of Renilla reniformis luciferase.* Biochemistry, 1977. **16**(1): p. 85-91.
136. Verhaegent, M. and T.K. Christopoulos, *Recombinant Gaussia luciferase. Overexpression, purification, and analytical application of a bioluminescent reporter for DNA hybridization.* Analytical chemistry, 2002. **74**(17): p. 4378-85.
137. Badr, C.E., et al., *A highly sensitive assay for monitoring the secretory pathway and ER stress.* PloS one, 2007. **2**(6): p. e571.
138. Chung, E., et al., *Secreted Gaussia luciferase as a biomarker for monitoring tumor progression and treatment response of systemic metastases.* PloS one, 2009. **4**(12): p. e8316.
139. Tseng, A.W., et al., *Detection of neuroendocrine tumors using promoter-specific secreted Gaussia luciferase.* International journal of oncology, 2016. **48**(1): p. 173-80.
140. Mazzoleni, S., et al., *Epidermal growth factor receptor expression identifies functionally and molecularly distinct tumor-initiating cells in human glioblastoma multiforme and is required for gliomagenesis.* Cancer research, 2010. **70**(19): p. 7500-13.
141. Clark, A.J., et al., *Stable luciferase expression does not alter immunologic or in vivo growth properties of GL261 murine glioma cells.* Journal of translational medicine, 2014. **12**: p. 345.
142. Yin, Y., et al., *Removal of transgene-expressing cells by a specific immune response induced by sustained transgene expression.* The journal of gene medicine, 2014. **16**(3-4): p. 97-106.
143. Campadelli-Fiume, G., et al., *Retargeting Strategies for Oncolytic Herpes Simplex Viruses.* Viruses, 2016. **8**(3): p. 63.
144. Manservigi, R., R. Argnani, and P. Marconi, *HSV Recombinant Vectors for Gene Therapy.* The open virology journal, 2010. **4**: p. 123-56.
145. Kemeny, N., et al., *Phase I, open-label, dose-escalating study of a genetically engineered herpes simplex virus, NV1020, in subjects with metastatic colorectal carcinoma to the liver.* Human gene therapy, 2006. **17**(12): p. 1214-24.

146. Kimata, H., et al., *Pilot study of oncolytic viral therapy using mutant herpes simplex virus (HF10) against recurrent metastatic breast cancer.* Annals of surgical oncology, 2006. **13**(8): p. 1078-84.
147. Nakao, A., et al., *A phase I dose-escalation clinical trial of intraoperative direct intratumoral injection of HF10 oncolytic virus in non-resectable patients with advanced pancreatic cancer.* Cancer gene therapy, 2011. **18**(3): p. 167-75.
148. Andtbacka, R.H., et al., *Talimogene Laherparepvec Improves Durable Response Rate in Patients With Advanced Melanoma.* Journal of clinical oncology : official journal of the American Society of Clinical Oncology, 2015. **33**(25): p. 2780-8.
149. Senzer, N.N., et al., *Phase II clinical trial of a granulocyte-macrophage colony-stimulating factor-encoding, second-generation oncolytic herpesvirus in patients with unresectable metastatic melanoma.* Journal of clinical oncology : official journal of the American Society of Clinical Oncology, 2009. **27**(34): p. 5763-71.
150. Louis, D.N.O., H.; Wiestler, O.D.; Cavenee, W.K., *World Health Organization Histological Classification of Tumours of the Central Nervous System. Revise 4th edition.*2016, Lyon: IARC Press.
151. Korn, T. and A. Kallies, *T cell responses in the central nervous system.* Nature reviews. Immunology, 2017. **17**(3): p. 179-194.
152. Louveau, A., T.H. Harris, and J. Kipnis, *Revisiting the Mechanisms of CNS Immune Privilege.* Trends in immunology, 2015. **36**(10): p. 569-77.
153. Thomas, E.D., et al., *IL-12 Expressing oncolytic herpes simplex virus promotes anti-tumor activity and immunologic control of metastatic ovarian cancer in mice.* Journal of ovarian research, 2016. **9**(1): p. 70.
154. Cody, J.J., et al., *Preclinical evaluation of oncolytic deltagamma(1)34.5 herpes simplex virus expressing interleukin-12 for therapy of breast cancer brain metastases.* International journal of breast cancer, 2012. **2012**: p. 628697.
155. Cheema, T.A., et al., *Multifaceted oncolytic virus therapy for glioblastoma in an immunocompetent cancer stem cell model.* Proceedings of the National Academy of Sciences of the United States of America, 2013. **110**(29): p. 12006-11.
156. Patel, D.M., et al., *Design of a Phase I Clinical Trial to Evaluate M032, a Genetically Engineered HSV-1 Expressing IL-12, in Patients with Recurrent/Progressive Glioblastoma Multiforme, Anaplastic Astrocytoma, or Gliosarcoma.* Human gene therapy. Clinical development, 2016. **27**(2): p. 69-78.

157. Uchida, H., et al., *Effective treatment of an orthotopic xenograft model of human glioblastoma using an EGFR-retargeted oncolytic herpes simplex virus.* Molecular therapy : the journal of the American Society of Gene Therapy, 2013. **21**(3): p. 561-9.
158. Menotti, L., et al., *HSV as a platform for the generation of retargeted, armed, and reporter-expressing oncolytic viruses.* Submitted.
159. Edelstein, A., et al., *Computer control of microscopes using microManager.* Current protocols in molecular biology, 2010. **Chapter 14**: p. Unit14 20.
160. Hausler, S.F., et al., *Ectonucleotidases CD39 and CD73 on OvCA cells are potent adenosine-generating enzymes responsible for adenosine receptor 2A-dependent suppression of T cell function and NK cell cytotoxicity.* Cancer immunology, immunotherapy : CII, 2011. **60**(10): p. 1405-18.
161. Trinchieri, G., *Interleukin-12 and the regulation of innate resistance and adaptive immunity.* Nature reviews. Immunology, 2003. **3**(2): p. 133-46.
162. Hellums, E.K., et al., *Increased efficacy of an interleukin-12-secreting herpes simplex virus in a syngeneic intracranial murine glioma model.* Neuro-oncology, 2005. **7**(3): p. 213-24.
163. Favaro, R., et al., *Sox2 is required to maintain cancer stem cells in a mouse model of high-grade oligodendroglioma.* Cancer research, 2014. **74**(6): p. 1833-44.
164. Saha, D., R.L. Martuza, and S.D. Rabkin, *Macrophage Polarization Contributes to Glioblastoma Eradication by Combination Immunovirotherapy and Immune Checkpoint Blockade.* Cancer cell, 2017. **32**(2): p. 253-267 e5.
165. Curry, W.T. and M. Lim, *Immunomodulation: checkpoint blockade etc.* Neuro-oncology, 2015. **17 Suppl 7**: p. vii26-vii31.
166. van der Woude, L.L., et al., *Migrating into the Tumor: a Roadmap for T Cells.* Trends in cancer, 2017. **3**(11): p. 797-808.
167. Carpenter, G. and S. Cohen, *Epidermal growth factor.* The Journal of biological chemistry, 1990. **265**(14): p. 7709-12.
168. Gullick, W.J., *Prevalence of aberrant expression of the epidermal growth factor receptor in human cancers.* British medical bulletin, 1991. **47**(1): p. 87-98.
169. Alessandrini, F., et al., *Noninvasive Monitoring of Glioma Growth in the Mouse.* Journal of Cancer, 2016. **7**(13): p. 1791-1797.

Non invasive monitoring of glioma growth in the mouse

J Cancer. 2016 Aug 12;7(13):1791-1797. eCollection 2016. PMID: 27698917

Francesco Alessandrini1, Davide Ceresa1, Irene Appolloni2, Daniela Marubbi1,2, Paolo Malatesta1,2§

1 Department of Experimental Medicine (DiMES), University of Genoa, Leon Battista Alberti 2, 16132,Genoa-Italy.

2 IRCCS-AOU San Martino-IST, Largo Rosanna Benzi 10, 16132, Genoa-Italy.

§ Author to whom correspondence should be addressed; E-Mail: paolo.malatesta@unige.it; Tel.: +39-010-5558403; Fax: +39-010-5558405.

Abstract

Malignant gliomas are the most common and deadly primary malignant brain tumors. In vivo orthotopic models could doubtless represent an appropriate tool to test novel treatment for gliomas. However, methods commonly used to monitor the growth of glioma inside the mouse brain are time consuming and invasive. We tested the reliability of a minimally invasive procedure, based on a secreted luciferase (Gaussia luciferase), to frequently monitor the changes of glioma size.

Gluc activity was evaluated from blood samples collected from the tail tip of mice twice a week, allowing to make a growth curve for the tumors. We validated the correlation between Gluc activity and tumor size by analysing the tumor after brain dissection. We found that this method is reliable for monitoring human glioma transplanted in immunodeficient mice, but it has strong limitation in immunocompetent models, where an immune response against the luciferase is developed during the first weeks after transplant.

IL-12 armed retargeted herpes simplex virus as therapy for a high-grade glioma preclinical model

Submitted (under revision)

Authors: Francesco Alessandrini, Laura Menotti, Elisa Avitabile, Irene Appolloni, Davide Ceresa, Daniela Marubbi, Gabriella Campadelli-Fiume, Paolo Malatesta

Affiliations: Department of Experimental Medicine, University of Genoa, Genoa, Italy. (F.A., D.C., D.M., P.M.). Department of Pharmacy and Biotechnology, University of Bologna, Bologna, Italy. (L.M., E.A.). Ospedale Policlinico San Martino – IRCCS per l'Oncologia, Genoa, Italy. (F.A., D.M., I.A., P.M.). Department of Experimental, Diagnostic and Specialty Medicine, University of Bologna, Bologna, Italy. (G.C.F.).

Abstract

Background: Oncolytic herpes simplex virus (oHSVs) are proving effective in clinical trials and practice against a number of cancers. Our aim was to determine the efficacy of a retargeted oHSV, fully virulent in its target cells and armed with mIL-12 (R-115), in counteracting glioblastoma, one of the most lethal and less treatable human cancer.

Methods: R-115 was designed to target cells expressing the human receptor tyrosine-protein kinase erbB-2 (hHER2), a receptor frequently expressed in glioblastomas, and carries no attenuation or deletion other than those required for retargeting. To evaluate R-115 efficacy in an immunocompetent environment, we expressed hHER2 in cells of a well-established glioma model, induced by overexpression of PDGF-B in murine neural progenitor cells. The model recapitulates the immunosuppressive features and lethality of human glioblastoma, invariably leading untreated animals to death.

Results: A single administration of low amount of R-115 was able to eradicate the gliomas in about 30% of treated animals and to increase significantly the overall survival time. R-115 strongly promoted the infiltration of tumor masses by lymphocytes. Long survivor mice developed resistance to the same neoplasia.

Conclusions: Such a high degree of protection upon a single viral dose was unprecedented; it was not observed before with the commonly used attenuated oHSVs, including oHSVs deleted in the γ134.5 virulence gene. This study highlights the advantages of a fully virulent retargeted mIL-12-expressing oHSV over attenuated oHSVs in counteracting high-grade gliomas, and suggests it is a candidate for oHSV-based glioblastoma treatment.